Determination of helix orientations in highly flexible DNA molecules

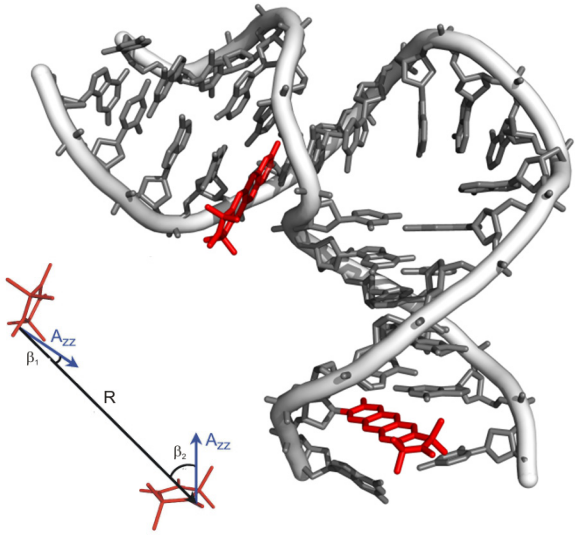

Dissertation

for attaining the PhD degree

of Natural Sciences

Submitted to the Department 14

of the Johann Wolfgang Goethe University

in Frankfurt am Main

by

Claudia Maria Grytz

from Offenbach am Main, Germany

Frankfurt am Main 2017

(D30)

Accepted by Department 14: biochemistry, chemistry and pharmacy
of the Johann Wolfgang Goethe University as a dissertation

Dean:	Prof. Dr. Clemens Glaubitz
First expert assessor:	Prof. Dr. Thomas F. Prisner
Second expert assessor:	Prof. Dr. Peter Güntert

Date of the disputation: **……**

„Es ist nicht genug, zu wissen, man muss auch anwenden;
es ist nicht genug, zu wollen, man muss auch tun.“

Johann Wolfgang von Goethe

Meinem Weggefährten und besten Freund
Pierre Eisenbrandt

Abstract

Pulsed electron-electron double resonance (PELDOR), also called Double Electron-Electron Resonance, (DEER) is a pulsed EPR technique that can provide structural information of biomolecules, such as proteins or nucleic acids, complementary to other structure determination methods by measuring long distances (from 1.5 up to 10 nm) between two paramagnetic labels. Incorporation of the rigid **Ç**-label pairwise into DNA or RNA molecules enables the determination not only of the distance but also of the mutual orientation between the two **Ç**-labels by multi-frequency orientation-selective PELDOR data (X-, Q- and G-band frequencies). Thus, information about the orientation of secondary structure elements of nucleic acids can be revealed and used as additional angular information for structure determination. Since **Ç** does not have motion independent from the helix where it resides, the conformational flexibility of the nucleic acid molecule can be directly determined. This thesis demonstrates the advancement of PELDOR spectroscopy, beyond its original scope of distance measurements, to determine the mutual orientation between two rigid spin labels towards the characterization of the conformational space sampled by highly flexible nucleic acid molecules. Applications of the methodology are shown on two systems: a three-way junction, namely a cocaine aptamer in its bound-state, and a two-way junction, namely a bent DNA.

More in detail, the conformational changes of the cocaine aptamer upon cocaine binding were investigated by analysis of the distance distributions. The cocaine-bound and the unbound states could be differentiated by their conformational flexibility, which decreases in the presence of the ligand. Moreover, the obtained distance distributions revealed a small change in the mean distance between the two spin labels upon cocaine binding. This indicates a ligand-induced conformational change, which presumably originates at the junction where cocaine is known to bind. The investigation of the relative orientation between the two spin-labeled helices of the aptamer revealed further structural insights into the conformational dynamics of the cocaine-bound state. The angular information from the orientation-selective PELDOR data and the *a priori* knowledge about the secondary structure of the aptamer were helpful in obtaining a molecular model describing its global folding and flexibility. In spite of a large flexible aptamer, the kink angle between the **Ç**-labeled helices was found to be rather well-defined.

As for the bent DNA molecule, a two-step protocol was proposed to investigate the conformational flexibility. In the first step, a database with all the possible conformers was

created, using available restraints from NMR and distance restraints derived from PELDOR. In a second step, a weighted ensemble of these conformers fitting the multi-frequency PELDOR data was built. The uniqueness of the obtained structural ensemble was checked by validation against an independent PELDOR data set recorded at a higher magnetic field strength. In addition, the kink and twist angle pairs were determined and the resulting structural ensemble was compared with the conformational space deduced both from FRET experiments and from the structure determined by the NMR restraints alone.

Overall, this thesis underlines the potential of using PELDOR spectroscopy combined with rigid spin labels in the context of structure determination of nucleic acids in order to determine the relative orientation between two helices, the conformational flexibility and the conformational changes of nucleic acid molecules upon ligand binding.

List of abbreviations

A	adenine
C	cytosine
Ç	C-Spin
CW	continuous wave
cryo-EM	cryo-electron microscopy
DEER	double electron-electron resonance
DNA	deoxyribonucleic acid
EPR	electron paramagnetic resonance
ESR	electron spin resonance
FRET	Förster resonance energy transfer
G	guanine
HWHM	half width at half maximum
mRNA	messenger RNA
MD	molecular dynamics
MM	molecular modelling
NMR	nuclear magnetic resonance
NOE	nuclear Overhauser effect
PELDOR	pulsed electron-electron double resonance
PRE	paramagnetic relaxation enhancement
pre-mRNA	pre-messenger RNA
RDC	residual dipolar coupling
RNA	ribonucleic acid

rRNA	ribosomal RNA
SDSL	site-directed spin labeling
snRNA	small nuclear RNA
T	thymine
tRNA	transfer RNA
TPA	2,2,5,5-tetramethylpyrrolin-1-yloxy-3-acetylene
U	uracil

Symbols

x	scalar
$\vec{x}$	vector
$\hat{x}$	operator
$\vec{\hat{x}}$	vector operator
$\underline{x}$	tensor

Table of contents

1 Introduction

1.1 Methods for structure and ensemble determination - An overview

Structure and dynamics of nucleic acids have major relevance in the determination of the specific biological function, such as replication, transcription, and gene regulation.[1-2] Their knowledge is also important for a rational design of drugs in the pharmaceutical industry.[3-4] Since many nucleic acids and their complexes with proteins or small molecules are highly flexible in nature, the complete structural ensemble, consisting of a set of conformations and their statistical weight, needs to be considered. Several biochemical and biophysical techniques have been applied for the study of the structure and dynamics[5] of nucleic acid molecules, giving mechanistic insights into their function.

X-ray crystallography, a common method for the characterization of structures at atomic resolution, requires crystals of the biomolecule in good quality. The conformation of the biomolecule in the crystal might not necessarily represent a biologically active conformation. Moreover, flexible structures decrease the experimentally accessible resolution.

Nowadays a rapidly growing field is cryo-electron microscopy (cryo-EM), which serves as a structure determination tool with a resolution up to 2.2 Å without need for crystallization of the sample.[6] Since the cryo-EM data have to be collected from images of many particles to generate a three-dimensional density map reconstruction, the particles have to be preferably structurally homogenous to achieve high resolutions. Moreover, since cryo-EM is a single-particle technique, different functional states might be distinguished. Software can assign single-particle images, differentiate between different functional states, and sort them into subsets provided that there is a small number of functional states and large structural differences between the particles. In the case of continuous structural heterogeneity of the studied particles, cryo-EM might not be the method of choice.

Nuclear magnetic resonance spectroscopy (NMR) is a well-established method for elucidating the secondary structure, compact tertiary structures and the dynamical behavior of biomolecules with atomic resolution.[7-8] Among various NMR techniques, the most relevant ones for structure determination are based on the nuclear Overhauser effect (NOE), residual dipolar coupling (RDC) and paramagnetic relaxation enhancement (PRE). The

measurement of a large number of cross-relaxation effects between close-by protons provide distance restraints mapping the proton-proton distances throughout the studied biomolecule. However, considering the small magnetic moment of the nuclear spins and the decrease of the NOE signal intensity with the 6th power of the distance, distance restraints obtained by NOE-based NMR experiments are usually restricted to less than 6 Å. Thus, a global fold of deoxyribonucleic acid (DNA) or ribonucleic acid (RNA)[9-10] with flexible regions is hard to determine unambiguously, if the network of restraints is not well connected through space. In many cases, the complete tertiary structure and the conformational heterogeneity of oligonucleotides cannot be deduced from NOE-derived short-distance contacts between secondary structure motifs, such as stems, bulges, and hairpin loops. This task becomes even more difficult if the size of the molecule is above 50 kDa due to the increased complexity of the spectra and line broadening. Restraints from RDCs[11], namely orientational restraints between different segments of the nucleic acid structure, have proven to be helpful in order to get information about global structures and are of great interest for structure refinement, fold assessment and quaternary structure determination of proteins and nucleic acids in many NMR studies. RDC experiments need residual order in the molecular orientation, *e.g.* induced by addition of an alignment medium[11-12] or by paramagnetic labels or metal ions (paramagnetically induced RDCs). In addition, attaching paramagnetic labels into the nucleic acid molecule induces paramagnetic effects such as pseudocontact shifts[13] and PREs[14-15], which offer other NOE-independent sources of long-distance information.[16] When measuring paramagnetic effects, a diamagnetic reference sample is of crucial importance, hence increasing the number of required samples. Information on dynamic processes can be inferred from relaxation dispersion experiments.[17-18] However, even using these techniques the number of high quality structural data remains low for large, flexible nucleic acid molecules and their complexes due to resonance overlap, line broadening, and low proton density.

Förster resonance energy transfer (FRET) and electron paramagnetic resonance (EPR) spectroscopy, also called electron spin resonance (ESR), require site-specific labeling with reporter groups to gain information on the studied biomolecule. The distance between those labels have to be in the nanometer-range to detect conformational changes of the biomolecule. FRET measures the electric dipole-dipole interaction between two chromophores attached to nucleic acids, thereby detecting the distance between those labels. However, the size of the labels and their flexibility limits the accuracy of distance determinations.[19-20] Advantages of this technique are the possibility to perform

measurements at physiological temperatures and on a single molecule level.

Continuous wave (CW) EPR spectroscopy in combination with the incorporation of two spin labels at specific sites of the nucleic acid by site-directed spin labeling (SDSL) techniques, reports on the magnitude of the magnetic dipole-dipole interaction between the two paramagnetic centers, revealing distances up to 2 nm.[21-23] In contrast, pulsed magnetic dipolar spectroscopies, among which the pulsed electron-electron double resonance (PELDOR)[24-25] spectroscopy, also called double electron-electron resonance (DEER), and the double-quantum EPR, enable access to distances between the two paramagnetic centers in the nanometer-range, more specifically from 1.5 up to 10 nm, with no limitations on the size of the studied biomolecule. The magnetic dipole-dipole interaction between two spins depends on the interspin distance as well as on the angle between the interspin distance vector and the external magnetic field. The strength of the dipole-dipole interaction scales with the inverse cube of the interspin distance. In the presence of rigid spin labels, the orientational part of dependence provides the opportunity to determine the mutual orientation between the spin labels, thus giving considerably more structural information. Compared with the amount of sample used *e.g.* in NMR spectroscopy or for X-ray crystallography, EPR requires substantially smaller amounts. For both CW and pulsed methods freezing of the sample is needed.

Structural and biochemical experimental methods can be complemented by molecular modelling (MM) and molecular dynamics (MD) simulations, which provide the ability to model and simulate nucleic acid structures as well as their dynamics. MM covers the calculation and representation of realistic three-dimensional molecular structures and their physicochemical properties. The most common procedures are knowledge-based approaches and force field methods for obtaining the low energetic structure of a molecule. A force field is a mathematical expression which describes the energy of a system in dependence on the coordinates of its atoms. The parameterization of the energy function is derived empirically from a collection of experimental data as well as quantum mechanical calculations. In contrast, MD is a method that can be used to follow the dynamics of atoms, molecules and biomolecules with propagation of time under the influence of a force field using the classical equations of motion. The main limitations of MD, especially for the simulation of RNA molecules, are the short time scale of the simulation and the quality of the force field.[26] Since MD is a computational intensive method, only short physical time-scales, presently ranging from microseconds to milliseconds, are achievable. This limit can be partially overcome by enhanced-sampling techniques. However, even the most detailed and accurate models used

to parameterize force fields are still approximations of the actual interatomic interactions, hence they are not able to predict completely all the properties of the studied system. In this respect, finding a better working compromise by using experimental data from EPR spectroscopy is an ongoing effort in our research group.

1.2 Motivation, goal and tasks

As outlined in the previous section, for the distance measurements between a pair of spin labels attached to nucleic acids PELDOR spectroscopy is a valuable tool that is complementary to other methods in structural biology. If the rigid **Ç**-label (C-Spin), an analogue of 2'-deoxycytidine, is used for such kind of measurements, not only the distance but also the mutual orientation of the two **Ç**-labels can be determined by multi-frequency orientation-selective PELDOR data (X-, Q- and G-band frequencies). Thus, the information about the orientation of two **Ç**-labeled double-stranded helices in nucleic acids can be used as additional angular information for structure determination, where ideally the obtained structural ensemble should represent all the experimental PELDOR data unambiguously. Furthermore, since **Ç** does not have motion independent from the one of the helix where it resides, the conformational flexibility of helical motives in nucleic acid molecules is directly accessible. Revealing this kind of information is the major goal of this thesis. In combination with additional knowledge about the topology of the nucleic acid and/or restraints from other techniques, the structural ensembles of highly flexible DNA motifs, namely a bent DNA and a three-way junction cocaine aptamer, were characterized. For the first task, the conformational changes of the cocaine aptamer upon cocaine binding were investigated by analysis of the distance distributions between two **Ç**-labels. Further structural insights were obtained by investigating the relative orientation between the two spin-labeled helices of the cocaine-bound state of the aptamer. The second task of this thesis is the study of the conformational flexibility of a bent DNA molecule with a 5-adenine bulge in the center, for which structural data from NMR and FRET are available; this allows a quantitative comparison of the structural ensembles obtained from the different techniques.

2 Structural aspects of nucleic acids

This chapter gives a brief overview about structural and dynamical aspects of nucleic acid molecules, especially DNA. Additional information can be found in textbooks and review articles.[27-28]

Since 1953, when James Watson and Francis Crick described the molecular structure of the DNA helix using the X-ray diffraction data from Rosalind Franklin,[29] the determination of DNA and RNA three-dimensional structures has been an active research field.

DNA contains the genetic information, whereas RNA has a broad range of different kind of functions, *e.g.* carrier of the genetic information, catalyst of biochemical reactions, structural scaffold in ribosomes or regulator of gene expression by RNA elements, called riboswitches, together with a wide variety of complex folding including the double helical form. Riboswitches consist of two domains: a metabolite-binding or aptamer domain, which recognizes the cognate small molecule. The binding is signaled to an effector domain or expression platform. This platform interfaces with the transcriptional, translational or post-transcriptional RNA modification machinery to modulate gene expression. DNA is present in all living beings and DNA viruses. In eukaryotes most of the DNA is present in the nucleus where it is organized as chromosomes, with a small amount of DNA being present in the mitochondria. Plants and algae also have DNA in their chloroplasts. In prokaryotes the DNA is mostly circular and it resides in the cytoplasm of cells which are called plasmids. The main task of DNA is the storage of genetic information as well as the control and regulation of the protein biosynthesis. The flow of the genetic information can be represented as follows:

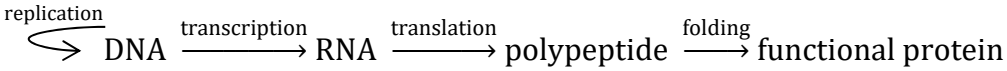

Protein biosynthesis is divided into transcription and translation. In the case of eukaryotes, the information in the DNA is first converted into the complementary base sequence of the pre-messenger RNA (pre-mRNA). This process, catalyzed by RNA polymerases, is referred to as transcription. Subsequently, the processing of the pre-mRNA follows, including the appending of the 5'cap structure, polyadenylation, RNA editing, and splicing. The messenger RNA (mRNA) is then transported into the cytoplasm outside of the nucleus and translated

into the amino acid sequence of the protein, where nucleotide triplets, called codons, encode the amino acids by means of the genetic code. This process is catalyzed by the ribosomes, which consist of a protein and a catalytically active ribosomal RNA (rRNA) moiety. At each step of the gene expression, regulatory proteins can bind to short specific DNA sequences and thus control temporally and locally the activation or suppression of the transcription of a specific DNA segment.

The duplication of the genetic information, called replication, is ensured by the production of two identical replica of the DNA during the interphase of the mitosis. The DNA is doubled by a semiconservative mechanism. The DNA double strands are separated by helicases. Next, a DNA polymerase adds new complementary nucleotides to each single strand of the DNA, which serves as template. Base mismatches may still occur due to incorrect replication. These mismatches are usually corrected by proofreading of the newly synthesized DNA strand. Nevertheless, the error rate of DNA replication is one to 10^{10} nucleotides.

Moreover, after replication the DNA structure can be damaged in different ways, for example by ultraviolet radiation or various chemical substances. Such damages can be characterized *e.g.* by base modifications, base loss or strand breaks. For this purpose, organisms have specific DNA repair mechanisms involving enzymes that register and repair damaged DNAs.

2.1 General structure of nucleic acid molecules

2.1.1 Building blocks of DNA and RNA

DNA and RNA are biopolymers and belong to the family of nucleic acids. They are built from monomers, called nucleotides. One nucleotide consists of a nitrogenous heterocyclic nucleobase (either a purine or a pyrimidine (*vide infra*)), a β-D-pentofuranose and a phosphate group. The individual nucleotides are linked to one another via 3'-5'-phosphodiester bonds (Figure 1), in which the sugar-phosphate backbone is negatively charged.

The DNA consists of two antiparallel strands, 5'→3' and 3'→5', which are held together by hydrogen bonding of the bases forming a double helix. There are four different nitrogen

heterocyclic bases in the DNA: adenine (A) and guanine (G), belonging to the bicyclic purine bases, and thymine (T) and cytosine (C), belonging to the monocyclic pyrimidine bases. In contrast, RNA has the pyrimidine base derivative, uracil (U), instead of T. Another important difference between DNA and RNA is the sugar moiety: RNA contains β-D-ribose, whereas DNA contains β-D-2-deoxyribose.

The structure of nucleic acids is subdivided into three levels: The primary structure describes the sequence of the nucleotides in the 5' → 3' direction (Figure 1A).

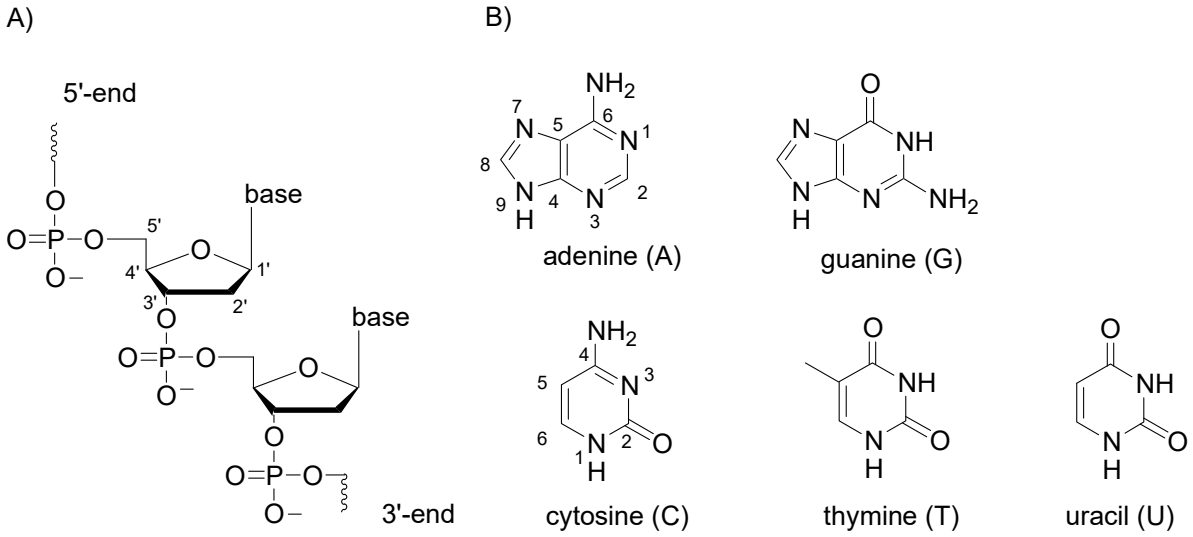

Figure 1: Chemical structure of building blocks of DNA and RNA. (A) Chemical structure of the deoxyribose-phosphodiester backbone (B) Chemical structure of the two purine and three pyrimidine bases in their prominent tautomeric mesomeric structure. Uracil is a base included in RNA. The purine bases are connected to the sugar-phosphate backbone at the N9 position and pyrimidine bases at the N1 position.

Secondary structure results if the complementary parts of two strands hybridize by base-pairing interactions to classical Watson-Crick base pairs (A=T and G≡C, Figure 2); non-complementary strands stay unpaired. In addition to the Watson-Crick base pairing, another common hydrogen bond pattern is the Hoogsten and Wooble (G=U) base pairing. Secondary structural elements are described in more detail in chapter 2.1.3.

Tertiary structure elements contain many interactions, such as Van der Waals contacts, specific hydrogen bonds and π-stacking, between different secondary structural elements defining the three-dimensional shape of the nucleic acid. Because of these interactions, regions of the secondary structure are kept spatially close. Two helices, two unpaired regions, or one unpaired region and a double-stranded helix (*e.g.* pseudoknots, kissing loops)

can be involved in those interactions, building a complex RNA tertiary structure.

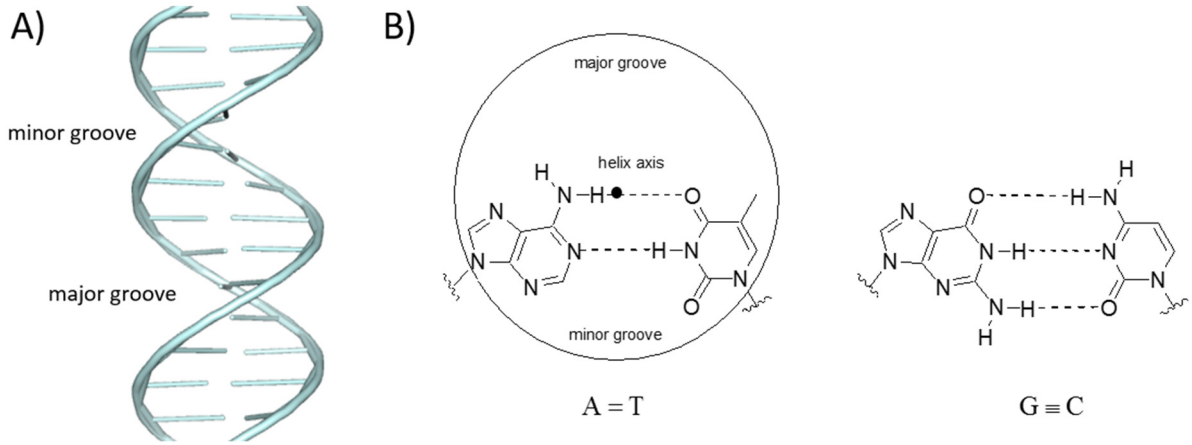

Figure 2: DNA structure and Watson-Crick base pair. (A) B-DNA double helix with major and minor groove. (B) Classical Watson-Crick base pair in DNA: A=T and G≡C. Each base pair has a more open side, which describes the major groove and a smaller defining the minor groove.

2.1.2 A-, B- and Z-DNA

The DNA double helix is primarily stabilized by hydrogen bonds between nucleotides of the opposite strand and by π-interactions among stacking bases. Depending on the polarity and salt content of the solvent and on the DNA base sequence, the DNA double helix can be present in three major conformations: A-, B- (Figure 2A) and Z-DNA (Table 1). The most common form under physiological conditions is the B-DNA, which was first described by Watson and Crick in 1953.[29] The DNA double helix prefers the A-form at low polarity of the solvent, and if the relative humidity is reduced to less than 75%. A-like conformations are found in double-stranded regions in RNA and RNA-DNA hybrids. For short oligonucleotides with an alternating sequence of pyrimidine and purine bases, the less common Z-form of the DNA double helix is found. Here, the phosphate groups in the backbone are arranged in a zigzag shape. In this case, a very high salt content is necessary in order to minimize electrostatic repulsions between the negatively charged phosphate groups of the backbone, which are spatially closer than in the A- and B-forms. In addition, the Z-DNA differs in its chirality from the A- and B-form. The biological relevance of Z-DNA is not fully understood; it shows, however, that the DNA is a flexible, very easily

deformable, dynamic molecule. This can also be observed in the case of transitions between the individual conformations upon changing the ambient conditions.

Table 1: Selected helical parameters to compare A-, B- and Z-DNA.[30-31]

Helix form	A-DNA	B-DNA	Z-DNA
Chirality of the helix	right-handed	right-handed	left-handed
Rise per base pair (nm)	0.25	0.34	0.37
Helix diameter (nm)	2.55	2.37	1.84
Glycosyl bond conformation	anti	anti	alternating syn (Purin bases)/ anti (pyrimi-dine bases)
Base pairs per helix turn	11	10	12
Base tilt (°)	20	-6	-7
Pitch height (nm)	2.53	3.54	4.56
Major groove	Tight and very deep	Broad and deep	flat
Minor groove	Very broad and flat	Tight and deep	Very tight and deep
Sugar pucker conformation	C3‘-endo	C2-endo	Pyrimidine bases: C2'-endo Purin bases: C3'-endo

2.1.3 Secondary structural elements of nucleic acids

Commonly occurring secondary structural elements, namely double-stranded regions, also referred to as stems or helices, single-stranded regions, mismatches, hairpins, junctions, loops and bulges (a special case of an internal loop) are summarized in Figure 3. They can be found especially in RNA. Such secondary structural elements have important functions, for example in the regulation of transcription, whereby they can serve as primers or as the catalytically active component of ribosomes in the form of rRNA.

Hairpin loops consist of a single strand, usually with a palindromic nucleotide sequence, which folds back on itself and forms a double helix bridged by a sequence of unpaired nucleotides. They are integrated *e.g.* in the cloverleaf structure of transfer RNAs (tRNAs). In an internal loop at least one nucleotide in both strands is unpaired between two paired regions.

In contrast to internal loops, where each strand has an interrupted base sequence, double strands with unpaired bases on only one of the two strands are structural motifs called bulges which induce a sharp kink into the helix axis, up to L-shaped molecules in extreme cases. The other strand has an uninterrupted base sequence. Bulges are an important factor as a structural element of nucleic acids for specific protein recognition. Bulges in DNA are possibly generated during recombination between imperfect homologous DNA sequences or by errors during the DNA replication.

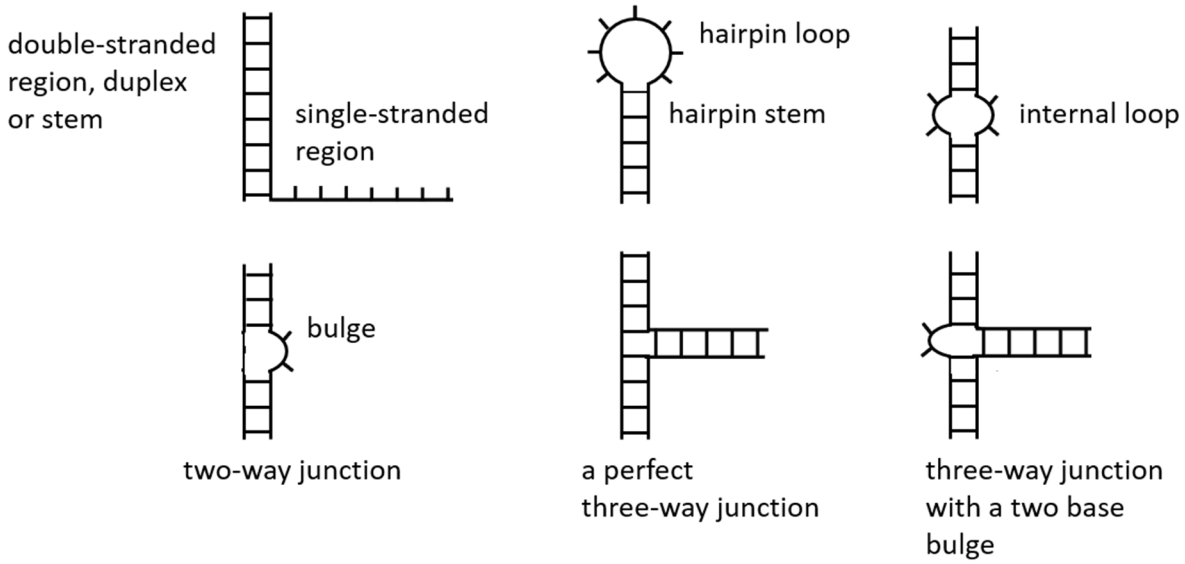

Figure 3: Schematic representation of secondary structural elements of nucleic acids.

Helical junctions are defined as branchpoints within the nucleic acid with axial interruptions, such that strands are exchanged between the different helical parts leading to more complex structures. A bulge is a special kind of a junction, namely a two-way junction. Junctions occur in DNA as well as in RNA. In DNA, four-way junctions serve as key intermediates in homologous and site-specific recombination processes, whereas in RNA junctions have a key architectural role in the organization of the tertiary structure. A known example for a DNA junction is the Holliday junction, a key intermediate during recombination, consisting of four helical sections.[32] Three- and four-way junctions are present in many functional

RNA, *e.g.* small nuclear RNA (snRNA), the hepatitis C virus internal ribosome entry site or the hammerhead ribozyme.[33-34] This latter can be considered as an imperfect three-way junction.

Two general folding possibilities can be considered in the context of branched nucleic acid molecules: on the one hand, due to the highly favorable energetic contributions of π-stacking interactions between the nucleobases to the overall stability of oligonucleotide structure, pairwise coaxial stacking of helical regions is enthalpically the most preferred folding principle. In this way, the RNA can achieve higher order organization. For example, four-way junctions have a strong preference for helix-helix stacking. On the other hand, since nucleic acids are highly negatively charged polyelectrolytes, metal ions can have huge influence in their folding (ion-induced folding principle). Without metal ions, the DNA four-way junction (but not the RNA four-way junction) is completely extended with no coaxial stacking of the four helices. In contrast, in the presence of metal ions the stacked X-shape of the four-way junction is stabilized due to charge neutralization of the DNA backbone.

In general, junctions can be perfectly paired or they can include mismatches or unpaired nucleotides. This is expected to have large influence to their conformation, especially in the case of three-way junctions. This kind of junction can assume different shapes depending on the local base sequence at the junction.[28] When the nucleobases at such junctions are perfectly paired, the three-way junction is a Y-shaped molecule without any coaxial helix stacking. This was originally shown by gel electrophoretic studies[35] and later confirmed by FRET experiments[36] and atomic force microscopy.[37] In general, the typical behavior of helices at three-way junctions is to be stacked. The Y-shaped junction does not follow any of the general folding principles.[28] However, the junction enables coaxial stacking of two helices to form a T-shaped molecule, by introducing additional conformational flexibility at the junction, such as unpaired nucleotides, sometimes along with a Y-shaped conformation, as determined by NMR spectroscopy.[28, 38-39] This is also the case for the cocaine aptamer, whose conformational changes upon cocaine binding are studied in this PhD thesis.

3 Spin labels for nucleic acid molecules

The investigation of the structure and conformational dynamics of biomolecules, which are usually diamagnetic, by EPR spectroscopy requires the incorporation of paramagnetic centers, called spin labels, at specific sites. The most common used spin labels are aminoxyl radicals, in the following referred to as nitroxides, which are chemically stable radicals under most of the biologically relevant conditions and can easily be modified by organic chemistry. A technique, referred to as SDSL, allows the site specific attachment of nitroxides to nucleic acids.

This chapter contains a small selection of different types of nitroxide spin labels used to study the structure and the (conformational) dynamics of nucleic acids. While this chapter focuses exclusively on the use of nitroxide spin labels, it should be also noted that a number of metal ions (*e.g.*, Mn^{2+}) are EPR active and have been used as spin labels for studying RNA.[40] A deeper discussion on synthetic details and further nitroxide spin labels can be found in several review articles.[41-42]

3.1 Site-directed spin labeling of nucleic acids

For SDSL at internal sites of nucleic acids several methods have been developed, both to introduce nitroxide spin labels at the sugar[43]-phosphate[44] backbone or at the nucleobase[45-46] (Figure 4). In total, there are three spin labeling strategies:

(1) The labeling of nucleic acids is done during its synthesis by automated chemical synthesis on a solid phase using modified phosphoramidites. This stepwise synthesis allows for the incorporation of modified nucleotides, containing a nitroxide radical, at chosen positions in the nucleic acid sequence.[45]

(2) Post-synthetic spin labeling refers to the incorporation of spin labels into the nucleic acid after their synthesis, either by chemical or enzymatic methods. Thereby, a reactive functional group has to be included at a specific site during the nucleic acid synthesis, which then reacts with a spin labeling reagent. This strategy is limited to attachments to specific sites since it requires chemically modified nucleotides. The tether that connects the spin label with the modified nucleotide is usually rather flexible. Moreover, incomplete labeling may require

purification from the non-labeled material, which may be nontrivial.
(3) Another strategy is non-covalent spin labeling[47] in which the intercalating spin label needs to bind non-covalently to an abasic site on the nucleic acid.

3.2 Internal motion of spin labels – An overview

Depending on the flexibility of the tether, the labeling position within the nucleic acid and the spin labeling strategy, the spin labels can have different characteristic internal motions: from rather flexible, *via* semi-flexible towards completely rigid spin labels, these latter giving additional angular information.
Translating measured interspin distances into structural information requires the knowledge of the internal motion of the spin labels in addition to the flexibility of the nucleic acid. Especially, if the tether is rather flexible (Figure 4, structure **1** and **2**) or semi-flexible the attached spin labels can move independently of the nucleic acid. Thus, the labels cannot directly report on the actual dynamics of the nucleic acid since both the internal motion of the spin labels and the nucleic acid flexibility contribute to the detected EPR signal. The degree of spin label flexibility can diminish the accuracy of EPR-based distance measurements and thus the determination of nucleic acid motions.
An example of a fairly rigid spin label is the five-membered ring nitroxide spin label 2,2,5,5-tetramethylpyrrolin-1-yloxy-3-acetylene (TPA, Figure 4, structure **3**), which provides well-defined distances for structural information on nucleic acid molecules. Hopkins and coworkers were the first that reported SDSL of nucleic acids *via* the TPA spin label by automated chemical synthesis of oligonucleotides and phosphoramidite chemistry.[45] Engels and coworkers incorporated the TPA-containing pyrimidine nucleosides, where the C2 position had been functionalized, into both DNA[48-49] and RNA[50] using a slightly different strategy. The same authors reported as well an adenosine derivative carrying the TPA at the position C2 for spin labeling of RNA. The short, semi-rigid acetylene bridge linker between the base and the nitroxide restricts the motion of the attached nitroxide relative to the nucleic acid, allowing the determination of accurate distances.[48-52] The TPA spin label projects into the major groove of the DNA helix, thus minimizing its influence on the native structure.
Gannett and coworkers designed a TPA spin label analogue (4-ethynyl-2,2,6,6-tetramethyl-3,4-dehydro-piperidine-1-oxyl nitroxide) (Figure 4, structure **4**) with a six-membered ring

nitroxide.[53] With respect to TPA the rotation of the single bonds on both sides of the acetylene triple bond does not displace the nitroxide group relative to the nucleobase, since these single bonds are on the same axis as the N–O bond of the nitroxide. This leads to more accurate distance measurements and narrower distance distributions between two labels using PELDOR spectroscopy.[53-55]

Sigurdsson and coworkers recently presented a new class of semi-rigid isoindoline-derived spin labels covalently attached to double-stranded DNA molecules linked by a single bond to a uridine (Figure 4, structure **5** and **6**).[56] Compared to the **Ç-**label (Figure 5, *vide infra*), their synthetic preparation is much easier. All semi-rigid isoindoline spin labels show some internal motion in addition to the mobility of the double-stranded DNA molecule itself, in contrast to the completely rigid spin label **Ç**. Quantitative simulation could separate between the conformational dynamics of the nucleic acid and of the spin label by explicitly taking into account the spin label dynamics.[57] The conformationally unambiguous ^{ExIm}U spin label (Figure 4, structure **6**) is designed to have a free rotation around a single bond flanking the acetylene group, which averages out orientation effects.[58] However, the rotation has no effect on the distance distribution since the N–O bond of the nitroxide and this single bond are aligned on the same axis. Thus, the ^{ExIm}U spin label enables direct and accurate distance measurements. In contrast to the ^{ExIm}U spin label, the semi-rigid spin labels ^{Im}U and ^{Ox}U (Figure 4, structure **5**) show restricted motion around the single bond linking them to the nucleobase.[56] The ^{Im}U spin label forms furthermore an intramolecular hydrogen bond between the NH of the benzimidazole and the O4 of the nucleobase (uracil). The authors reported that the ^{Im}U and ^{Ox}U spin labels show clearly visible orientation behavior in the orientation-selective PELDOR measurements with minimal intrinsic motion.

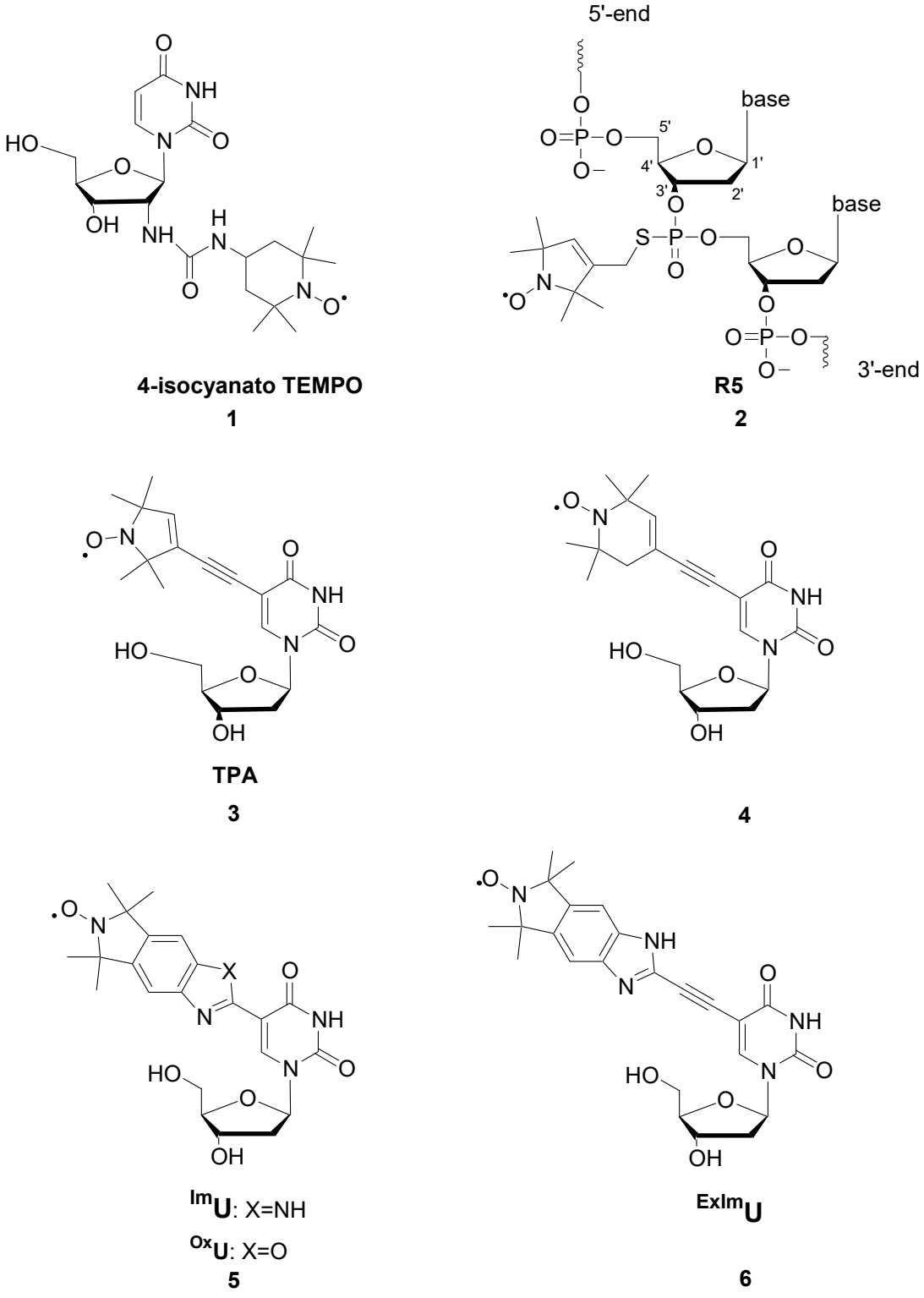

Figure 4: Examples of different nitroxide spin labels. Nitroxides that have been conjugated to the 2'-position of sugar (**1**[43]), and to the phosphate backbone of nucleic acids (**2**[44]). Pyrimidine nucleosides that contain spin labels at their 5-positions (**3**[45], **4**[53], **5**[56], **6**[56]). The rigid **Ç**-label is presented in Figure 5.

3.3 The rigid Ç-label

For the precision of the obtained distances between the spin labels, one has to take into account the inherent mobility of the spin labels for the interpretation of the PELDOR measurements. To overcome this drawback, the rigid **Ç**-label ('C-spin') was developed. Here, the nitroxide spin label is fused to the nucleobase via a heterocyclic six-membered ring, thus minimizing the motion of the spin label that is independent of the base. The spin label **Ç**, a 2'-deoxycytidine-analogue,[59-61] is designed, synthesized and incorporated into the nucleic acid by the group of Prof. Dr. Sigurdsson from the University of Island. The design was inspired by the spin-labeled nucleoside **Q** from the group of Hopkins which is base paired with the non-natural 2-aminopurine base.[62-63] **Ç** forms a Watson-Crick base pair with guanine (G) (**Ç**: X = H, Y = H in Figure 5) and stacks on the neighboring bases, thereby fixing its orientation within the DNA stem pointing into the major groove of the DNA duplex, thus the influence of **Ç** on the native structure is reduced to an minimum.[64]

The synthesis of **Ç** and the incorporation into DNA is described previously by automated chemical synthesis, using the phosphoramidite derivative of **Ç**.[59, 61] It should be also mentioned that Sigurdsson and coworkers showed noncovalent labeling of **Ç** to an abasic site in a DNA duplex which binds through hydrogen bonding with guanine and π-stacking with neighboring bases.[65]

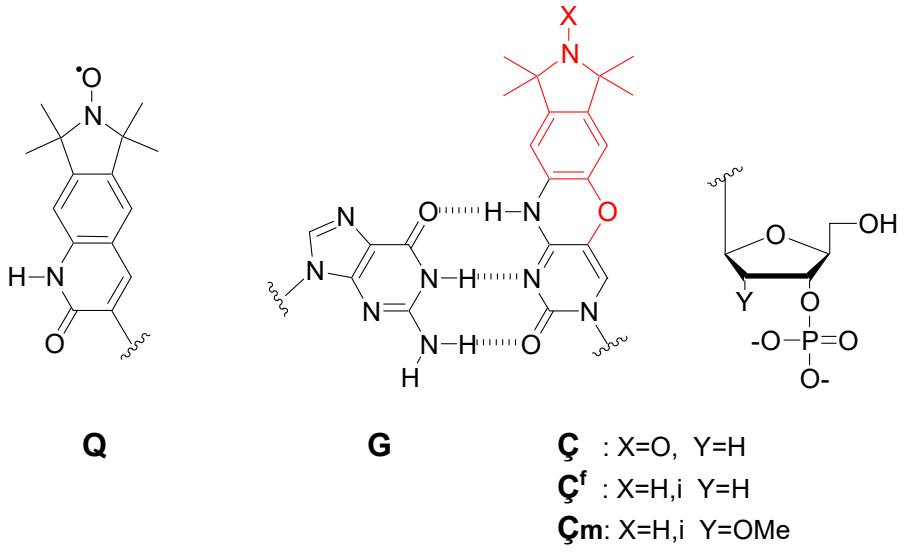

Figure 5: The rigid spin label Ç. Spin label **Q**[62-63] and spin label **Ç**[59-61], an analogue of 2'-deoxycytidine (modification in red), base-paired to guanine. **Ç**[f66-67] fluorescent probe and **Çm**[68-69] the RNA analogue of **Ç**.

The rigid **Ç**-label has two major advantages compared to previously reported spin labels for nucleic acids described in the literature, which leads to extended applications in contrast to flexible spin labels.

Firstly, the spin label itself introduces almost no additional flexibility (negligibly small compared to the DNA motion). Therefore, the application of PELDOR spectroscopy using this kind of spin label gives more accurate distances between the two labels compared to nitroxide spin labels with flexible tethers. Recently, PELDOR spectroscopy using the rigid **Ç**-label showed that small conformational changes can be observed, thereby differentiating between different dynamic models describing the stretching, twisting and bending of a double-stranded DNA.[70] The limited spin label mobility within a DNA duplex enables studying the conformational flexibility of highly flexible or partially disordered nucleic acid molecules directly, without need to consider any conformational flexibility of the spin label. Secondly, two labels fixed in space are expected to enable the determination of the relative orientation between the two spin labels in addition to the distance by PELDOR spectroscopy studies. This additional angular information of the rigid spin label strongly reduces the total number of required spin-labeled samples for determining the structure of the nucleic acid and directly relates to more detailed structural information on the DNA molecule itself. Recently, it has been shown that **Ç** enables the determination of the structure and conformational flexibility of double-stranded DNA molecules with high accuracy.[70-72] Specifically, the relative orientation of the two **Ç**-labels could be deduced by orientation-selective PELDOR measurements at X- and G-band frequency (9 GHz/0.3 T and 180 GHz/6.4 T, respectively).

The design of this spin label, an analogue of the base cytidine, allows the determination of the relative orientation of two **Ç**-labels, which are rigidly incorporated in different helices of the nucleic acid. Since each spin label is fixed in its orientation with respect to the helix where it resides, the relative orientation and the conformational flexibility of double-stranded helical motives in nucleic acids can be determined and modelled. This is the main topic discussed in this thesis.

The RNA analogue of **Ç**, called 2′-O-methylribonucleoside **Çm** (X = H, Y = OMe in Figure 5), is applicable for EPR studies to elucidate structural and dynamical aspects of folded RNA molecules.[68] Circular dichroism (CD) spectroscopy and melting experiments reveal that **Çm** is well tolerated in an A-form RNA helix like the **Ç**-label in a B-form DNA helix. A decrease in the melting temperature compared to the non-labeled RNA indicates that the 2′-OMe group stabilizes the overall structure of the **Çm**-modified RNA. It was reported

that PELDOR experiments with RNA samples containing two **Çm-**labels have the potential to report angular correlations in terms of a biradical structure.[69]

Upon reduction of the nitroxide spin label **Ç** to the corresponding hydroxyl amine, another important property of this spin label arises: it becomes fluorescent and thereby opening the opportunity for structural studies of nucleic acids by both EPR and fluorescence spectroscopy. This fluorescent probe (X = H, Y = H in Figure 5), called **Ç^{f}**, quenches the fluorescence upon base pairing.[66] **Ç^{f}** clearly differentiates between different base pairing partners in duplex DNA with significant fluorescence intensity, thereby detecting single-base mismatches.[67] Furthermore, the bispectroscopic activity of the spin label enables the preparation of nucleic acids that contain a redox-active sensor, since after oxidation to **Ç** fluorescence is quenched. The group of Prof. Dr. Wachtveitl is currently investigating further fluorescence properties of **Ç^{f}**.

4 Theoretical basics of PELDOR spectroscopy

Paramagnetic species, like radicals or transition metal ions, can be studied by EPR spectroscopy. For that, the macroscopic magnetization of a sample is manipulated in the presence of a microwave irradiation perpendicular to the direction of an applied external magnetic field. Electrons and several nuclei have a spin, which enables the study of their mutual interactions and their interactions with the magnetic field by dipolar or hyperfine spectroscopy. The following chapter introduces the basics for the interpretation of PELDOR experiments. It gives an overview about spin interactions which underlie the interpretation of EPR spectra on the basis of standard textbooks.[73-74]

4.1 The electron spin

Stern and Gerlach conducted one of the fundamental experiments of today's physics at the University of Frankfurt in 1922.[75-76] They found that the electron magnetic moment is only allowed to take discrete orientations either parallel or antiparallel with respect to an applied static magnetic field.[77] Three years later, Goudsmit and Uhlenbeck interpreted this result quantum mechanically: The electron has an intrinsic angular momentum, the so-called electron spin. Every particle with a spin angular momentum, a mass and a charge has an intrinsic magnetic moment. For a free electron, the corresponding vector operator $\hat{\vec{\mu}}_e$ is

$$\hat{\vec{\mu}}_e = -g_e \mu_B \hat{\vec{S}} = \hbar \gamma_e \hat{\vec{S}} \qquad \textbf{eq. 1}$$

with the electron spin vector operator $\hat{\vec{S}}$, $\mu_B = 9{,}274015 \cdot 10^{-24}\,\mathrm{Am^2}$ is the Bohr magneton, $\hbar$ is the reduced Planck constant, $\gamma_e = 1.760859644 \cdot 10^{-21}\,\mathrm{rad{\cdot}s^{-1}{\cdot}T^{-1}}$ the gyromagnetic ratio and $g_e = 2.00231930436182$ accounts for the g-factor of the free electron.

4.2 The spin Hamilton operator

The complete spin Hamilton operator $\widehat{H}$, which was introduced by Abragam und Pryce in 1951, allows the characterization and interpretation of EPR spectra.[78] For a system of two $S = 1/2$ (electron spin magnetic quantum numbers $m_s = \pm 1/2$) electrons A and B, each coupled to a ^{14}N-nucleus ($I(^{14}\mathrm{N}) = 1$ (nuclear spin magnetic quantum numbers $m_I = \pm 1, 0$) $\widehat{H}$ has the following terms

$$\widehat{H} = \underbrace{\mu_B \cdot \vec{\hat{S}}_A \cdot \underline{g}_A \cdot \vec{B} + \mu_B \cdot \vec{\hat{S}}_B \cdot \underline{g}_B \cdot \vec{B}}_{\widehat{H}_{EZ}} \underbrace{-g_{IA} \cdot \mu_I \cdot \vec{B} \cdot \vec{\hat{I}}_A - g_{IB} \cdot \mu_I \cdot \vec{B} \cdot \vec{\hat{I}}_B}_{\widehat{H}_{NZ}} \quad \textbf{eq. 2}$$

$$\underbrace{+\vec{\hat{S}}_A \cdot \underline{A}_A \cdot \vec{\hat{I}}_A + \vec{\hat{S}}_B \cdot \underline{A}_B \cdot \vec{\hat{I}}_B}_{\widehat{H}_{HF}} + \underbrace{\vec{\hat{S}}_A \cdot \underline{D} \cdot \vec{\hat{S}}_B}_{\widehat{H}_{dip}}$$

where $\vec{\hat{S}}_A$, $\vec{\hat{S}}_B$ are the electron spin vector operators and $\vec{\hat{I}}_A$, $\vec{\hat{I}}_B$ are the nuclear spin vector operators. The nuclear Zeeman interaction has been considered to be isotropic and the nuclear quadrupole interaction, present for systems with nuclear spin $I > 1/2$, has been omitted. In the course of the chapter the terms of $\widehat{H}$ (eq. 2), especially the electron dipole-dipole interaction, will be described.

The e**lectron Zeeman interaction** describes the interaction of the electron magnetic moment with the external magnetic field $\vec{B}$ For a two-electron spin system the electron-Zeeman Hamiltonian operator $\widehat{H}_{EZ}$ is

$$\widehat{H}_{EZ} = \mu_B \cdot \vec{\hat{S}}_A \cdot \underline{g}_A \cdot \vec{B} + \mu_B \cdot \vec{\hat{S}}_B \cdot \underline{g}_B \cdot \vec{B} \quad \textbf{eq. 3}$$

$\underline{g}_A$ and $\underline{g}_B$ are the g-tensors for electrons A and B. Deviations of the g-tensor from the free electron g-factor are the result of spin-orbit coupling with the orbital angular momentum from excited states.

If the molecule tumbles fast compared to the anisotropy of the magnetic interactions (fast motion regime, namely rotational correlation time <10 ps for nitroxides at X-band frequencies), only the isotropic part of the electron Zeeman interaction needs to be

considered. The isotropic part of the g-tensor is given by one third of the trace of the matrix

$$g_{iso} = \frac{1}{3}(g_{xx} + g_{yy} + g_{zz}) = \frac{1}{3}Tr\left(\underline{g}\right) \qquad \textbf{eq. 4}$$

This value can be experimentally obtained using *e.g.* room-temperature CW-EPR spectroscopy at X-band frequencies.

The g-tensor expressed in its principal axes system (PAS), which is a molecule-fixed frame, is represented as a diagonal matrix.

$$\underline{g}_{\mathrm{PAS}} = \begin{pmatrix} g_{xx} & 0 & 0 \\ 0 & g_{yy} & 0 \\ 0 & 0 & g_{zz} \end{pmatrix}$$

$\underline{g}_{\mathrm{PAS}}$ contains the principal values g_{xx}, g_{yy} and g_{zz}. The geometric interpretation of the g-tensor is an ellipsoid where the effective g-factor g_{eff} for an arbitrary orientation of the magnetic field is the distance from the origin to the surface of the ellipsoid. For a given orientation of the external magnetic field $\vec{B}$ the electron Zeeman interaction can be described by means of the effective g-factor, which is given by[73]

$$g_{eff}(\Theta, \varphi) = \sqrt{(g_{xx}\cos\varphi\, sin\Theta)^2 + \left(g_{yy}\sin\varphi\sin\Theta\right)^2 + (g_{zz}\cos\Theta)^2} \qquad \textbf{eq. 5}$$

g_{eff} is symmetric with respect to the origin of the coordinate system: $g_{eff}(\Theta, \varphi) = g_{eff}(\pi - \Theta, \pi + \varphi)$.

With higher magnetic fields (for nitroxides at least 3.4 T, *vide infra*) the differences in the magnetic field positions between the three principle values of the g-tensor increase, which usually leads to better resolved EPR spectra and therefore enables the determination of the principle values.

The second term, the **nuclear Zeeman interaction**, represents the interaction of the nuclear spins with the external magnetic field.

$$\hat{H}_{NZ} = -g_{IA} \cdot \mu_I \cdot \vec{B} \cdot \hat{\vec{I}}_A - g_{IB} \cdot \mu_I \cdot \vec{B} \cdot \hat{\vec{I}}_B \qquad \textbf{eq. 6}$$

with the nuclear angular momentum $\vec{\mu}_I = g_I \cdot \mu_I \cdot \hat{\vec{I}}$, where μ_I is the nuclear magneton and

g_I the nuclear g-factor.

The **hyperfine interaction**, described by the hyperfine coupling tensor $\underline{A}_A$ and $\underline{A}_B$, represents the interaction between the electron spin and the neighboring nuclear spins.

$$\hat{H}_{HF} = \vec{\hat{S}}_A \cdot \underline{A}_A \cdot \vec{\hat{I}}_A + \vec{\hat{S}}_B \cdot \underline{A}_B \cdot \vec{\hat{I}}_B \qquad \textbf{eq. 7}$$

The hyperfine interaction can be divided into an isotropic and a purely anisotropic part. The isotropic part is due to the electron density at the nucleus. The electrons in s-orbitals have a non-zero probability density at the nucleus ($|\Psi_0(r=0)|^2 > 0$) and give rise to Fermi contact interactions. The Fermi contact interaction is completely isotropic and is given by

$$\hat{H}_{HF,iso} = a_{iso,A} \cdot \vec{\hat{S}}_A \cdot \vec{\hat{I}}_A + a_{iso,B} \cdot \vec{\hat{S}}_B \cdot \vec{\hat{I}}_B \qquad \textbf{eq. 8}$$

with the isotropic hyperfine coupling constant $a_{iso} = \frac{2\mu_0}{3h} g_e \mu_B g_N \mu_N |\psi_0(r=0)|^2$ in frequency units (MHz).

The anisotropic part, the electron nuclear magnetic dipole-dipole coupling is described by

$$\hat{H}_{HF,dip} = \vec{\hat{S}}_A \cdot \underline{T}_A \cdot \vec{\hat{I}}_A + \vec{\hat{S}}_B \cdot \underline{T}_B \cdot \vec{\hat{I}}_B \qquad \textbf{eq. 9}$$

where $\underline{T}_A$ and $\underline{T}_B$ are the symmetric and traceless electron-nuclear spin dipolar coupling tensors.

The effective value of the hyperfine coupling is given by

$$A_{eff} = \sqrt{(A_{xx}\cos\varphi\, sin\Theta)^2 + \left(A_{yy}\sin\varphi\sin\Theta\right)^2 + (A_{zz}\cos\Theta)^2} \qquad \textbf{eq. 10}$$

The influence of the above-mentioned interactions will be explained on the shape of a CW-EPR spectrum for a nitroxide radical. Figure 6A shows the corresponding energy level diagram. The energy of the spin sublevels are defined as the eigenvalues of the spin Hamiltonian operator. Upon irradiation, the spins can flip if the quantum $h\nu$ matches the energy difference ΔE between the energy levels. Such a resonance transition has to fulfill the selection rules $\Delta m_s = \pm 1$ and $\Delta m_I = 0$. The corresponding characteristic EPR spectrum

for nitroxide radicals in the fast motion regime consists of three lines with a separation by the isotropic hyperfine coupling constant a_{iso} of about 47 MHz. The resonance position of the central line $|m_I\rangle = |0\rangle$ at X-band frequencies is defined by the isotropic g-factor g_{iso} of about 2.0057 (Figure 6B).[79] Typical anisotropic values for the g- and the A-tensor for the nitroxide TEMPONE are $g_{xx} = 2.0088, g_{yy} = 2.0061, g_{zz} = 2.0027, A_{xx} = 5.8$ G, $A_{yy} = 5.8$ G, $A_{zz} = 30.8$ G, where the principal axes of the two tensors are collinear.[80]

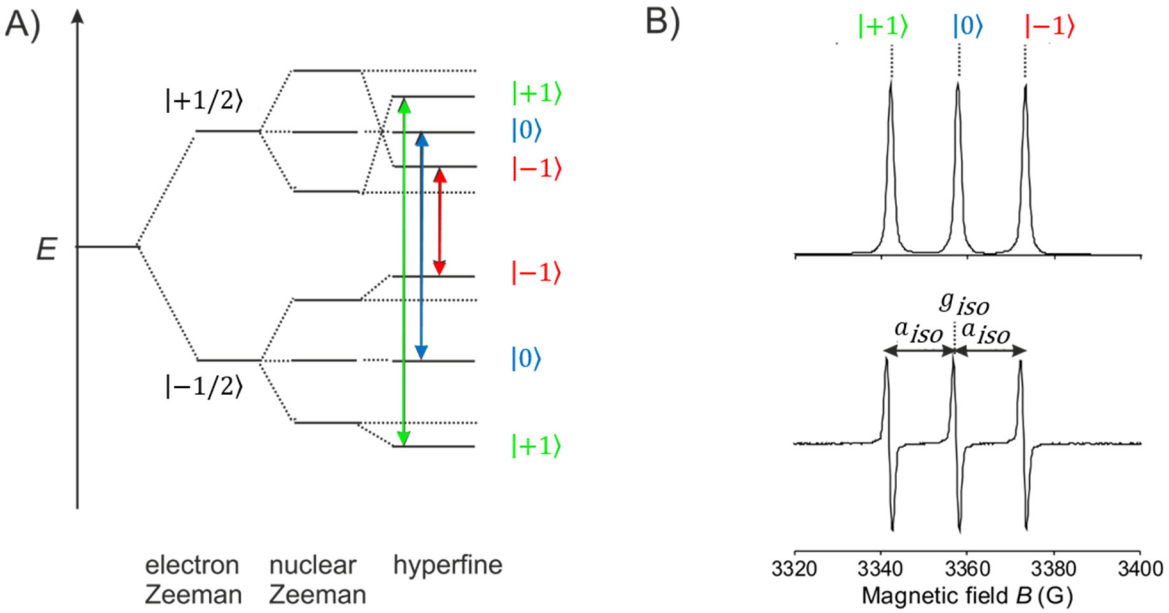

Figure 6: Energy level diagram and isotropic CW-EPR spectra of a nitroxide radical. (A) Energy level diagram in a fixed magnetic field of a nitroxide radical with S = ½ and I(14N) = 1. The electron and the nuclear Zeeman levels and the hyperfine splitting and corresponding resonance transitions for the nitrogen nuclear spin states $|m_I\rangle$, ($|+1\rangle$ (green), $|0\rangle$ (blue) and $|-1\rangle$ (red)) are shown. (B) Isotropic nitroxide CW-EPR spectra of TEMPO at room temperature (top) at X-band frequencies and the first derivative (bottom) with the isotropic g-factor g_{iso} and the isotropic hyperfine coupling constant a_{iso}.

The EPR spectra of immobilized systems in amorphous samples (frozen solution) are generally broader and the interplay of the g- and hyperfine anisotropies leads to more complicated EPR spectra, usually referred to as 'powder spectra'. The solid-state spectrum at X-band frequencies is dominated by a strong ^{14}N-hyperfine interaction of the unpaired electron with the ^{14}N-nucleus. The width of the nitroxide spectrum can be approximately described by $2A_{zz}$. The x- and y-components of the hyperfine coupling tensors, A_{xx} and A_{yy}, and the principle values of the g-tensor are unresolved within the inhomogeneous linewidth of the central peak (Figure 7A). With increasing magnetic field strength the components of the g-tensor get partially resolved (Figure 7B). At a microwave frequency of 95 GHz (W-

band frequencies) and above the three principal values of the g-tensor are resolved and dominate the width of the nitroxide EPR spectrum (Figure 7C. The field-swept powder absorption EPR spectrum at G-band frequencies is shown).

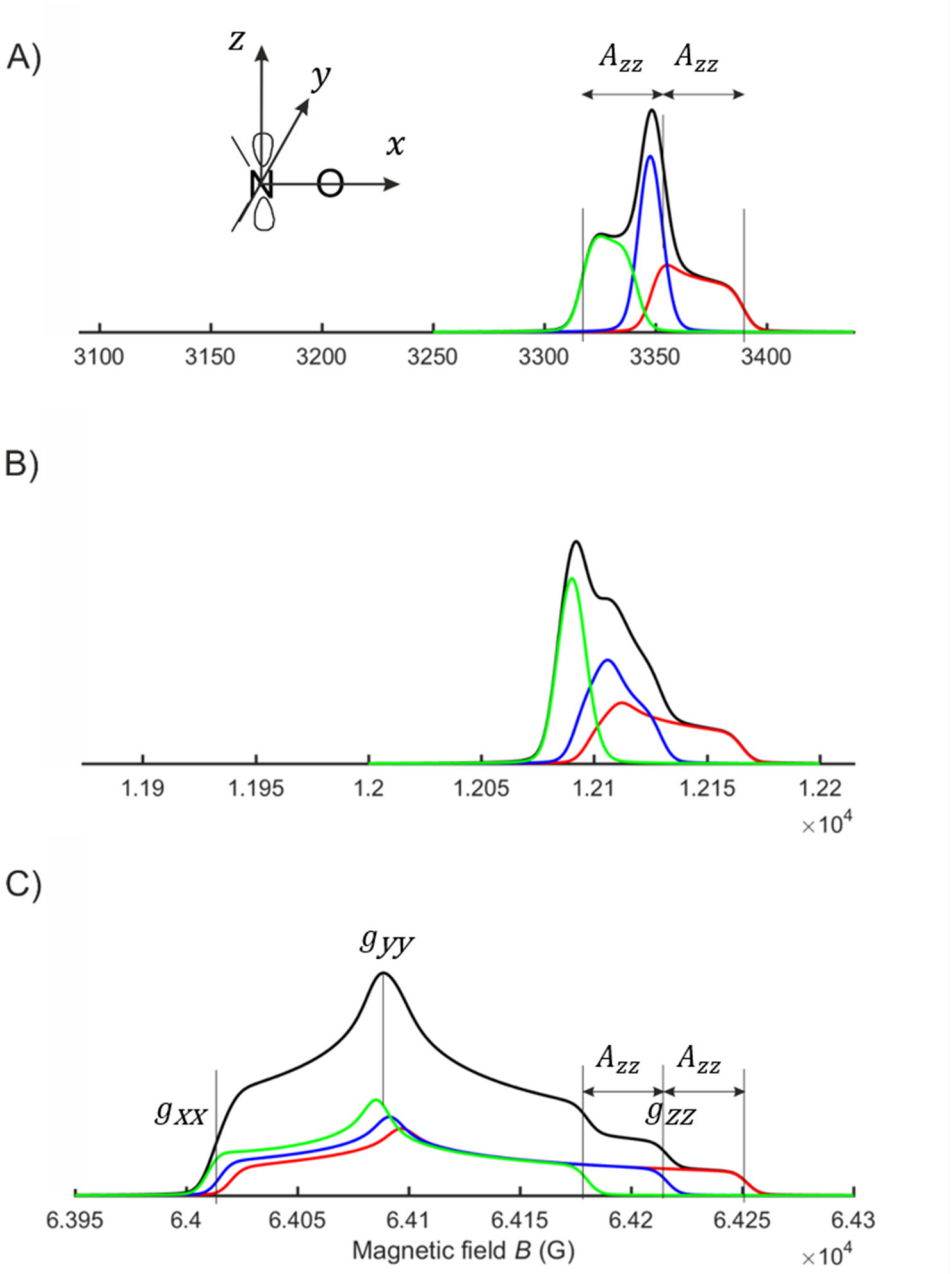

Figure 7: Field-swept powder absorption nitroxide EPR spectra at different frequencies and magnetic field strengths (black). (A) The EPR spectra were recorded at X-band (9 GHz/0.3 T), (B) at Q-band (33.6 GHz/1.2 T) and (C) at G-band (180 GHz/6.4 T) frequencies. The resonance transitions for the nuclear spin magnetic quantum numbers $|+1\rangle$ (green), $|0\rangle$ (blue) and $|-1\rangle$ (red) are highlighted. The definition of the nitroxide molecular frame and p_z-orbital is given in the inset. The x-axis is parallel to the N-O bond and the z-axis is oriented perpendicular to the nitroxide plane. The y-axis is the cross product of x and z.

The **electron-electron interaction** accounts for the interaction between the two electron spin magnetic dipole moments. This interaction has two components: the exchange interaction *J,* depending on the overlap between the orbitals, and the electron dipole-dipole interaction D. This latter interaction is purely anisotropic. For the studied nucleic acid molecules, the J-coupling can be neglected since the orbitals of the two unpaired electrons do not overlap. The Hamiltonian for the electron dipole-dipole interaction is

$$\hat{H}_{dip} = \vec{\hat{S}}_A \cdot \underline{D} \cdot \vec{\hat{S}}_B \qquad \textbf{eq. 11}$$

where $\underline{D}$ is the electron dipole-dipole interaction tensor.

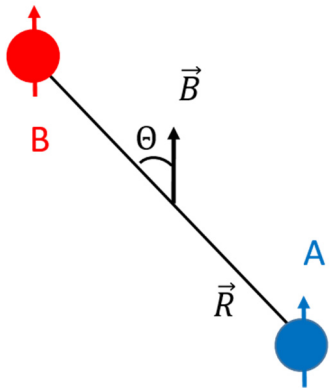

Figure 8: Two coupled magnetic dipoles A and B and their axis system with respect to the external magnetic field. Θ describes the angle between the interspin distance vector $\vec{R}$ and the external magnetic field axis $\vec{B}$.

The dipolar interaction energy U of two coupled magnetic dipole moments (Figure 8), $\vec{\mu}_A$ and $\vec{\mu}_B$, which are separated by the interspin distance vector $\vec{R}$, is described classically by

$$U = \frac{\mu_0}{4\pi}\left[\frac{\vec{\mu}_A \cdot \vec{\mu}_B}{|\vec{R}|^3} - \frac{3(\vec{\mu}_A \cdot \vec{R})(\vec{\mu}_B \cdot \vec{R})}{|\vec{R}|^5}\right] \qquad \textbf{eq. 12}$$

For the equivalent quantum mechanical expression, the magnetic moments are replaced by the corresponding operators (see eq. 1) under application of the correspondence principle. The point-dipole approximation the Hamiltonian in angular frequency units is given by

$$\hat{H}_{dip} = D_{dip}\left[\frac{\hat{\vec{S}}_A \cdot \hat{\vec{S}}_B}{\left|\vec{R}\right|^3} - \frac{3\left(\hat{\vec{S}}_A \cdot \vec{R}\right)\left(\hat{\vec{S}}_B \cdot \vec{R}\right)}{\left|\vec{R}\right|^5}\right] \qquad \textbf{eq. 13}$$

$$D_{dip} = \frac{\mu_0 g_A\, g_B\, \mu_B^2}{4\pi\hbar}$$

with the dipolar coupling constant D_{dip}. If $\vec{R}$ is expressed in spherical coordinates $\vec{R} = \begin{pmatrix} R\sin\Theta\cos\varphi \\ R\sin\Theta\sin\varphi \\ R\cos\Theta \end{pmatrix}$, $\hat{H}_{dip}$ can be rewritten as

$$\hat{H}_{dip} = \frac{D_{dip}}{R^3}\left(\hat{A} + \hat{B} + \hat{C} + \hat{D} + \hat{E} + \hat{F}\right) \qquad \textbf{eq. 14}$$

where $R = \left|\vec{R}\right|$. The terms $\hat{A}$ - $\hat{F}$ of the 'dipolar alphabet' represent products of spin operators and angular expressions. The individual terms are as follows:

Term	products of spin operators	angular expression
$\hat{A} =$	$\hat{S}_{zA}\hat{S}_{zB} \cdot$	$(1 - 3\cos^2\Theta)$
$\hat{B} =$	$-\frac{1}{4}\left(\hat{S}_{+A}\hat{S}_{-B} + \hat{S}_{-A}\hat{S}_{+B}\right) \cdot$	$(1 - 3\cos^2\Theta)$
$\hat{C} =$	$-\frac{3}{2}\left(\hat{S}_{+A}\hat{S}_{zB} + \hat{S}_{zA}\hat{S}_{+B}\right) \cdot$	$\sin\Theta\cos\Theta \cdot e^{-i\varphi}$
$\hat{D} =$	$-\frac{3}{2}\left(\hat{S}_{-A}\hat{S}_{zB} + \hat{S}_{zA}\hat{S}_{-B}\right) \cdot$	$\sin\Theta\cos\Theta \cdot e^{i\varphi}$
$\hat{E} =$	$-\frac{3}{4}\hat{S}_{+A}\hat{S}_{+B} \cdot$	$\sin^2\Theta \cdot e^{-2i\varphi}$
$\hat{F} =$	$-\frac{3}{4}\hat{S}_{-A}\hat{S}_{-B} \cdot$	$\sin^2\Theta \cdot e^{2i\varphi}$

$\hat{S}_x$ and $\hat{S}_y$ are expressed in terms of the shift operators, the raising and lowering operators being defined as $\hat{S}_\pm = \hat{S}_x \pm i\hat{S}_y$.

In the high-field approximation (where the electron Zeeman interaction is larger than the dipolar interaction) and if the interaction of both magnetic dipole moments with the external magnetic field is approximately isotropic and dominates all other contributions, the dipole quantization axes are aligned parallel to the external magnetic field $\vec{B}$. Therefore, only the

terms $\hat{A}$ (secular term) and $\hat{B}$ (pseudo secular term) of the dipolar alphabet in the Hamiltonian have to be considered and term $\hat{C} - \hat{F}$ (non-secular terms) can be neglected. If relaxation effects are taken into account, all terms of the 'dipolar alphabet' have to be considered.
In the weak coupling limit the dipolar coupling frequency ω_{dip} is much smaller than the difference between the resonance frequencies of spin A and B $|\omega_A - \omega_B|$, which is usually the case in pulsed EPR experiments. Under these conditions, only the $\hat{A}$-term needs to be considered (secular approximation):

$$\hat{H}_{dip} = \frac{D_{dip}}{R^3}\hat{A} \qquad \textbf{eq. 15}$$

The dipolar coupling frequency ω_{dip} can be defined as

$$\hat{H}_{dip} = \omega_{dip}\hat{S}_{zA}\hat{S}_{zB} \qquad \textbf{eq. 16}$$

$$\omega_{dip}[\mathrm{rad/s}] = 2\pi\nu_{dip}[1/\mathrm{s}] = \frac{D_{dip}}{R^3}\cdot(3\cos^2\Theta - 1) \qquad \textbf{eq. 17}$$

$$\nu_{dip}[\mathrm{MHz}] = \frac{52{,}16\,[\mathrm{MHz\cdot nm^3}]}{R^3[\mathrm{nm^3}]} \text{ for } g_A = g_B = 2{,}005\,,\Theta = 90° \qquad \textbf{eq. 18}$$

R is the interspin distance in nm and Θ is the angle between the distance vector $\vec{R}$ and the external magnetic field $\vec{B}$. The constant 52.16 MHz·nm^3 in eq. 18 includes the effective values of the g-tensor, g_A and g_B , for a pair of nitroxides radicals. These are assumed to be equal and isotropic. The strength of the dipolar coupling frequency ω_{dip} depends on R (eq. 17 and eq. 18). This opens the opportunity for an assessment of the distance between two spin labels in a biomolecule from a measurement of the coupling frequency, giving information regarding the structure of the studied system. This is valid for electron-electron as well as for electron-proton interactions (anisotropic part of the hyperfine interaction). Moreover, the angular dependence of the dipole-dipole interaction $(1 - 3\cos^2\Theta)$ provides the possibility to unravel the relative orientation of two rigid spin labels, thus yielding considerably more structural information.
Using the orthogonal basis functions $|m_{SA}m_{SB}\rangle = |\alpha_A\alpha_B\rangle, |\alpha_A\beta_B\rangle, |\beta_A\alpha_B\rangle, |\beta_A\beta_B\rangle$, the matrix representation of the electron Zeeman and electron-electron dipolar terms of the spin Hamiltonian for the described system gives

$$\widehat{H}_{EZ} = \frac{1}{2}\begin{pmatrix} +(\omega_A + \omega_B) & & & 0 \\ & +(\omega_A - \omega_B) & & \\ & & -(\omega_A - \omega_B) & \\ 0 & & & -(\omega_A + \omega_B) \end{pmatrix}$$

$$\widehat{H}_{dip} = \frac{1}{4}\begin{pmatrix} \omega_{dip} & & & 0 \\ & -\omega_{dip} & & \\ & & -\omega_{dip} & \\ 0 & & & \omega_{dip} \end{pmatrix}$$

eq. 19

The diagonal elements of the Hamilton $\widehat{H} = \widehat{H}_{EZ} + \widehat{H}_{dip}$ are the eigenvalues ε. Therefore, for a two-electron spin system without hyperfine couplings there are four energy states

$$\begin{aligned} \varepsilon_{|\alpha_A\alpha_B\rangle} &= +\frac{1}{2}(\omega_A + \omega_B) + \frac{1}{4}\omega_{dip} \\ \varepsilon_{|\alpha_A\beta_B\rangle} &= +\frac{1}{2}(\omega_A - \omega_B) - \frac{1}{4}\omega_{dip} \\ \varepsilon_{|\beta_A\alpha_B\rangle} &= -\frac{1}{2}(\omega_A - \omega_B) - \frac{1}{4}\omega_{dip} \\ \varepsilon_{|\beta_A\beta_B\rangle} &= -\frac{1}{2}(\omega_A + \omega_B) + \frac{1}{4}\omega_{dip} \end{aligned}$$

eq. 20

Figure 9A shows the resulting allowed EPR transitions, as described by

$$\begin{aligned} \varepsilon_{|\alpha_A\alpha_B\rangle} - \varepsilon_{|\beta_A\alpha_B\rangle} &= \omega_A + \frac{\omega_{dip}}{2} \\ \varepsilon_{|\beta_A\alpha_B\rangle} - \varepsilon_{|\beta_A\beta_B\rangle} &= \omega_B - \frac{\omega_{dip}}{2} \\ \varepsilon_{|\alpha_A\alpha_B\rangle} - \varepsilon_{|\alpha_A\beta_B\rangle} &= \omega_B + \frac{\omega_{dip}}{2} \\ \varepsilon_{|\alpha_A\beta_B\rangle} - \varepsilon_{|\beta_A\beta_B\rangle} &= \omega_A - \frac{\omega_{dip}}{2} \end{aligned}$$

eq. 21

The final EPR spectrum shows at each resonance positions ω_A and ω_B a doublet, which is split by $|\omega_{dip}|$ (Figure 9B). For distances above 1.5 nm ($\nu_{dip} = 15.45$ MHz), the dipolar splitting is covered by the inhomogeneous line width, which includes line broadening from the anisotropy of the g- and A-tensors and the dipolar coupling.

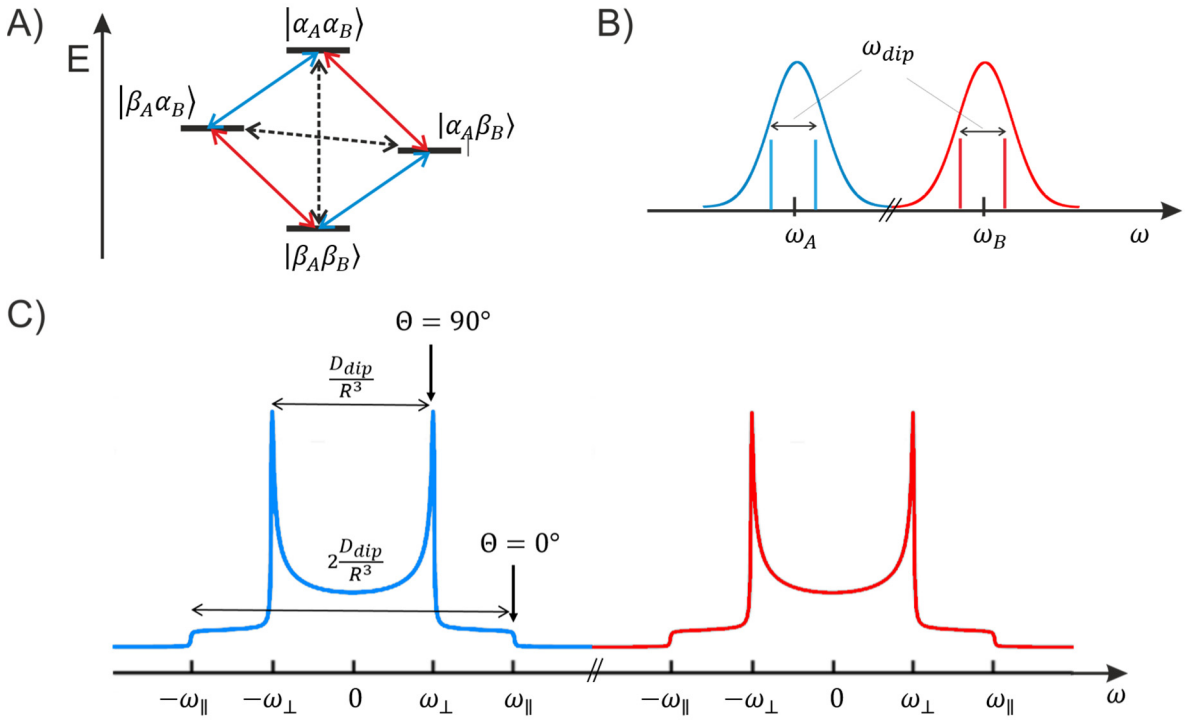

Figure 9: Energy scheme, CW-EPR spectrum and Pake pattern of a two-electron spin system. (A) Energy scheme of a two-electron spin system with the allowed (solid blue and red line) and forbidden (dashed line) EPR transitions. The transitions of the A- and B-spins are colored in blue and red, respectively. Hyperfine couplings are not considered in this representation for simplicity. (B) CW-EPR spectrum of an isolated electron spin-pair, whose resonance lines are covered by the inhomogeneous linewidth. (C) Pake pattern of an electron spin-pair for disordered powder samples.

Taking into account a disordered powder sample, where the molecules are randomly distributed with respect to the external magnetic field $\vec{B}$, the integration of the dipolar frequencies ω_{dip} over the angle Θ (Figure 8) on the unit sphere results in a symmetric Pake pattern (powder averaging) (Figure 9C). Two turning points of the Pake pattern can be distinguished: the perpendicular component ($\Theta = 90°$ at $\pm\,\omega_\perp$, highest intensity features) are separated by $\frac{D_{dip}}{R^3}$ and the parallel component ($\Theta = 0°$ at $\pm\,\omega_\parallel = 2\omega_\perp$, lowest intensity peaks) separated by $2\frac{D_{dip}}{R^3}$. In principle, the interspin distance R between the two spins can be directly determined by the dipolar coupling frequency ω_{dip} at $\Theta = 90°$ using eq. 18, if a single distance with a narrow distribution is present. In the presence of a distribution of distances the turning points are broadened, which makes it more difficult to extract the distances directly from the frequency spectrum.

4.3 Description of PELDOR experiments

This chapter introduces the pulsed EPR method, called PELDOR, which reveals dipolar coupling frequencies from interacting spin pairs allowing distance measurements from 1.5 nm up to 10 nm. For a more detailed discussion, see the following textbooks and review articles.[73, 81-82]

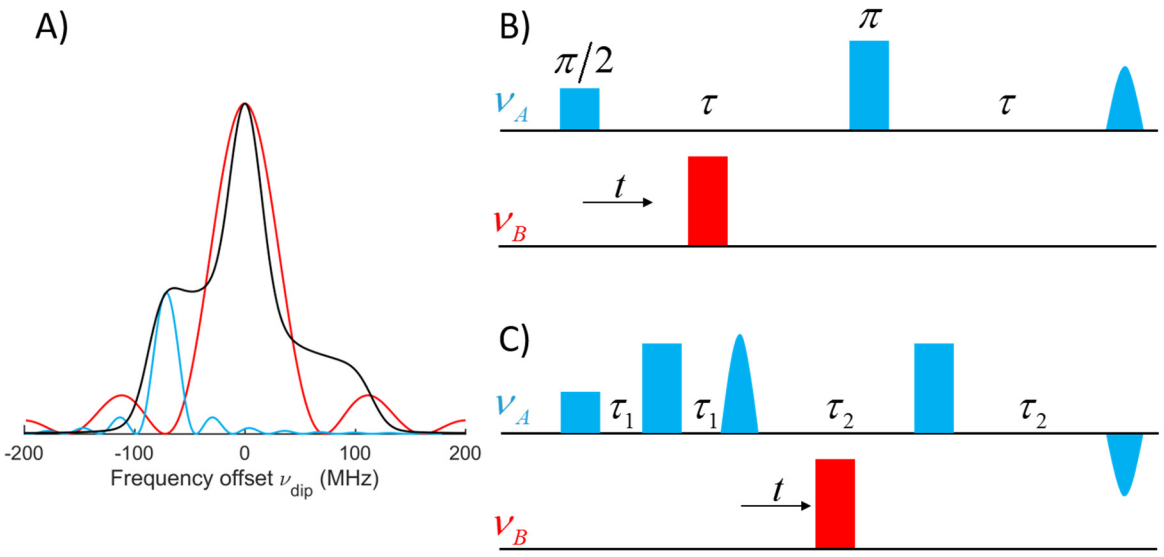

Figure 10: PELDOR pulse sequences. (A) Field-swept powder absorption nitroxide EPR spectra at X-band frequencies with the spectral profiles of pump (red) and probe (blue) pulses separated by a pump-probe frequency offset $\Delta\nu$ of 70 MHz typically used for flexible nitroxide spin labels. The calculation was done for a pulse length of 12 ns for the pump pulse and 32 ns for the probe pulses. (B) 3-pulse PELDOR sequence[83-84] (C) Dead-time-free 4-pulse PELDOR sequence.[85-86]

The basic principle of a PELDOR experiment is easily explained by the 3-pulse PELDOR sequence (Figure 10B), which was originally introduced by Milov *et al.*.[83-84] PELDOR is a two frequency experiment which detects on the A-spins (probed spins) using a Hahn-echo sequence and pumps on the B-spins (pumped spins) that belong to the dipolar interacting A-B-spin system.

The Hahn-echo sequence, whose frequency ν_A is resonant to the Lamor frequency of the A-spins, causes a Hahn-echo, thereby refocusing the interactions of the A-spin with the environment (including the electron dipole-dipole interaction). τ is the pulse separation time, which is kept constant during the experiment. An additional π-pulse (pump pulse), whose frequency ν_B is resonant to the Lamor frequency of the B-spins, inverts the B-spins at the

delay time *t*. This changes the local magnetic field at the A-spins, leading to a change in the Lamor frequency of the A-spins by the dipolar coupling frequency of ± ω_{dip}. Hence, the A-spins precess with this modified frequency in the transversal plane and accumulate a phase factor of $\pm\omega_{dip}t$ depending on the pump pulse delay time t. This leads to an imperfect refocused Hahn-echo at time 2τ. By varying the pump pulse position t, the amplitude of the detected echo signal $V(t)$ oscillates with the dipolar coupling frequency ω_{dip} of spin A and B, according to

$$V(t) = V_0 \cos(\omega_{dip} t) \qquad \textbf{eq. 22}$$

where V_0 is the echo intensity at $t = 0$.

Nowadays, the 3-pulse sequence is extended by an additional π-pulse in the detection sequence. This 4-pulse PELDOR sequence was introduced by Spiess to avoid the dead time-problem of the 3-pulse sequence by replacing the π/2-pulse by a π/2 - τ_1 - π - τ_1 sequence (Figure 10C).[85-86] Thus, the zero time of the modulation corresponds to the position of the first Hahn-echo. The time t is incremented between the second and the third pulse of the detection sequence.

The A-spin of an A-B spin pair does not only interact with the intramolecular B-spin but also has spin-spin couplings to other spins of neighboring spin pairs (intermolecular contribution). These additional dipolar couplings cause a decay of the echo signal $V(t)$ depending on the local spin concentration and spatial distribution. In the case of a homogeneous three-dimensional distribution of radicals without excluded volume, the signal is described by a monoexponential decay.[87] The total PELDOR signal consists of the product of the intramolecular $V_{intra}(t)$ and the intermolecular contribution $V_{inter}(t)$.

$$V(t) = V_{intra}(t) \cdot V_{inter}(t) \qquad \textbf{eq. 23}$$

In the following, $V_{intra}(t)$ is discussed and the index 'intra' is omitted.

The PELDOR experiment is generated by several not overlapping pulses (neither in time nor in frequency). The EPR spectra of two nitroxide spin labels overlap completely. In a PELDOR experiment, the EPR spectrum is only partly excited by each pulse. A partly excited spectrum also means that certain orientations of the nitroxide relative to the magnetic field are more likely to be inverted than others due to the anisotropic contributions of the

nitroxide orientation in the external magnetic field to the EPR spectrum (*vide ante*). Upon applying the pulse at the second frequency the signal decays to a non-zero value $V_0(1-\lambda)$ for times $t \to \infty$.

$$V(t \to \infty) = V_0(1-\lambda) \qquad \textbf{eq. 24}$$

λ is the modulation depth, later also called orientation intensity function, describing the fraction of inverted B-spins by the pump pulse which are coupled to the detected A-spins. If the B-spins are completely excited, $\lambda = 1$. By combining eq. 24 with eq. 22 gives the expression for the intermolecular term

$$V(t) = V_0\left(1-\lambda+\lambda\cos\left(\omega_{dip}t\right)\right) \qquad \textbf{eq. 25}$$

In the case of a macroscopically disordered powder sample (frozen solution sample), all orientations of the A-B spin pairs relative to the external magnetic field will have the same probability. Therefore, the total signal $V(t)$ is given by the sum over the sphere of the contributions of each single molecular orientation depending on all magnetic field orientations and weighted by $\sin(\Theta)$.

$$V(t) = V_0\int_0^{2\pi}\int_0^{\pi}\left(1-\lambda(\Theta)+\lambda(\Theta)\cos\left(\omega_{dip}(\Theta)\,t\right)\sin(\Theta)d\Theta d\varphi\right) \qquad \textbf{eq. 26}$$

The dependence $\lambda(\Theta)$ will be discussed later in this chapter. The Fourier transformation of this equation gives the dipolar spectrum, whose shape is an undistorted Pake pattern.
By using two flexible spin labels, the relative orientation between them is almost randomly distributed due to their intrinsic flexibility. Now, $V(t)$ is integrated over all dipolar angles Θ. In this case, the modulation depth parameter λ is independent of the relative orientation between the two spin labels. λ is constant and thus does not depend on the angle Θ.

$$V(t) = V_0\left(1-\lambda+\lambda\int_0^{\pi/2}\cos\left(\omega_{dip}t\right)\sin(\Theta)d\Theta\right) \qquad \textbf{eq. 27}$$

The PELDOR signal can be described by a Fredholm integral equation of the first kind with the normalized PELDOR signal $S(t) = V(t)/V_0$ and ω_{dip} (eq. 18).

$$S(t) = 1 - \lambda + \lambda \int_0^{\pi/2} \cos\left[\left(\frac{D_{dip}}{R^3} \cdot (3\cos^2\Theta - 1)\right)t\right] \sin(\Theta) d\Theta \qquad \textbf{eq. 28}$$

The description of the PELDOR signal given above assumed a single conformation of the biomolecule with a fixed interspin distance. Since biomolecules are dynamic in nature and undergo fluctuations in liquid solution, an ensemble of *i*=1, …, *N* molecular structures with distributed distances R_i is necessary to describe the PELDOR signal in a realistic manner. PELDOR experiments have to be performed using an immobilized sample (*e.g.* frozen solution) on the one hand to slow down the fast electron spin relaxation and on the other hand to immobilize the molecules hence preventing the complete averaging of the dipolar coupling. The thermal distribution of conformational states is assumed to be preserved in the frozen state. Therefore, the signal is given by the average over the ensemble.

$$\begin{aligned} S(t) = {} & 1 - \lambda + \lambda \frac{V_0}{N} \sum_{i=1}^{N} \int_0^1 \cos\left[\left(\frac{D_{dip}}{{R_i}^3} \cdot (3x^2 - 1)\right)t\right] dx \\ & = 1 - \lambda + \lambda \int_{R_{min}}^{R_{max}} K(t,R) P(R) dR \\ & K(t,R) = \int_0^1 \cos\left[(3x^2 - 1)\omega_{dip}(R)t\right] dx \end{aligned} \qquad \textbf{eq. 29}$$

where $x = \cos(\Theta)$. $P(R)$ is the distance distribution function (describing the distribution of distances between two spin labels) and $K(t,R)$ is the integral kernel function. If the conformational flexibility of the biomolecule increases, and thus the width of the distance distribution, the dipolar oscillations are damped faster and the $\cos(\omega_{dip}t)$ terms interfere to zero for times $t \to \infty$. The characteristics of the Pake pattern are less defined and it is no longer possible to determine reliable distances from the Fourier transform of the PELDOR time traces. The calculation of the PELDOR signal $V(t)$ from a known distance distribution $P(R)$ is straightforward, if no angular correlations between the two spins exists, whereas the

extraction of distances from the PELDOR time trace, the inverse problem, does not admit a unique solution, especially considering the presence of noise in the experimental time trace. Small changes in the input data $V(t)$, *e.g.* due to noise or small errors in background correction, can lead to different solutions for the output data $P(R)$. Tikhonov regularization is one way to overcome this issue giving consistent and stable results of such ill-posed problems. Tikhonov regularization is implemented *e.g.* in the DeerAnalysis Software packet[88]. Tikhonov regularization makes a compromise between smoothness of the distance distribution and goodness of the fit using the regularization parameter α. The optimum distance distribution $P(R)$ is given by minimization of the following function

$$G_\alpha\big(P(R)\big) = \left\|V_{sim}(t) - V_{exp}(t)\right\|^2 + \alpha \left\|\frac{d^2}{dR^2}P(R)\right\|^2 = \rho(\alpha) + \alpha\,\eta(\alpha) \qquad \textbf{eq. 30}$$

$\rho(\alpha)$ is the mean square deviation between the experimental $V_{exp}(t)$ and the simulated signal $V_{sim}(t)$. $\eta(\alpha)$ is the square norm of the second derivative of $P(R)$ and describes the smoothness of $P(R)$. The optimum regularization parameter is found by application of the L-curve criterion (plot of $\log\eta(\alpha)$ against $\log\rho(\alpha)$) determining over- and undersmoothing of the distance distributions.

4.3.1 Orientation-selective PELDOR experiment

The PELDOR signal $V(t)$, described above, was calculated for two flexible spin labels with a random orientation distribution relative to each other and to their interspin distance vector $\vec{R}$ (fully uncorrelated spin pairs). A full orientational correlation between two spin labels exists, if two rigidly attached spin labels have a fixed relative orientation of their molecular frames and of their connection vector $\vec{R}$ with respect to these frames. In this case, the PELDOR signal $V(t)$ refects this orientation correlation and the PELDOR time trace will differ depending on the spectral position of the pump and probe pulses. This PELDOR property is called orientation selection.[89-90] For an ensemble of *N* doubly rigid labeled molecules in a macroscopically disordered sample, the total signal $V(t)$ is given by the

expression

$$V(t) = \frac{V_0}{N}\sum_{i=0}^{N}\left(1 + \int_0^{\pi/2} \lambda_i(\Theta)\left(\cos\left(\omega_{dip,i}(R,\Theta)t\right) - 1\right)\sin(\Theta)d\Theta\right) \qquad \textbf{eq. 31}$$

where the weights of different dipolar axis orientations contributing to the PELDOR time traces are $P_i(\Theta) = \lambda_i(\Theta)\sin(\Theta)$. The usual weighting factor $\sin(\Theta)$ accounts for the presence of a macroscopically disordered sample. The additional weighting factor $\lambda_i(\Theta)$ arises from the observer spin A, since at a given excitation position a subensemble of orientations of the molecular frame of the A-spin with respect to the external magnetic field is selected. At X-band frequencies, the molecular frames of both spin labels are predominantly selected due to the A-anisotropy and at G-band frequencies due to the g-tensor anisotropy (*vide infra*). By this mechanism, a subensemble of orientations of the interspin vector with respect to the magnetic field is selected, since the orientation of the interspin distance vector in the molecular frame is fixed. Likewise, a specific selection of the molecular frame of the B-spins occurs, due to the fixed orientation of spin B relative to spin A within a dipolar interacting A-B spin system. In addition, the modulation depth λ is sensitive to the fraction of inverted B-spins by the pump pulse. Thus, the modulation depth depends also on the angle Θ. The calculation of λ is explained in more detail later.

It is worth noting that the orientation intensity function $\lambda_i(\Theta)$ depends not only on the geometry of the two spin labels but also on experimental parameters such as spectral position, microwave power, resonator bandwidth, pulse lengths and B_1 homogeneity over the sample length. Due to the dependency of the dipolar coupling frequencies $\omega_{dip,i}(R,\Theta)$ on Θ, the weights $P_i(\Theta)$ cause a selection of dipolar frequencies in the dipolar spectrum and thus the Fourier transformation of the PELDOR signal does no longer have the shape of a standard Pake pattern. In summary, on the one hand the excitation of spin A leads to a non-random distribution of dipolar angles Θ and on the other hand the weights $P_i(\Theta)$ and the dipolar coupling frequencies $\omega_{dip,i}(R,\Theta)$ depend on the angle Θ in a nontrivial way and thus on the relative orientation between both spin labels.

4.3.1.1 Orientation-selective PELDOR experiment at X-, Q- and G-band frequencies

In order to selectively probe the relative orientation between two radicals and observe the dipolar oscillation by PELDOR spectroscopy, the pump and the probe pulses need to excite separately both radicals (*vide ante*). From an experimental point of view, several time traces are recorded by moving the position of pump and probe pulses. A single PELDOR time trace is usually not sufficient, since it does not obtain enough independent information to obtain unique solutions of the angles describing a given geometry. Thereby, orientations are selected, which depend on the particular magnetic field positions. In doing so, the Θ-dependency can be observed in a change in oscillation frequency, modulation depth and damping of the PELDOR signals as a function of the spectral position at which the PELDOR time traces are recorded. How the orientation-selective PELDOR experiment is performed is shown by means of two rigid nitroxide spin labels recorded at X-, Q-, and G-band.

Excitation probabilities in dependence of the magnetic field orientation in the molecular axis system of the nitroxide radical can be represented on a sphere (Figure 11).

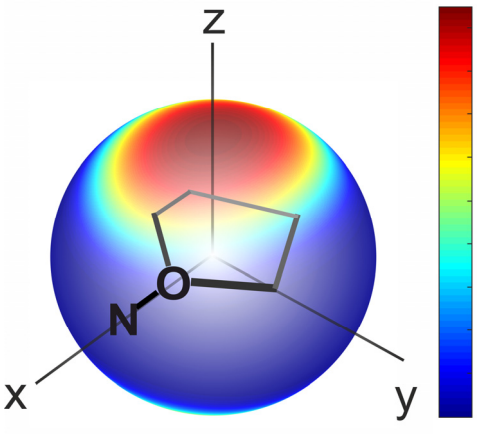

Figure 11: Definition of the molecular axis system of the nitroxide radical and sphere of excited molecular orientations. The color code gives the excitation probability, increasing from blue to red, in dependence of the molecular orientation. The simulations were performed using the EasySpin toolbox.[91] The excitation bandwidth was within 30 MHz. Here, the orientation resolution is shown for an X-band spectrum at the low-field edge of the nitroxide spectrum.

Figure 12 shows the excitation probabilities in dependence of the magnetic field orientation for different magnetic field positions within the field-swept powder absorption spectra recorded at X-, Q- and G-band frequencies.

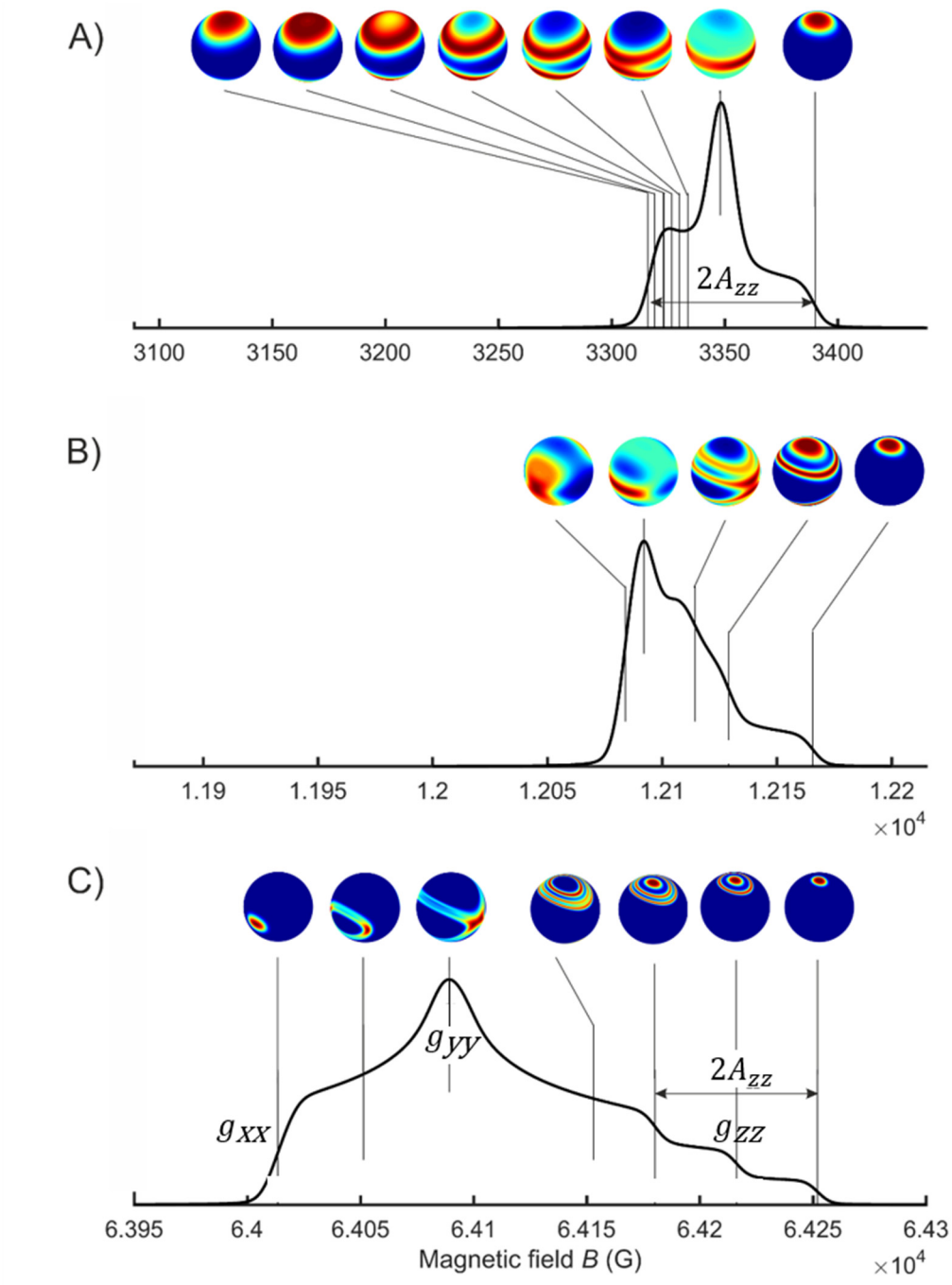

Figure 12: Excited orientations (orientation selections) on the unit sphere for nitroxides at different frequencies and magnetic field strengths. (A) Field-swept powder absorption nitroxide EPR spectra at X-band frequencies and orientation selections on the unit sphere for nitroxides. Excited orientations for the pump pulse and for the detection sequence from $\Delta\nu$ = 40, 50, …, 90 MHz. (B) Field-swept powder absorption EPR spectra at Q-band frequencies and orientation selections. (C) Field-swept powder absorption EPR spectra at G-band frequencies and orientation selections shown along the principal axis directions of the g-tensor. For the calculations, an excitation bandwidth of 30 MHz was chosen.

The X-band nitroxide spectrum is dominated by the strong anisotropic hyperfine interaction of the unpaired electron with the ^{14}N-nucleus, which has a large A_{zz}-component, whereas the g- tensor is unresolved within the inhomogeneous linewidth (Figure 12A). In this case, the non-selective pump pulse exciting the B-spins is typically located at the maximum of the anisotropic powder spectrum, predominentely selecting nearly all orientation within the nitrogen nuclear spin sublevel with the nitrogen nuclear spin states $|m_I\rangle = |0\rangle$. Thus, almost all molecular orientations of the nitroxide radical with respect to the external magnetic field are excited. In order to gain information about the interspin distance and the relative orientation of two rigid spin labels, the PELDOR experiments at X-band frequencies are performed with a fixed pump frequency ν_B and a series of probe frequencies ν_A with a frequency offset $\Delta\nu = \nu_A - \nu_B$ varied from 40 to 90 MHz relative to the pump frequency. Increasing $\Delta\nu$ excites less of A_{xx} and A_{yy} and more of A_{zz} (Figure 12A). At the high-field edge of the X-band EPR spectrum ($|m_I\rangle = |-1\rangle$) the molecular nitroxide plane of the A-spins is perpendicular to the magnetic field $\vec{B}$, and consequentially a molecular z-axis almost parallel to $\vec{B}$ (Figure 11) is selected. Therefore, by the choice of the probe frequency a well-defined subensemble of specific nitroxide orientations relative to the external magnetic field can be selected. If the system is rigid, this results in a selection of the allowed orientations of the interspin distance vector $\vec{R}$ with respect to $\vec{B}$. This orientation selection can be observed in the orientation-selective PELDOR experiments (evolution time t vs. pump–probe frequency offset $\Delta\nu$) as a change in the shape of the PELDOR signals as a function of the frequency offset. This complex pattern of time traces indicates that the relative orientation between two spin labels contributes to the spectral shape, and thus that the former can be inferred from such a set of PELDOR time traces. In contrast, if no angular correlations exist between two spin labels, *e.g.* in the case of flexible spin labels, all time traces recorded with different frequency offset are identical. At X-band frequencies, the g-anisotropy is not resolved and the x- and y-components of the hyperfine tensor are also not distinguishable. The orientational resolution is therefore only clearly defined at the edge of the EPR spectrum due to the large A_{zz}-component. As shown later, orientational information related to the g-anisotropy can be retrieved at high magnetic fields due to the resolution of the g-tensor components.

In contrast to what is described for X-band, the orientational resolution at Q-band frequencies is weak and not intuitive (Figure 12B), although the z-component of the g-tensor becomes partially resolved (whereas the x- and y-components of the g-tensor are still not

distinguishable).

At even higher magnetic fields and microwave frequencies, namely at a frequency of 95 GHz or above, all the components of the anisotropic g-tensor are spectrally resolved (Figure 12C). This is due to the fact that the g-tensor is rhombic for nitroxide radicals. Here, many combinations of pump and probe frequencies will lead to a complex pattern of the orientation-selective PELDOR time traces due to the selectivity of probe and pump pulse in equal ways. Therefore, it is necessary to test different separations between pump and probe frequencies and/or to vary the magnetic field positions in the EPR spectrum to gain the complete angular information content. For the current G-band spectrometer setup used in our research group, the magnetic field position is varied and the frequency separation $\Delta\nu$ is usually kept constant. The application of a dual-mode cavity would give more freedom in tuning the frequency separation. For instance, the W-band spectrometer of the research group of Prof. Dr. Bennati permits a frequency separation up to 800 MHz.[69, 92] In summary, the advantage to perform PELDOR at high magnetic fields is the strong and clear orientational resolution in spite of technical difficulties related to the handling of high-field spectrometers.

Since the PELDOR experiments have to be performed at different field positions and frequencies to gain the complete angular information, the experiments themselves are more time consuming, yet each time trace set results in more than just distance information. New techniques, like broadband SIFTER, were proposed to get the orientational information in one experiment.[93-94] This is for the moment limited to X- and, more recently, Q-band frequencies.

4.3.1.2 Orientational information from orientation-selective PELDOR data

The nitroxide molecular frame is defined such that its x-axis is along the N-O bond and its z-axis is oriented perpendicular to the nitroxide plane, *i.e.* perpendicular to the plane containing the N-O bond and the connecting carbons that are bound to the N-O group. The y-axis is the cross product of x and z and thus perpendicular to both axes. This definition of the axes coincides with the principal axes of the g- and the hyperfine interaction tensors.

The geometry of two nitroxide spin labels can be characterized by six parameters: The interspin distance R, two polar angles and three Euler angles (Figure 13B). The interspin distance R is approximately between the midpoints of the two N-O bonds of both nitroxides.

The two polar angles define the orientation of the interspin distance vector (dipolar frame $\{x, y, z\}$) with respect to the molecular frame of spin A $\{x_1, y_1, z_1\}$. The three Euler angles describe the relative orientation of the molecular frame of spin B $\{x_2, y_2, z_2\}$ with respect to the molecular frame of spin A.

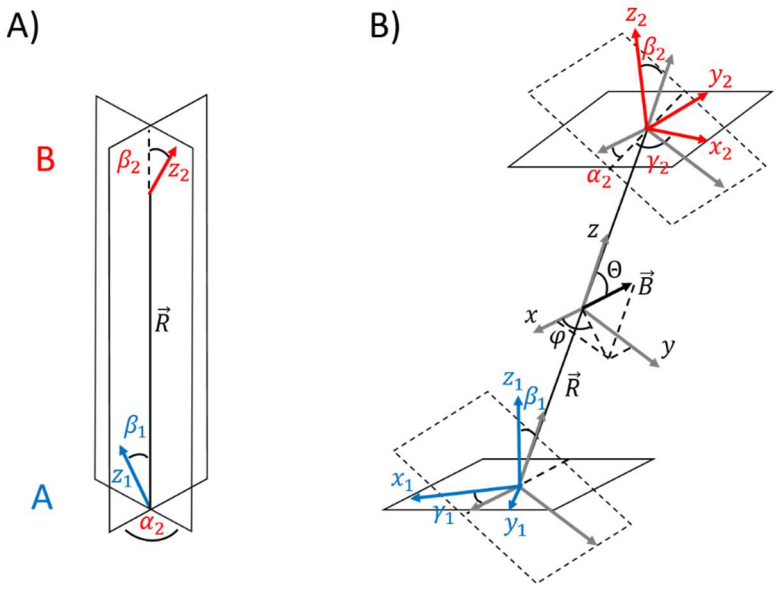

Figure 13: Coordinate system and angles definition of the geometry of two dipolar coupled nitroxide spin labels and angular information provided by orientation-selective PELDOR data at X- and G-band frequencies. (A) Angular information provided by orientation-selective PELDOR data at X-band frequencies. Only the angles $(\alpha_2, \beta_1, \beta_2)$ determine the shape of a PELDOR signal due to the symmetry of the A-tensor. (B) Coordinate system and angles definition of the geometry of two dipolar coupled nitroxide spin labels connected by an interspin distance vector $\vec{R}$ (dipolar frame $\{x, y, z\}$). The molecular frame of spin A $\{x_1, y_1, z_1\}$ relates to the molecular frame of spin B $\{x_2, y_2, z_2\}$ each described by the three Euler angles, $\alpha_{1,2}, \beta_{1,2}, \gamma_{1,2}$, respectively, whereas the orientation of the magnetic field vector $\vec{B}$ is described by the two polar angles φ and Θ. The molecular frame axes coincide with the principle axes of the g- and the hyperfine interaction tensors. The z-axis of the dipolar frame is aligned with the interspin distance vector $\vec{R}$, whereas the x-axis is oriented orthogonally to the plane of the z- and z_1-vectors.

The following definition of the relative orientation of two nitroxide spin label A and B is introduced, to be consistent with the work of Marko *et al.*.[95] The relative orientation of two nitroxides A and B with respect to the common interspin distance vector is defined by two consecutive rotations, first from the g-frame of nitroxide B into the principal axis system of the dipolar tensor, whose z-axis is aligned with the interspin axis, $D_2(\alpha_2, \beta_2, \gamma_2)$ and second from the latter into the g-frame of nitroxide A, $D_1(\alpha_1, \beta_1, \gamma_1)$. Here, the relative orientation of two nitroxide spin labels

with respect to the dipolar tensor is described by the Euler angles $\vec{o}_A \equiv (\alpha_1, \beta_1, \gamma_1)$=$(0, \beta_1, \gamma_1)$ and $\vec{o}_B \equiv (\alpha_2, \beta_2, \gamma_2)$ (Figure 13B). It should be noted that without losing generality $\alpha_1$is set to zero, and thus effectively only 5 angles describe the orientation of both nitroxides, due to the axial symmetry of the dipolar interaction tensor. The five Euler angles characterizing the biradical geometry are in the ranges $0 \leq \alpha_2 < 2\pi$, $0 \leq \beta_{1,2} < \pi$ and $0 \leq \gamma_{1,2} < 2\pi$.

If angular contributions to the spectral shape are observable in the orientation-selective PELDOR data, angular information of a geometrically correlated spin pair can generally be extracted. However, the angular information content (number of angles) achievable differs at different magnetic field strengths. X-band orientation-selective PELDOR data provide information on three angles: the angles between each nitroxide out-of-plane normal, the A_{zz}-axes, and the interspin distance vector ($\beta_{1,2}$) and the angle between both A_{zz}-axes (α_2) (Figure 13A). This is due to the dominance of the anisotropic hyperfine interaction of the unpaired electron with the nitrogen nucleus, which has a large A_{zz}-component, to the X-band nitroxide spectrum (Figure 7A). In order to gain information regarding all five angles (β_1, γ_1 and α_2, β_2, γ_2), PELDOR measurements have to be performed at high magnetic field strength, where the x- and y-components of the anisotropic g-tensor are spectrally resolved (Figure 7C). There are a few aspects which have to be taken into account. In the first place, the inversion symmetry of the spin Hamiltonian gives additional ambiguities to the solutions. Moreover, due to the complete overlap between the EPR spectra of both nitroxide spin labels these latter are indistinguishable and each can act as pump or observer spin. In principle, these ambiguities can be solved in combination with specific knowledge of the structure and labeling scheme to gain a complete description of the relative orientation of the molecular frames of two nitroxide spin labels.

4.3.1.3 Separation of distance and orientation information from orientation-selective PELDOR data

The separation of the dependencies on R and Θ in eq. 17 can generally be achieved by a quantitative analysis or fitting procedure of the PELDOR time traces as a function of the probe frequency or the magnetic field position. For the analysis of orientation-selective PELDOR data several approaches were proposed in recent years. In order to calculate only

the distance distribution function out of a set orientation-selective PELDOR time traces $S(t)$, the PELDOR time traces cannot be directly transferred to a distance distribution $P(R)$, as described in chapter 4.3. If the simple extraction of $P(R)$ is applied, artificial peaks could occur to compensate the orientational correlations. To get around this, the PELDOR time traces are summed up over all measured frequency offsets $\Delta\nu_i$ at X-band frequencies, giving the orientation-averaged time trace $W(t)$.

$$W(t) = \sum_i V(t, \Delta\nu_i \text{ or } \Delta B_i) \qquad \textbf{eq. 32}$$

This procedure is a good approximation to average out the orientation information and to obtain an accurate distance distribution function by using afterwards Tikhonov regularization as suggested by Godt *et al*.[96] and supported by simulations.[70, 97]
In order to get angular information, the signal $V(t)$ can easily be predicted according to eq. 31 in a straightforward manner from a well-known structure of the molecule, since the spin Hamiltonian parameters of nitroxides and the experimental parameters are well known. Structures obtained by techniques like NMR or X-ray can be successfully used as molecular models to define the orientations of the spin labels and thence predict PELDOR time traces.

$$\{Orientation,\ distance\} \xrightarrow{unique} PELDOR\ signal$$

One of the first examples in the literature is the determination of the relative orientation between two monomers of the ribonucleotide reductase dimer with tyrosyl radicals.[98-99] There are several other examples applied on nitroxide biradicals[96, 100-104], trityl-nitroxide biradicals[105] and metal-nitroxide or metal-metal complexes[106-107]. In the case of the rigid **Ç**-label, which is fixed within the framework of the DNA/RNA helix, two **Ç**-labels can be easily modelled into a high-resolution structure by replacing existing bases C. The resulting relative orientation and the distance vector between these two **Ç**-labels can be used to simulate the corresponding PELDOR time traces. To gain insight in the dynamical behavior of a biomolecule, an ensemble of structures can be furthermore extracted from MD simulation trajectories. Another approach to create an ensemble of structures is based on educated guesses using simple geometric models of the studied molecule.[71, 100, 108-110]
In the last step, the predicted PELDOR time traces can be compared quantitatively with the

experimental time traces. In comparison with other classes of biological systems, this procedure is not so easy to transfer to biomolecules labeled with flexible spin labels, such as the MTS spin label used for many applications on proteins. Due to the internal flexibility of such spin labels, their flexibility has to be taken into account with an absolute accuracy of around 0.3 nm between the predicted and the measured distance R. Fast and mostly reliable approaches for the prediction of spin label conformations are available using the software MMM[111] or MtsslWizard[112], which are both based on rotamer library approaches.[113-114]
The reverse way, extracting the relative orientation of two rigid spin labels and distance from the orientation-selective PELDOR time traces directly, is not so straightforward.

$$\{Orientation,\ distance\} \xleftarrow{ambiguous} PELDOR\ signal$$

A fundamental problem in the determination of the relative orientation between the two spin label molecular frames from the orientation-selective PELDOR time traces is the existence of several sets of Euler angles giving the same PELDOR time traces. The ambiguity of the PELDOR time traces is due to the inversion symmetry of the spin Hamiltonian regarding the magnetic field orientation $\vec{B}$. For instance, if a nitroxide is rotated by 180° around any axis of its molecular frame the effective tensor values (eq. 5 and eq. 10) do not change, hence the resonance frequency and λ remain the same and thus the time traces are identical (eq. 34, *vide infra*). The equivalence of the PELDOR signals caused by symmetry has been already analyzed in the work of Abé *et al*..[115] Additional ambiguity is usually introduced by the fact that the two attached nitroxide spin labels are indistinguishable. Especially in the case of flexible systems, when many conformers coexist, the number of possible solutions get even more ambiguous, since different ensembles of spin label conformations might represent the same orientation-selective PELDOR data. No derivation of a closed mathematical relation is available so far, which would allow a direct determination of the angles describing the relative orientations from a set of experimental PELDOR data. However, the experimental PELDOR time traces can be reconstructed by fitting the experimental data through the selection of a subset out of a set of presimulated time traces that were derived from a library of possible spin-spin orientations and distances.[95]
This approach consists of two steps. In the first step, a library S_{lib} of all orientation-selective PELDOR data sets which can occur at X-band frequencies for nitroxide radical pairs with arbitrary orientations and interspin distances, is created. The angles and distances are for this

purpose chosen within the experimentally accessible range. Only the angles $\alpha_2, \beta_1, \beta_2$ and the interspin distance R are varied to create the library of signals needed for the fitting procedure, since only the z-component of the nitrogen hyperfine tensor is resolved at X-band frequencies. The remaining angles, γ_1 and γ_2, are not taken into account, since they cannot be determined from X-band PELDOR measurements. The calculation of the PELDOR signals for a powder sample with a given fixed orientation between the A- and B-spin is described in the following using the definitions to describe the orientation between two rigid spin labels: the resonance frequencies $\omega_{A,B}$ of spin A and spin B are determined by the orientation of each nitroxide in the external magnetic field $\vec{B}$

$$\omega_{A,B}\left(\Theta, \varphi, \vec{o}_{A,B}, m_{A,B}\right) = \gamma_e \left[\frac{\vec{B} g_{eff}\left(\Theta, \varphi, \vec{o}_{A,B}\right)}{g_e} + m_{A,B} A_{eff}\left(\Theta, \varphi, \vec{o}_{A,B}\right) + \delta b_{A,B}\right] \quad \textbf{eq. 33}$$

with $g_{eff}\left(\Theta, \varphi, \vec{o}_{A,B}\right)$ the effective value of the anisotropic Zeeman interaction tensor (eq. 5) and $A_{eff}\left(\Theta, \varphi, \vec{o}_{A,B}\right)$ the effective value of the hyperfine interaction tensor for the coupling of the electron spin with the ^{14}N-nucleus (eq. 10). $m_{A,B}$ are the nuclear spin magnetic quantum numbers for spin A and spin B. The resonance frequency also depends on local field fluctuations, which leads to inhomogeneous line broadening, here described by $\delta b_{A,B}$. λ is an averaged sum of the product of the spin echo magnetization of each electron m_x and the flip probability of spin B p_B.

$$\lambda = \frac{1}{2} \sum_{m_A, m_B} \langle m_x(\omega_A, \nu_A) p_B(\omega_B, \nu_B) + m_x(\omega_B, \nu_A) p_B(\omega_A, \nu_B) \rangle_{\varphi, \delta b_A, \delta b_B} \quad \textbf{eq. 34}$$

where the m_x and p_B are given by

$$m_x\left(\omega_{A,B}, \nu_A\right) = \frac{1}{4}\left[\frac{\gamma_0 B_{1A}}{\Omega_A(A,B)}\right]^5 \sin\left(\Omega_A(A,B) t_{A,\frac{\pi}{2}}\right)\left[1 - \cos\left(\Omega_A(A,B) t_{A,\pi}\right)\right]^2 \quad \textbf{eq. 35}$$

$$p_B(\omega_{A,B}, \nu_B) = \frac{{\gamma_0}^2 {B_{1B}}^2}{2{\Omega_B}^2(i)}\left[1 - \cos\left(\Omega_B(A,B)t_{B,\pi}\right)\right] \qquad \textbf{eq. 36}$$

with the Rabi frequencies of spin A and B

$${\Omega_{A,B}}^2(i) = {\gamma_0}^2 {B_{1A,B}}^2 + \left(2\pi\nu_{A,B} - \omega_{A,B}\right)^2 \qquad \textbf{eq. 37}$$

$t_{B,\pi}$ is the length of the microwave pump pulse and $B_{1A,1B}$ are the magnitudes of the microwave probe and pump pulses, respectively. In summary, λ depends on the Euler angles $\vec{o}_{A,B}$ since the functions $m_x(\omega_{A,B}, \nu_A)$ and $p_B(\omega_{A,B}, \nu_B)$ depend both on the resonance frequencies of spin A and B. For the calculation of the PELDOR signals, λ is inserted in eq. 31.

In the second step of the two-step approach, an optimal combination of these pre-simulated PELDOR time traces is estimated by application of the algorithm which reproduces the experimental orientation-selective PELDOR data. In each iterative step *n* the fitting algorithm searches for the element $S_n \in S_{\text{lib}}$ which corresponds to the signal of the spin label conformer minimizing the error function Err_n. Err_n is the difference between the experimental data set of signals S_{exp} and the sum of the simulated signals squared from the previous selection of calculated signals $S_1,\ldots S_{n-1}$ plus S_n:

$$Err_n = \min_{S_n \in S_{\text{lib}}} \left(S_{\text{exp}} - \frac{1}{n}\sum_{i=1}^{n} S_i \right)^2 \qquad \textbf{eq. 38}$$

In the first iteration a simulated set of orientation-selective PELDOR data, representing a spin label conformer giving the lowest Err_n, is selected. In each subsequent step of the iterative fitting procedure an additional simulated orientation-selective PELDOR data set is picked and added to the previous such that Err_n is further minimized. These steps are repeated until satisfactory agreement is reached with all experimental PELDOR time traces. Each spin label conformer can be selected several times. Thus, in the final ensemble a single spin label conformer can have possible multiple occurrence.

5 Results - Determination of structural ensembles of highly flexible nucleic acid molecules

The determination of structural ensembles and the characterization of the conformational dynamics of complex and highly flexible nucleic acids is a challenging task in structural biology. In principle PELDOR data reflect the sum of contributions from each conformation in the sample since the experiments are performed in frozen solution, and thus reflect the conformational flexibility of the nucleic acid at the freezing temperature. Therefore, this allows the determination of structural ensembles, which represent the overall flexibility of the studied biomolecule. However, the time scales of conformational transitions cannot be accessed by PELDOR spectroscopy. The motion of the nucleic acid is superimposed with the internal motion of the spin label by using flexible spin labels and have to be considered in the analysis of the PELDOR data. Since the rigid **Ç**-label is sensitive to the motion of the base and thereby to the motion of helices, when the spin label is paired with guanine in a duplex region, analysis of the PELDOR data directly enables the determination of the conformational flexibility of the nucleic acid. In addition, the relative orientation between two helices can be estimated from the relative orientation between two **Ç**-labels, if the spin labels are incorporated into each helix. This enables the determination of both the conformational flexibility and the structure of the nucleic acid molecules.[97,116-118]

It was shown that unambiguous determination of the orientation between two rigid spin labels out of orientation-selective PELDOR data from a well-defined rigid structure is possible.[95] However, if the DNA molecule is highly flexible a single conformer alone cannot explain the experimental PELDOR data. In such a case, the extraction of angular information from orientation-selective PELDOR data in a straightforward manner is not always possible, as was discussed in previous studies.[95, 117] It might be that different structural bundles represent the same orientation-selective PELDOR time traces. This is especially the case for the study of flexible systems, where many conformers of the nucleic acid molecules coexist, and it becomes a challenge for the determination of the structural ensemble by using PELDOR spectroscopy. However, experimental PELDOR time traces can be reconstructed in a two-step approach to fit the data selecting a subset from a set of presimulated time traces that were derived from a library of possible spin-spin orientations (chapter 4.3.1.3).[95] This approach considers two rigid nitroxide spin labels in free space without any knowledge of

the biomolecular structure between them. However, the biomolecule restricts the number of possible angles and distances between the two spin labels. At this point, the question arises whether complete native structures of spin-labeled DNA exist that are in agreement with the found spin label conformations. Therefore, a different strategy was chosen in this thesis to characterize the conformational spaces of the highly flexible DNA motifs, the cocaine aptamer in the presence of cocaine and a bent DNA. To shed light on the conformational dynamics of both systems, a PELDOR data-guided selection of conformers from a spin label conformation library or structure library were applied, respectively. Generally, this is a two-step protocol based on the search algorithm mentioned above. In the literature, such a protocol is classified as sample-and-select method.[119-120]

For the first example, the cocaine aptamer[117], the classical two-step approach to find possible spin label conformations which reproduces the experimental orientation-selective X-band PELDOR data was applied followed by the generation of the corresponding topologically allowed inter-helical orientations. Since there is no NMR or X-ray structure available, *a priori* knowledge about the secondary structure of the aptamer was used. For this purpose, topological restrictions were introduced based on steric clashes and distances between points of inter-helical connectivity not exceeding the maximum length of the bulge linker. Using this topological restrictions combined with the assumption of ideal B-DNA helices as rigid bodies, a molecular model describing the global folding and conformational flexibility of the aptamer was obtained.

In contrast, for the second system, the bent DNA,[118] spectroscopic data from NMR spectroscopy was available. Dornberger *et al.* have solved the three-dimensional structure of this DNA (PDB entry: 1QSK).[121] The same distance and angular restraints derived from NOESY-type experiments and from J-coupling measurements were combined with long-distance ranges from PELDOR.

In the first step, a library was created with a broad collection of conformers that are in agreement with topological constraints, NMR restraints and distance ranges derived from PELDOR. In the second step, a weighted structure ensemble of these conformers was chosen such that it fits simultaneously the orientation-selective X-band PELDOR time traces of all doubly **Ç**-labeled samples. In the literature there are examples for the first step of this two-step approach through sampling of inter-helical Euler angles[122] or by using molecular dynamic simulations[123] to generate structure libraries followed by a fit on experimental NMR data in the second step.

For the studied bent DNA molecule, the ^{1}H-^{1}H NOEs and angular restraints from the

available NMR data set are sufficient to describe precisely the structure of the helices; they furthermore partially restrict the conformation of the bulge defining the topology of the studied DNA. Using the available NMR data for the bent DNA allows determination of atomistic high-resolution structures and facilitate the modelling of the rather short helices. (The bent DNA helices have a length of six base pairs, whereas a complete turn of a B-DNA helix consists of about 10 base pairs.) On the other hand, long-distance restraints from PELDOR measurements are useful to restrict the conformational space which describes the global arrangement of the two helices relative to each other. Thus, the resulting structural bundle, which is characterized in atomic detail, describes the dynamic nature of this bent DNA molecule.

A combination of NMR and EPR has previously been successfully applied to study the structures of a homodimeric protein complex,[124] of partially folded proteins,[125] and of a protein-RNA complex[126] using flexible spin labels. Kennedy and coworkers showed that NMR restraints combined with a few additional long-distance restraints from PRE and PELDOR allowed the determination of the structure of the homodimer Dsy0195.[124] Ulmer and coworkers identified dominant ensemble subpopulations in partially folded proteins by such a combined approach.[125] Recently, Duss *et al.* included calculation of the spin label distribution centers for a flexible IA-proxyl spin-labeled RNA into the structure calculation of a protein-RNA complex.[126] However none of these studies utilized orientation-derived information, which is facilitated by the use of rigid spin labels.

The kink and twist motions between the helical parts were quantitatively determined for both systems to obtain a picture of their conformational spaces. For the bent DNA, the obtained structural ensemble was compared with the structure bundles derived from the published NMR structures[121] and the FRET study[20].

5.1 Application on two DNA model systems

5.1.1 Flexibility and conformation of the cocaine aptamer studied by PELDOR

In order to study the conformational changes of the cocaine aptamer upon binding of cocaine using PELDOR spectroscopy, the rigid **Ç**-label was incorporated pairwise into helices II and III of the cocaine aptamer (Figure 14). The synthesis of the spin label and of all the DNA samples used in this thesis were performed by Dr. Cekan a former group member in the research group of Prof. Dr. Sigurdsson from the University of Iceland.

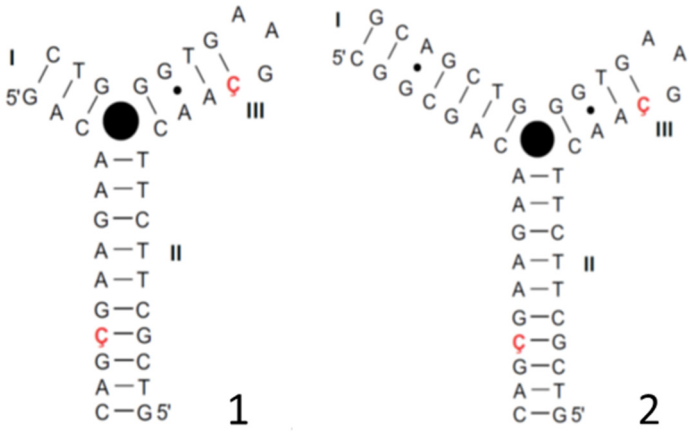

Figure 14: Secondary structures of cocaine aptamer 1 and 2. Helices II and III of the cocaine aptamers **1** and **2** share the same sequence and labeling positions. However, aptamer **2** has an elongated helix I. The ligand cocaine is represented by the filled black circle at the junction where the cocaine is known to bind. The **Ç**-labeled positions in helix II and III are highlighted in red and bold.

In the literature, Stojanovic and coworkers have described the construction of the DNA-based cocaine aptamer as an aptamer-based fluorescent sensor for cocaine (Figure 14).[127] The design of this construct was chosen such that it is a single strand in the absence of cocaine. The aptamer folds up into a three-way junction upon binding to cocaine[128] with the dissociation constant in the micromolar range[66, 128-129] as detected by fluorescence spectroscopy. The research group of Prof. Dr. Sigurdsson has previously incorporated the rigid **Ç**-label (Figure 14) into single sites of this cocaine aptamer construct and studied its folding upon cocaine binding by CW-EPR and fluorescence spectroscopy (using the analogue fluorescence chromophore **Ç**^{f}). The interpretation of their data was in agreement with a model in which the aptamer was partially folded up into two co-axially stacked helices

in the absence of cocaine, giving a T-shaped molecule (helices II and III, Figure 14). Upon concomitant binding to cocaine and formation of helix I, the co-axially stacked helices would tilt relative to each other forming a Y-shaped junction (Figure 14).

5.1.1.1 Orientation-selective PELDOR experiments

In order to obtain information regarding both the distances and the mutual orientations between the two **Ç**-labels, orientation-selective PELDOR experiments at X-band frequencies were performed (see also chapter 4.3.1.1) on both cocaine constructs in absence and presence of cocaine (Figure 15).

An important parameter for the characterization of a PELDOR time trace is the modulation depth parameter λ, which describes the decay of the echo signal to a non-zero value (1−λ). The error of reproducibility from experiment to experiment at X-band frequencies on the modulation depth λ is 5–10%, if the experiments are performed under the same conditions.[130]

If angular correlations between both spin labels exist, the modulation depth as well as the oscillation frequency depend on the frequency offset between pump and probe pulses, with a pattern that reflects the specific geometry between both spin labels. In the orientation-selective PELDOR experiments in 3 out of the 4 aptamer samples (Figure 15B-D) variations of the modulation depth as a function of the frequency offset are easily visible.

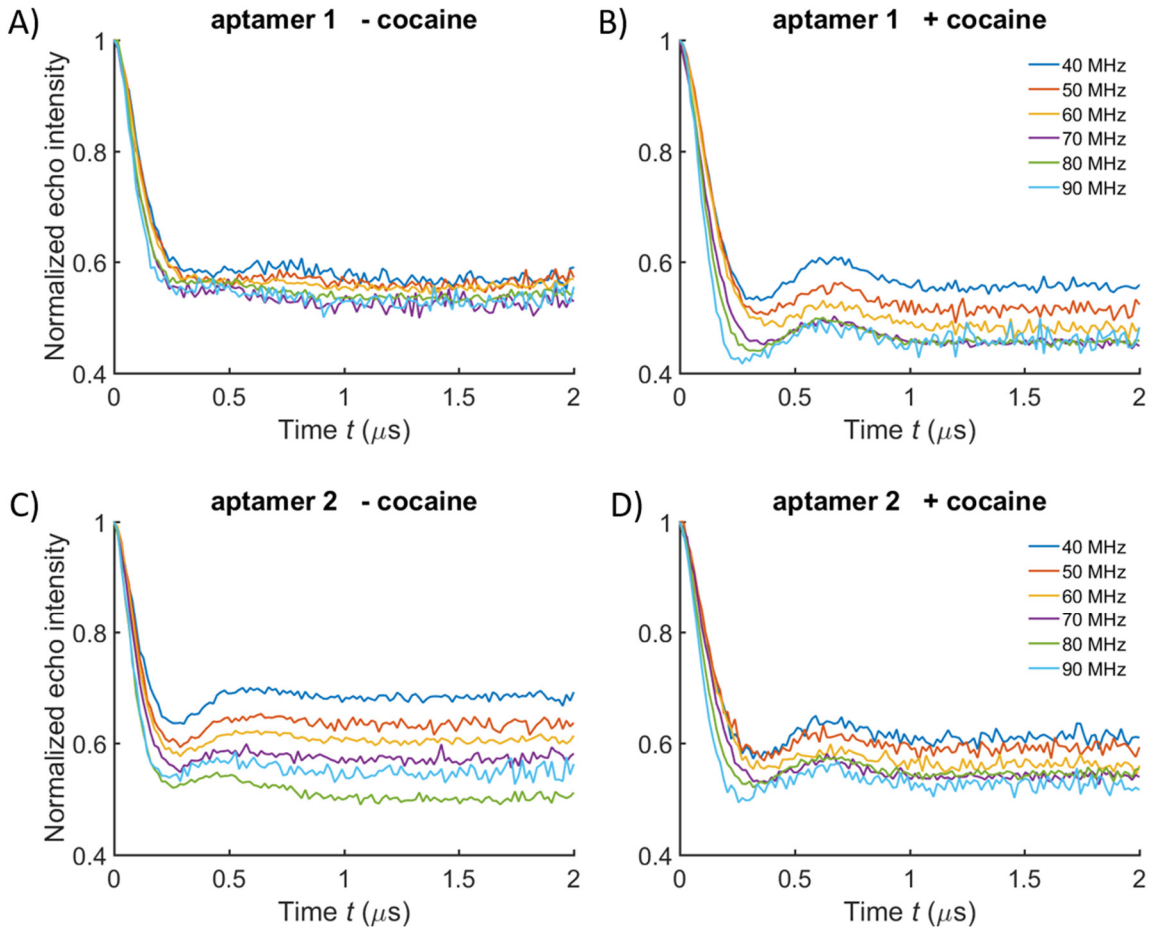

Figure 15: Experimental background-divided PELDOR time traces recorded at X-band frequencies for the cocaine aptamer constructs. Experimental background-divided PELDOR time traces measured at frequency offsets Δν ranging from 40 to 90 MHz at X-band frequencies for the spin-labeled aptamer constructs **1** in the absence (A) and presence of cocaine (B) and **2** in the absence (C) and presence of cocaine (D). The raw time traces and experimental details can be found in the appendix.

5.1.1.2 Determination of distances and distance distributions - Flexibility of the cocaine aptamer in absence and upon binding of cocaine

For distance determination, the X-band PELDOR time traces (Figure 15) measured with different frequency offsets $\Delta\nu$ were summed up (see also chapter 4.3.1.3). Figure 16 shows the averaged time traces and the corresponding distance distributions obtained by Tikhonov regularization.

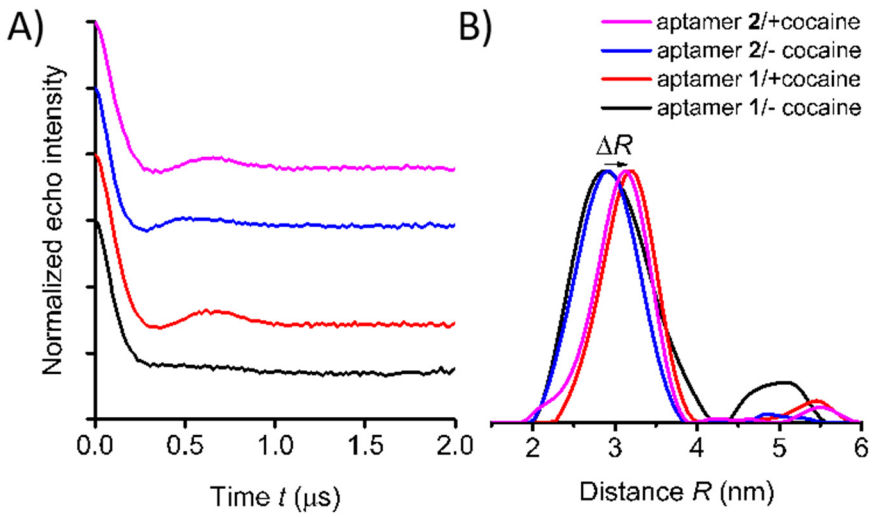

Figure 16: Averaged time traces and corresponding distance distributions for the cocaine aptamer constructs. (A) Averaged and background-divided time traces of both spin-labeled cocaine aptamer constructs **1** in the presence (red) and absence of cocaine (black) and **2** in the presence (magenta) and absence of cocaine (blue) at X-band frequencies. For better visualization, the upper three time traces have been shifted in the vertical direction. (B) Distance distributions based on a Tikhonov regularization for aptamers **1** and **2** in the presence and absence of cocaine. The arrow depicts the shift of the mean distance ΔR induced by the binding of cocaine.

The movement of **Ç** is restricted to the one of the helix where it resides, as explained in chapter 3.3. Thus, in addition to accurate distance measurements between two **Ç**-labels, the damping of the dipolar oscillations in the PELDOR time traces gives detailed information on the conformational flexibility of the DNA molecule.[97] The oscillations in the PELDOR signals for both aptamers **1** and **2** are more strongly damped (Figure 15 and Figure 16) compared to the study of the bent DNA (*vide infra*) or to previous studies on double-stranded DNAs[70]. Moreover, the orientation-selective PELDOR data show less pronounced variations in the oscillation frequency as a function of the frequency offset (Figure 15). This confirms

that both constructs have considerable conformational flexibility in the absence of cocaine, albeit less in the cocaine-bound state. In summary, these data show that the cocaine aptamer can be considered as a rather flexible junction, especially in the absence of cocaine.

The distance distributions of aptamers **1** and **2** show a well-defined distance at 2.9 nm in the absence of cocaine (Figure 16B), indicating that helices II and III already formed without cocaine. This is in agreement with the previously published study of the cocaine aptamer using fluorescence and CW-EPR spectroscopy.[66] This study pointed out, an increase in fluorescence of **Ç**$^{\mathbf{f}}$ upon addition of cocaine, which was incorporated in helix II close to the junction This was ascribed to helical stacking of aptamer **1** in the absence of cocaine, suggesting a T-shape junction.[66] An additional broad and low populated distance at around 4.8 nm can be observed in the distance distributions obtained by Tikhonov regularization of aptamer **1** in absence of cocaine (Figure 16, black curve), whereas all the other samples show only one distance. These two distances might reflect the presence of two conformations with a difference in interspin distance between the two spin labels of around 1.9 nm. The observation of two distances in the distance distributions would be consistent with the previously proposed two-state model for folding of the cocaine aptamer by Sigurdsson.[66] The model consists of a T- and a Y-shaped junction that are expected to give different distances. Since the reliability of distance distributions depends strongly on the maximum dipolar evolution time t_{max},[131] time traces with an extended dipolar evolution time up to 5 µs were recorded with samples of aptamer **1** with and without addition of cocaine in deuterated solvent (Figure 17). These measurements were performed at Q-band frequencies, to avoid artifacts induced by a poor signal-to-noise ratio. In comparison to measurements at X-band frequencies, measurements at Q-band have higher sensitivity and a somewhat reduced orientation selectivity which is due to the strong interplay between g- and hyperfine anisotropy at this magnetic field strength, resulting in strong spectral overlap of different molecular orientations. A second peak in the distance distribution of aptamer **1** without cocaine can also be observed in the distance distributions from the time trace recorded at Q-band frequencies (Figure 17). The PELDOR data for the aptamer bound to cocaine display also a second distance, but with considerably reduced intensity. It should be noted that the shape and width for the second longer distance population cannot be interpreted in consideration of the given experimental maximum dipolar evolution time t_{max}.[131] In addition, to exclude misinterpretations due to uncertainties in background correction, a validation of the distance distribution against the choice of the background was performed using the DeerAnalysis Software package[88]. Although the longer distance cannot be entirely

suppressed, it can barely survive validation.

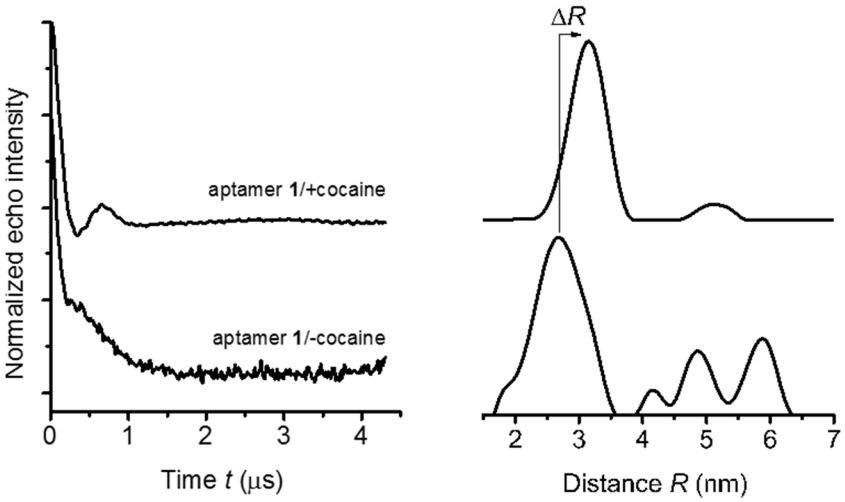

Figure 17: Experimental background-divided PELDOR time traces with a dipolar evolution time t_{max} of 5000 ns recorded at Q-band frequencies and corresponding distance distributions. Background-divided time traces of spin-labeled cocaine aptamer **1** before and after addition of cocaine in a deuterated solvent at Q-band with a dipolar evolution time t_{max} of 5000 ns. Each PELDOR time trace was recorded with a single frequency offset of 50 MHz, since orientation selection was expected to be weak at Q-band frequencies. Distance distributions were obtained by Tikhonov regularization. The time traces were vertically shifted for better visualization. The raw time traces and experimental details can be found in the appendix.

Aptamer **1** is a construct of the cocaine aptamer that was designed by Stojanovic and coworkers such that helices I and III are unfolded in the absence of cocaine,[127] whereas in aptamer **2** helix I has been extended to stabilize the formation of a three-way junction.[128] In the absence of cocaine construct **2** containing the elongated helix I, displays a clearly visible oscillation in the averaged PELDOR signal (Figure 16) and a dependence of the modulation depth as a function of the probe frequency offset in the orientation-selective PELDOR data (Figure 15). This was not the case for the construct with the short helix I (Figure 15 and Figure 16). Therefore, extension of helix I yields a stiffer structure, despite the fact that a similar mean interspin distance was observed for both aptamers in the absence of cocaine (Figure 16B). The main difference in the distance distribution functions of both aptamer constructs in the absence of cocaine is the broad peak at large distances which is required to simulate the fast damping of the dipolar oscillations of aptamer **1**.

Upon addition of cocaine to both constructs, the PELDOR data explicitly shows that

the structure and conformational flexibility of the aptamers change. Moreover, a pronounced oscillation appeared in the time traces for aptamer **1** and for aptamer **2** (Figure 15 and Figure 16). From these observations it can be deduced that, the cocaine aptamers rearrange to a more rigid structure and the Y-shaped structure is stabilized by the binding of cocaine.

The averaged time traces and distance distributions are almost identical for aptamers **1** and **2** in the presence of cocaine, which demonstrates that elongation of helix I in aptamer **2** has no influence on the structure of the cocaine-bound state (Figure 16). The variations of the modulation depth and of the dipolar oscillation frequency of the elongated aptamer construct **2** without cocaine resemble also already very much the data set of the cocaine-bound aptamer **1**, although with a stronger damping for the former construct. This is in agreement with previous results reporting that the formation of both helix I and the aptamer is stabilized by the ligand cocaine.[66, 127, 129] In addition, a change ΔR of the mean interspin distance of about 0.3 nm can be observed upon binding of cocaine for both constructs **1** and **2** in the distance distributions. This indicates a ligand-induced conformational change, which presumably originates at the junction where the cocaine is known to bind.[127-128] The shift of the maximum peak is clearly visible for both aptamer samples and for all control PELDOR experiments recorded at X- and Q-band frequencies in non-deuterated as well as deuterated solvent (Figure 15, Figure 16 and Figure 17). The distance shift obtained from the experiment recorded at Q-band is slightly longer than at X-band. This is tentatively attributed to residual orientation selection effects. Had more flexible spin labels been used, a change of the rotameric state of the spin label itself could also have been the cause of such a shift. This can be excluded for the rigid spin label **Ç**, which demonstrates again the ideal features of this spin label regarding quantitative distance determinations.

5.1.1.3 Extracting angular information from orientation-selective PELDOR data - Determination of the kink angle between helices I and III of the cocaine-bound aptamer

In addition to the interspin distance the relative orientation between two spin labels can be determined, if a strong dependence of the PELDOR time traces on the frequency offset between pump and probe pulses is visible in the orientation-selective PELDOR data (*vide ante*).[70-71] For both aptamer constructs, whether in presence or in absence of cocaine, the oscillation frequency and the damping of the PELDOR signals change only weakly as a function of the frequency offset, confirming a high flexibility of the aptamer at the junction between helices II and III. However, most of the orientation-selective PELDOR data sets, except the data for aptamer **1** in the absence of cocaine, show a variation of the modulation depth as a function of the offset frequency $\Delta\nu$ (Figure 15). These variations of the modulation depth are attributed to non-random orientations of the angle Θ and reflect different conformational distributions of relative orientations between two spin labels.

Therefore, a quantitative analysis of the orientation-selective PELDOR time traces recorded at X-band frequencies was performed using a numerical algorithm, developed by Dr. Marko in our research group, as outlined in chapter 4.3.1.3.[97] Figure 18A shows that the selected ensemble of spin-spin orientations reproduces the experimental PELDOR time traces of the cocaine-bound aptamer **1** very well including the modulation depth. This ensemble consists of 100 spin-spin orientations with possible multiple occurrence of one spin-spin orientation, since 100 iterative fitting steps were performed and each spin label conformer can be selected several times. Herein, the fitting procedure founds 53 non-redundant spin label conformers for the aptamer in its cocaine-bound state (Figure 18B). A set of angles (α_2, β_1, β_2) and the distance between the spin labels R describe the conformation of a spin label pair. A clustering of all spin label conformers in the β angle range of 60-90° is obvious, since two nitroxide spin labels cannot be distinguished and therefore β_1 and β_2 are interchangeable.

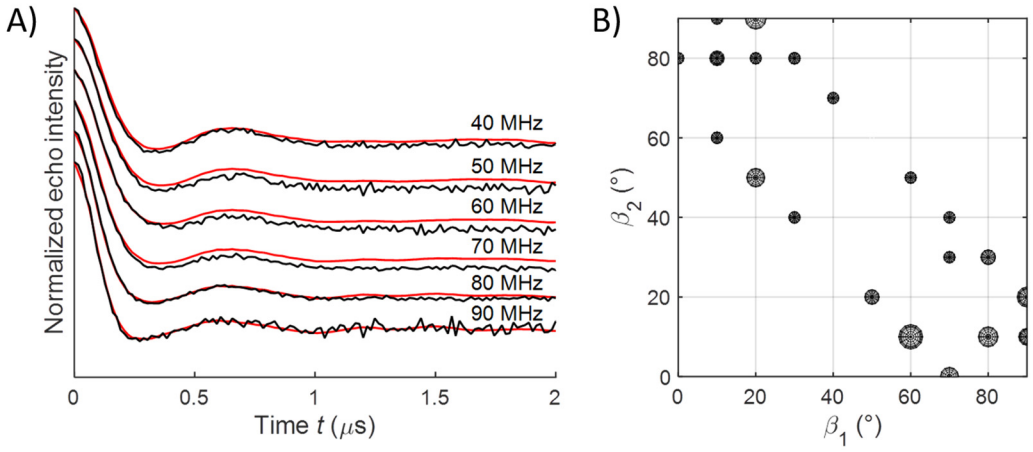

Figure 18: Fit by an ensemble of spin label conformers and density plot of the angles β_1 and β_2 for the aptamer 1 in the presence of cocaine. (A) Experimental X-band orientation-selective PELDOR data for the aptamer **1** in the presence of cocaine (black) and fit by an ensemble of spin label conformers (red). The time traces have been shifted in the direction of the y-axis for an easier visual inspection. (B) Angles β_1 and β_2 of the 53 spin label conformers, which were selected to fit the experimental orientation-selective PELDOR data. Non-redundant spin label conformers are represented by circles, and their weights in the fit by the radius of the circles.

The same procedure has been applied to the orientation-selective PELDOR data set of aptamer **1** in the absence of cocaine. No clear offset dependence can be observed in this data and, as expected, a much broader orientation distribution results from the fit procedure (Figure 19B). This indicates that aptamer **1** shows high conformational flexibility in the absence of the ligand, whereas the cocaine-bound state of the aptamer is more structured (Figure 18B).

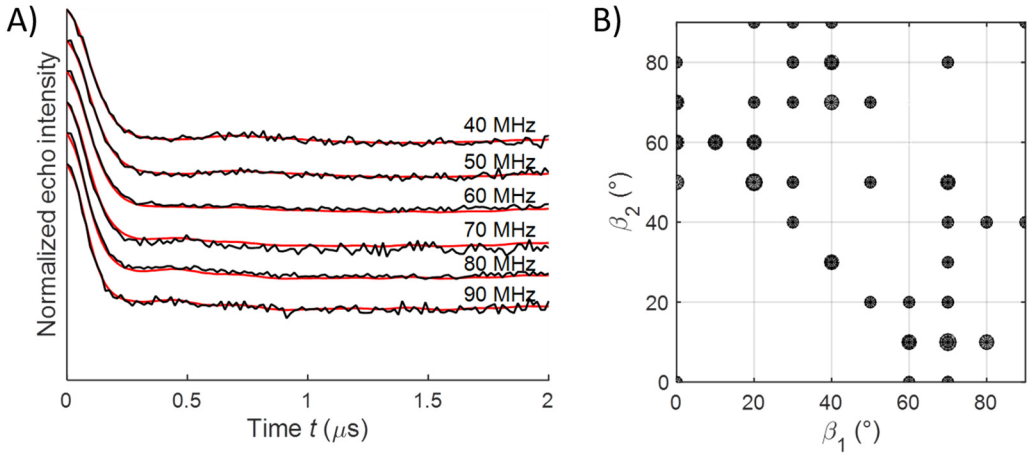

Figure 19: Fit by an ensemble of spin label conformers and density plot of the angles β_1 and β_2 for the aptamer 1 in the absence of cocaine. (A) X-band PELDOR signals from the database providing the best fit (red curves) to the experimental orientation-selective PELDOR data (black curves) of aptamer **1** in the absence of cocaine. The time traces have been shifted in the direction of the y-axis for an easier visual inspection. (B) Angles β_1 and β_2 of the spin label conformers selected during the fit procedure. A spin label conformer is represented by a circle and the weight of this spin label conformer in the fit by the radius of the circle.

Next, *a priori* knowledge about the secondary structure of the cocaine aptamer was used to generate physically possible solutions describing the relative orientation between the helices (helix II and III). In this context, the angular information and interspin distance $(\alpha_2, \beta_1, \beta_2, R)$ obtained by the fitting algorithm was used.

The web interface software w3dna[132] was used to construct the two spin-labeled B-DNA helices. For modelling of helix II the sequence 5'd-(AAGAAGCGAC)-3' was paired with 5'd-(GTCGCTTCTT)-3', and for modelling of helix III the sequence 5'-d(GTTG)-3' was paired with 5'-d(CAAC)-3'. The GA mismatch in helix III was not taken into account. The rigid nitroxide **Ç**-label was modeled into both DNA helices by a rigid superposition of the equivalent atoms of **Ç** and C at the labeling positions. The **Ç**-labeled DNA helices were treated as rigid bodies within the following analysis. Their mutual orientations were modeled according to the nitroxide spin label orientations found by the fitting algorithm using a custom written Matlab program, which consist of the following steps. The coordinates of the modelled **Ç**-labeled helices were loaded into the program, which orients both **Ç**-labeled DNA helices according to the Euler angle β_1 for nitroxide 1 and the Euler angles (α_2, β_2) for nitroxide 2 and varies the γ_1 and γ_2 angles. The second spin-labeled helix was additionally translated by the distance R between the two electron spins located each

in the middle of the NO-bond. In addition, because spin A and spin B are able to act both as pumped and as observer spins the two nitroxide spin labels cannot be distinguished. It was therefore necessary to consider all possible solutions for spin label 1 in helix II and spin label 2 in helix III and *vice versa*. It was also considered that the nitroxide radical normal ($\vec{A}_{zz}$) of each **Ç**-label can point up or down, which turns the helix upside down. All possible helix orientations were modeled for each $\alpha_2, \beta_1, \beta_2, R$ set that best fits the experimental orientation-selective PELDOR data.
Some of the generated structural models could be discarded since not all of these models for the cocaine-bound state are compatible with the basic geometrical knowledge of the aptamer structure. All helix orientations were verified by using three conditions, which are based on the secondary structure of the cocaine aptamer. The first condition is referred to the covalent connection between helix II and helix III (Figure 14). A threshold value was chosen that allows stretching of a helix by no more than 0.8 nm since the junction might stretch the pitch height. Structural models with a separation distance between the P-atom at the 5‘-end of Cytosine 24 and the 3‘-OH at Thymine 23 longer than 0.8 nm were discarded. To complete the geometry of the three-way junction, the maximum and the minimum space required by the non-labeled helix I (The diameter of a B-DNA helix is 2 nm.) has to be considered additionally. All structures with a separation between the 3‘-OH at the 3‘-end of helix III and the P-atom at the 5‘-end of helix II (deoxyadenosine 14) outside of the range 1.5 nm and 2.7 nm were filtered out. The values for the criteria were chosen by visual inspection of the structural models using the molecular visualization software PyMOL. Finally, steric clashes between helix II and helix III were prevented by discarding all structural models that cause steric conflicts between the two helices. To calculate the van der Waals repulsion between the helices, the plugin ‘Show bumps’ was slightly modified and used in PyMOL (http://www.pymolwiki.org/index.php/Show_bumps). The number of possible structural models was reduced by using these three filter threshold conditions yielding an ensemble of 1125 possible structural models from 549504 possible helix orientations. The criteria for the threshold conditions were chosen such that the experimental PELDOR data could still be satisfactorily simulated with the structural models which were not discarded. The corresponding simulated PELDOR time traces show that the frequency is very well described, which confirms that the interspin distance distribution still matches (Figure 20).

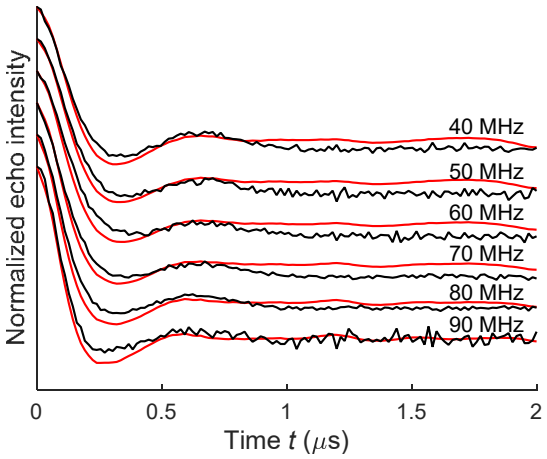

Figure 20: Simulation of the orientation-selective PELDOR data (red) resulting from non-filtered structural models of aptamer 1 in presence of cocaine. The same statistical weight was used as in the original database fit. The simulation (red) is compared to the experimental data (black). The time traces have been shifted in the direction of the y-axis for an easier visual inspection.

The model sketched in Figure 21 defines the geometry between the aptamer helices II and III. The angle between the helix axes of each stem of the DNA describes the kink angle φ between both helices, whereas the twist angles ψ, θ define the rotation around each helix axis. Due to the design of the **Ç**, the nitroxide molecular frame (see Figure 11) represents the helix frame to which **Ç** is attached. The normal ($\vec{A}_{zz}$) of **Ç** is parallel to the helix axis. Therefore, the kink angle φ is the angle between $\vec{A}_{zz,II}$ and $\vec{A}_{zz,III}$ and the two twist angles θ and ψ are the rotations between the two nitroxide NO-vectors $\vec{A}_{xx,II}$ ($\vec{A}_{xx,III}$, respectively) and the projection vectors $\vec{A}'_{xx,III}$ ($\vec{A}'_{xx,II}$, respectively) of the respective helix axis described in the molecular frame of the spin label. The kink angle φ can be directly extracted from the angles β_1 and β_2. In contrast, the twist angles ψ and θ are only restricted by the geometrical constraints imposed by the *a priori* knowledge from the secondary structure of the cocaine aptamer. The calculation of these angles can be found in the appendix, chapter 10.3.

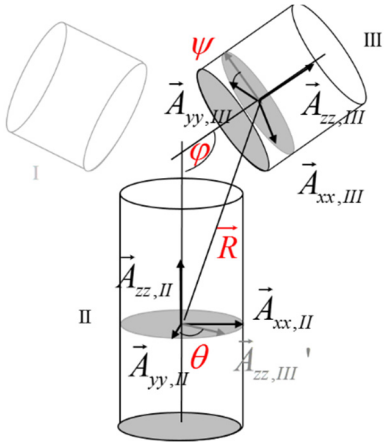

Figure 21: Definition of kink φ and twist angles θ and ψ. The cylinders represent the helices. Further details for the calculation of these angles can be found in the appendix.

Figure 22 demonstrates that the kink angle is very well conserved within the conformational ensemble for the cocaine-bound aptamer **1**. A weighted mean kink angle of 85 ± 20° was obtained. The twist angles θ and ψ are much more distributed but with some correlation between them.

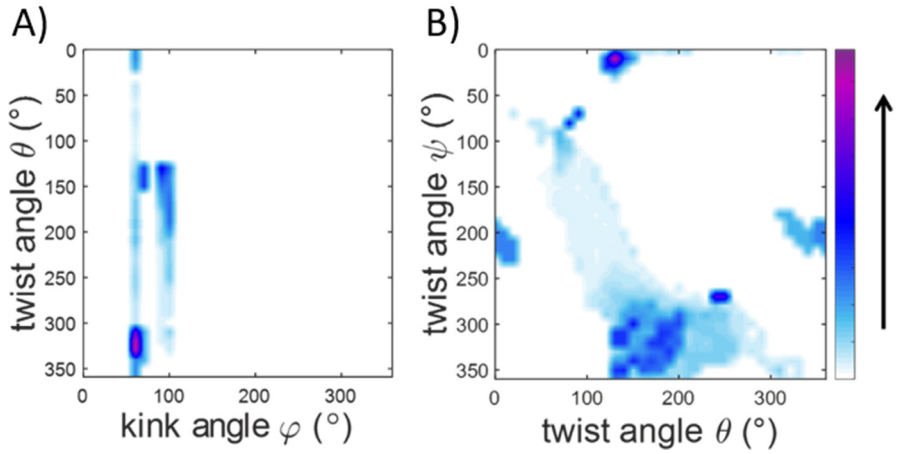

Figure 22: Density plot of twist and kink angles. (A) Density plot of the twist angle θ against the kink angle φ and (B) density plot of the twist angle ψ against the twist angle θ for the conformers found from the modelling of the helix orientation for aptamer **1** in the presence of cocaine. The color specifies the weight of the conformers. The data points are interpolated. It should be pointed out that the resolution of the angles of the PELDOR library ($\alpha_2, \beta_1, \beta_2$ for X-band frequencies) is in 10° steps, whereas the density plots have a resolution of 1°.

Two representative structural models from the conformational ensemble found by the analysis are shown Figure 23.

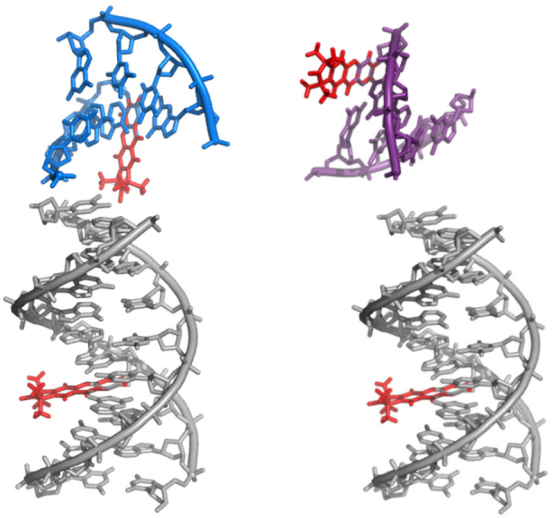

Figure 23: Two different representative structural models from the conformational ensemble found by the analysis of the angular contributions for aptamer 1 in the cocaine-bound state. In the structural models, helix II is identically orientated (colored in grey). The twist and kink angles for the left structural model (helix III is colored in blue) are $\varphi = 110°$, $\psi = 270°$ and $\theta = 240°$, $\varphi = 70°$, $\psi = 10°$ and $\theta = 130°$ for the right structural model (helix III is colored in purple). The **Ç**-label is colored in red.

5.1.2 Determination of helix orientations in highly flexible DNAs by multi-frequency EPR spectroscopy

The investigated bent DNA molecule is a two-way junction with a five-adenine bulge between its two helices, which induces a kink in the DNA structure (Figure 24). It can be considered as a model for locally damaged DNA or more complex nucleic acids containing bulges, loops, junctions, or kinks. In order to perform orientation-selective PELDOR experiments, one rigid **Ç**-label was incorporated into each stem of the bent DNA. In total, three DNA samples were prepared, each containing two spin labels: **DNA5,16** is labeled at C5 and C16, **DNA2,13** carries the two spin labels at positions C2 and C13, and **DNA2,16** has labels at positions C2 and C16 (Figure 24).

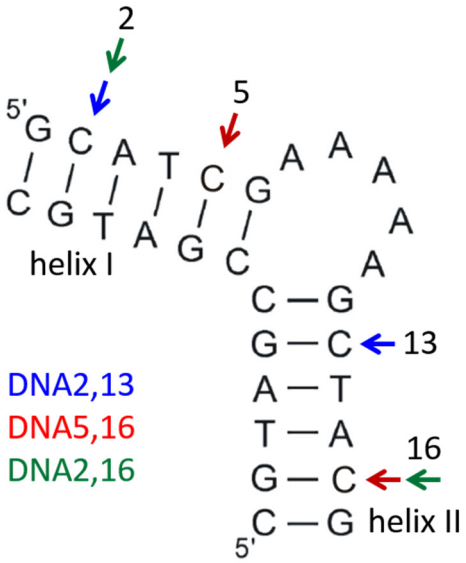

Figure 24: Secondary structure of the studied DNA and its three Ç-labeled constructs DNA2,13, DNA5,16 and DNA2,16. The flexible 5-nucleotide bulge with the sequence dAAAAA (dA-bulge) is located between the two helical regions (helix I and helix II). The labeling positions are marked by arrows.

5.1.2.1 Orientation-selective PELDOR experiments

Orientation-selective PELDOR measurements were performed at multi-frequency, X-, Q- and G-band frequencies, in order to obtain information regarding the distances and the relative orientations between the pairs of **Ç-**labels.

At X-band frequencies, the pump pulse with the frequency ν_B was set to the maximum of the nitroxide spectrum to excite all molecular orientations. The frequency offset $\Delta\nu = \nu_A - \nu_B$ was varied from 40 to 90 MHz in steps of 10 MHz to select different orientations of the nitroxide radicals due to the anisotropic nitrogen hyperfine tensor (see also chapter 4.3.1.1). The oscillation frequency, the modulation depth and the damping of the PELDOR signals change as a function of the selected frequency offset $\Delta\nu$, as shown in Figure 25. Such a frequency offset dependency indicates that the relative orientation between the two **Ç-**labels contributes to the pattern of the PELDOR signal. The damping of the dipolar oscillations for **DNA5,16** becomes more pronounced with decreasing the frequency offset $\Delta\nu$ from 90 to 40 MHz. The time traces of **DNA2,13** show the opposite effect. The PELDOR signals for **DNA2,16**, which is **Ç-**marked close to the end of each helix depend weakly on the frequency offset, on the other hand, the orientation effect is strongest for sample **DNA5,16**.

The distance distributions were calculated for the three spin-labeled DNAs from the orientation-averaged time traces (Figure A5 in the appendix) by Tikhonov regularization. Analysis in terms of the mean distance and HWHM yields the following results: the sample **DNA5,16** has a interspin distance of 2.7 ± 0.3 nm. The sample **DNA2,13** has the longest distance of 3.3 ± 0.3 nm and a distance of 3.0 ± 0.5 nm was obtained for **DNA2,16**. Stronger damping of the oscillation is correlated with an increase in the width of the distance distribution and thus with an increased conformational flexibility of the biomolecule. Here we observe a relatively strong damping of the oscillations in the time traces and in the corresponding broad distance distributions. We infer from this that the experimental PELDOR data indicate a high conformational flexibility of the DNA structure. The spin label, which is stacked within the helix, does not exhibit independent flexibility and therefore the higher flexibility observed here is a direct result of the flexibility of the DNA (*vide ante*).

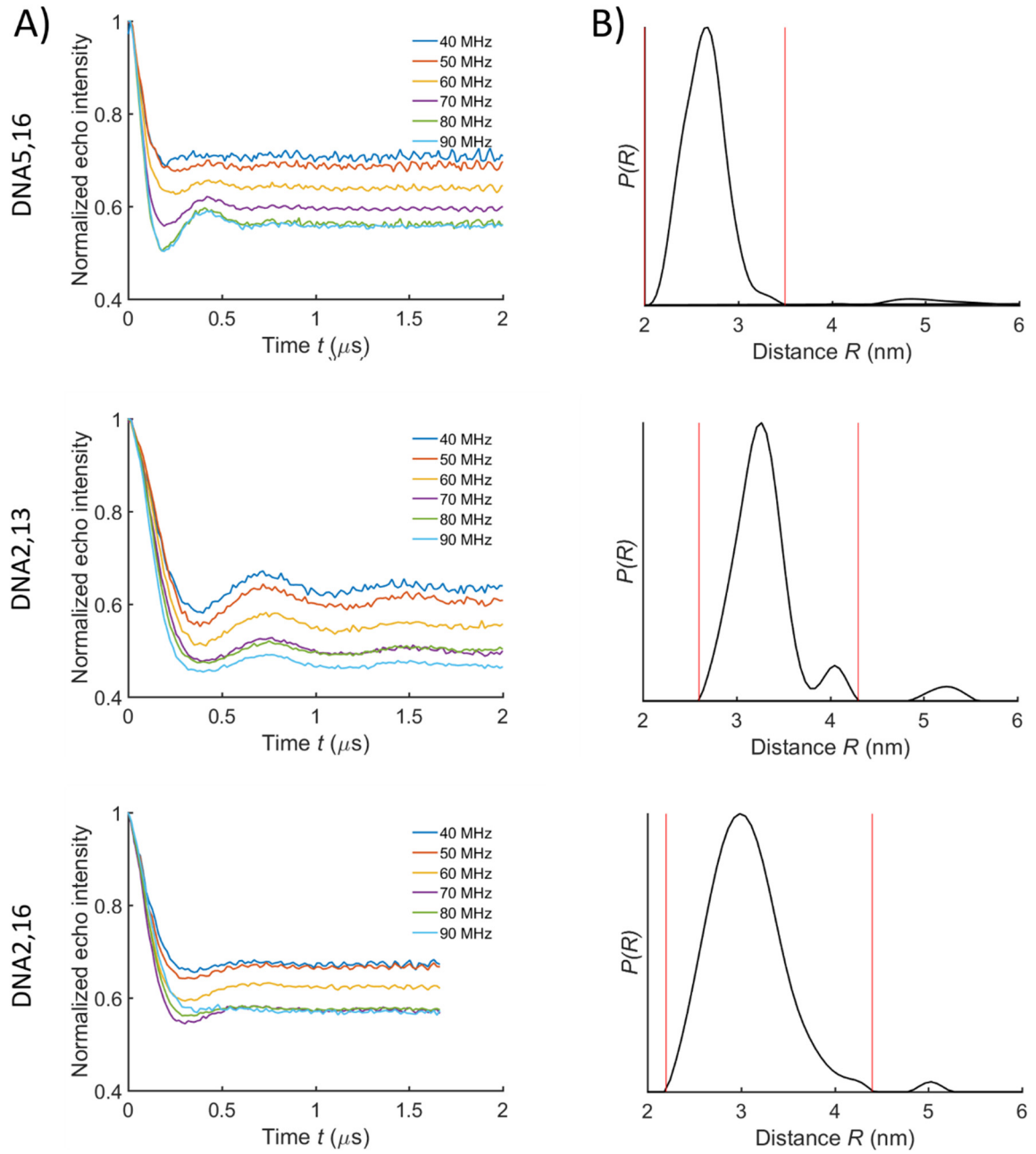

Figure 25: Experimental background-divided PELDOR time traces recorded at X-band frequencies for DNA2,13, DNA5,16 and DNA2,16 and corresponding distance distributions. (A) Experimental X-band PELDOR time traces recorded with different frequency offsets $\Delta\nu$ ranging from 40 to 90 MHz for **DNA5,16**, **DNA2,13** and **DNA2,16**. (B) Distance distributions obtained by a Tikhonov regularization of the orientation-averaged X-band PELDOR time trace. The orientation-averaged and background-divided time traces of **DNA5,16**, **DNA2,13** and **DNA2,16** at X-band frequencies can be found in the appendix (Figure A5). The raw time traces and experimental details can be found in the appendix.

The Q-band PELDOR time traces show negligible orientation dependency (Figure 26). A slightly stronger angular correlation effect can be observed for **DNA5,16** which was also observable in the PELDOR data at X-band frequencies.

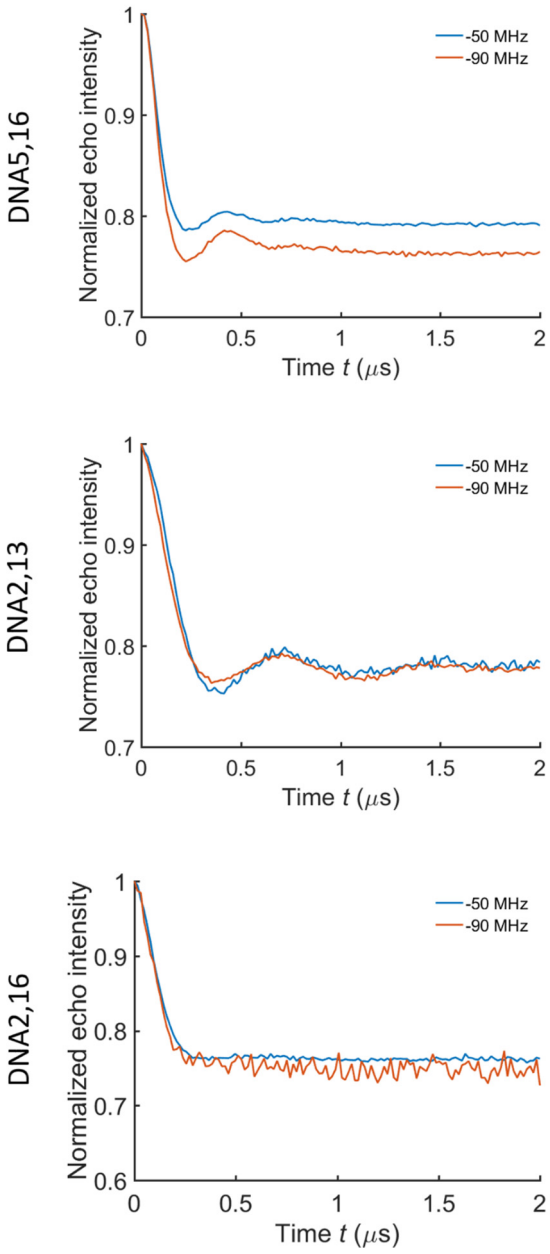

Figure 26: Experimental PELDOR time traces with a frequency offsets Δν of 50 and 90 MHz for DNA5,16, DNA2,13 and DNA2,16 recorded at Q-band frequencies. The raw time traces and experimental details can be found in the appendix.

The PELDOR experiments at G-band frequencies were performed on a home-built 180 GHz pulsed EPR spectrometer[36-37] for the samples **DNA2,13** and **DNA2,16**. The external magnetic field position was varied and the frequency offset $\Delta\nu$ was kept constant ($\Delta\nu$ = 60 MHz) to record the PELDOR time traces. The modulation frequency, depth and damping of the PELDOR signals change as a complex function of pump and probe position in the EPR spectra, as shown in Figure 27. This is a clear indication that the two **Ç**-labels have a specific relative orientation to each other. The most pronounced dipolar oscillation

appeared on a time trace recorded half way between the low field edge (g_{xx} position) and the maximum of the EPR spectrum (g_{yy} position) for **DNA2,13**. Dipolar oscillations could be observed in all PELDOR time traces until detecting at the high-field edge (g_{zz} position) (Figure 27A). However, the g_{zz} position at the high-field edge was not detectable due to a weak signal-to-noise ratio. These experimental G-band data were both used as an independent test of the structural model obtained from the analysis of X-band PELDOR time traces and later for a global fit.

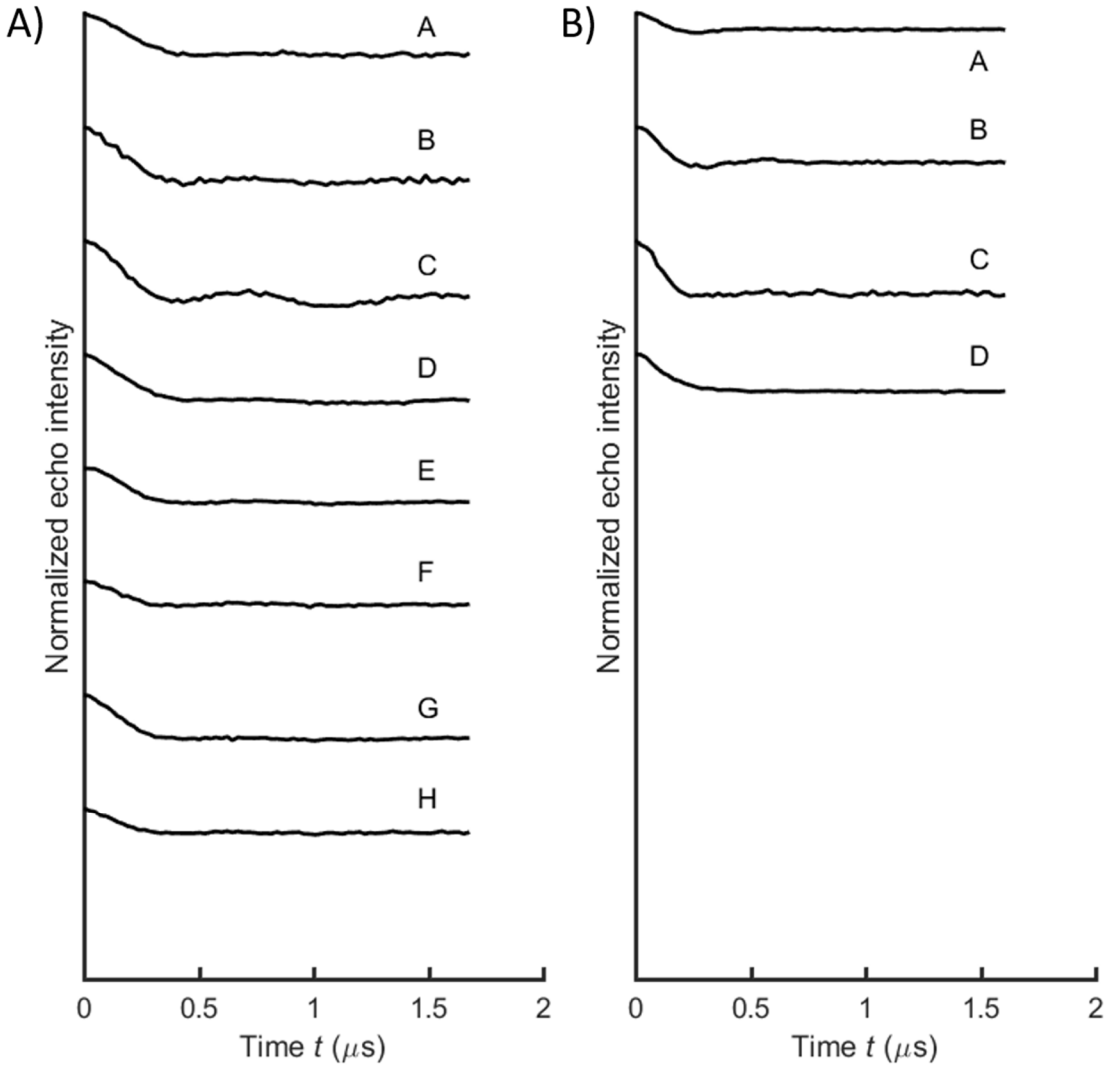

Figure 27: Experimental PELDOR time traces recorded at G-band frequencies. Time traces are recorded for (A) **DNA2,13** and (B) **DNA2,16**. The field positions A-H are marked in Figure A2 in the appendix. The raw time traces and experimental details can be found in the appendix. The time traces have been shifted in the direction of the y-axis for an easier visual inspection.

5.1.2.2 Protocol for ensemble determination

In order to gain insight into the conformational flexibility of the bent DNA, a quantitative analysis of the orientation-selective PELDOR data was performed. Figure 28 shows schematically the two-step strategy that was utilized. The structure calculations were done by Dr. Kazemi using CYANA[133-134], a program for the calculation of three-dimensional structures of biomolecules, the research group of Prof. Dr. Güntert.

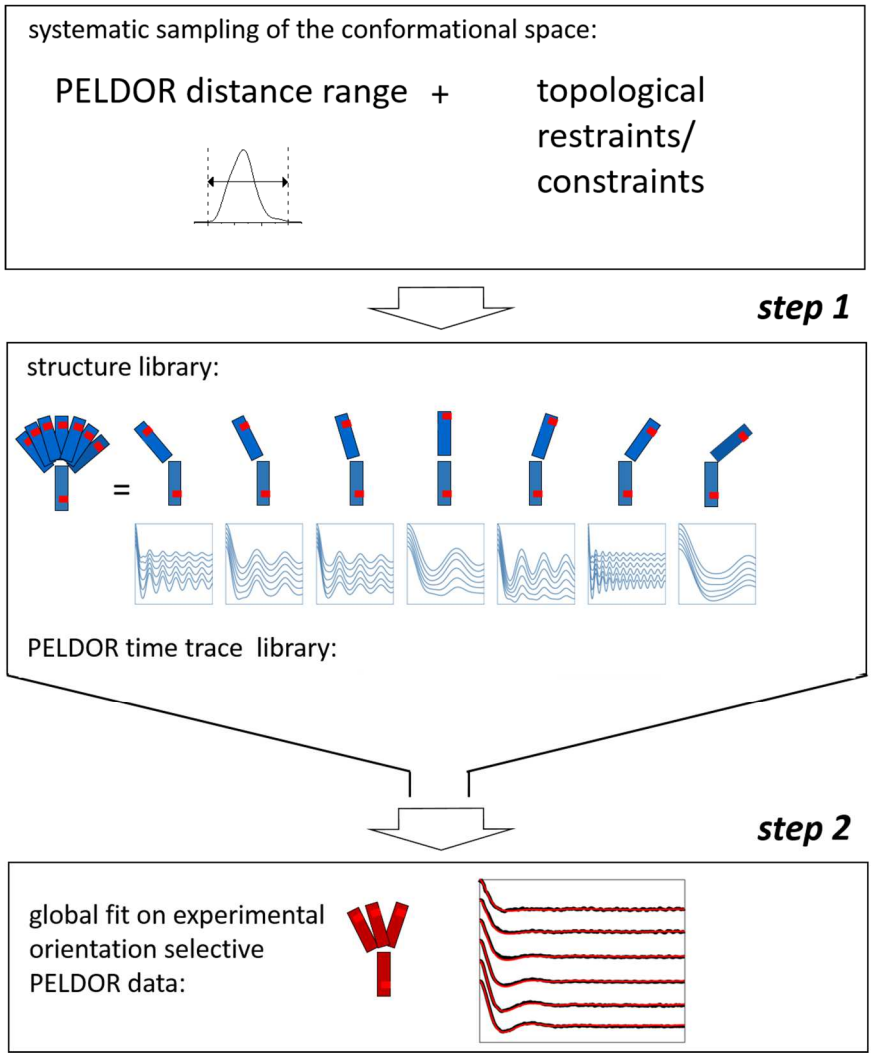

Figure 28: Schematic representation of the structure determination protocol using distance and orientation PELDOR information and distance restraints derived from NMR. In the first step (step 1) a broad conformational library was generated using the NMR restraints and the distance ranges obtained by PELDOR. Next the corresponding orientation-selective X-band PELDOR data is simulated for each structure in the structure library. In the final step (step 2) the library of time traces is used to fit the experimental time traces. Thereby, a small subset of pre-simulated PELDOR time traces that best fit the experimental time traces is selected from the library.

Step 1:

In the first step of the protocol, a library of about 15,000 structures containing a broad variety of conformations was generated that broadly samples the conformational space restricted by the PELDOR restraints. NMR restraints and PELDOR distance ranges were used; however there are examples in the literature where sampling of inter-helical Euler angles[122] or molecular dynamic simulations[123] have been used to generate such libraries. Three distance restraints between the **Ç**-pairs, each situated in one of the three DNA constructs, were added to the NMR restraint set and systematically varied in length (in steps of 0.5 Å with lower and upper distance bounds set at ± 0.25 Å from the target distance of each distance restraint). The distance ranges, from which the distance values were selected, were based on the PELDOR distance distributions (Figure 25B, The distances were restricted for **DNA5,16** to 2.0–3.5 nm, for **DNA2,13** to 2.6–4.3 nm and for **DNA2,16** to 2.2–4.4 nm). A 10 times higher weight than for the NMR distance restraints was chosen for the PELDOR-derived, to guarantee the fulfillment of these additional distance restraints during the structure determination. 500 structures were calculated and the 20 conformers with the lowest CYANA target function were kept for each combination of the three distance values. The target function, defined as the sum of the squared deviations with respect to the NMR restraints, the PELDOR distances, and the steric lower distance bounds, permits a measure of how well these restraints are fulfilled. Those structures showing a CYANA target function value below a threshold of 4.0 $Å^2$ were taken to guarantee the agreement of the generated structures with the NMR data. This cutoff value was set below the maximum target function value found among the 20 best conformers which were obtained in a CYANA structure calculation using only the NMR data. The calculated structures are in agreement with the NMR data as good as the structures calculated without any additional PELDOR restraint. In total, 14,254 structures were calculated which are in agreement with all types of restraints using this procedure.

The generation of a structure library that takes into account the additional long distance PELDOR data directs the conformational sampling towards structures of the bent DNA molecule that are not favored by using NMR restraints alone. It is worth noting that, notwithstanding this, the value of the CYANA target function remained low within the distance ranges obtained by PELDOR, as shown Figure 29. Only distance restraints that were set to values outside of the experimental PELDOR distance boundaries lead to a significant rise in the CYANA target function. This indicates that more conformations than

those in the published bundle[121] are in agreement with the NMR restraints. Reversely, this also means that the NMR data lack information on the relative orientation of the stems, and therefore about the global structure and conformational dynamics of the bent DNA.

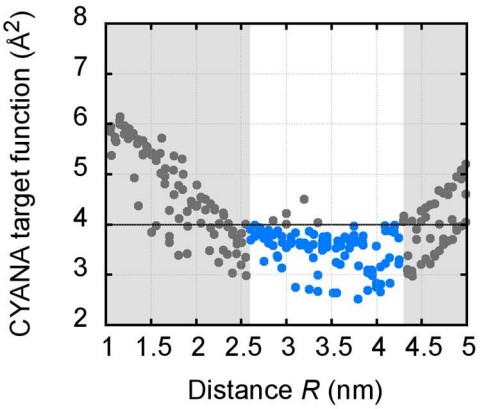

Figure 29: CYANA target function values as a function of the spin-spin distance between the Ç spin labels is shown exemplarily for DNA2,13. The other distance restraints were as the original NMR structure. The target function cutoff for accepted structures is indicated by the black line at 4 Å^2. All structures were in very good agreement with the NMR data (blue), within the corresponding PELDOR distance range (white) and under the target function value of 4 Å^2.

Next, for each of the $N = 14{,}254$ obtained NMR structures in the structure library the corresponding orientation-selective X-band PELDOR data were simulated. Each structure was represented by 18 time traces (3 labeling positions and 6 frequency offsets) in the library of the PELDOR time traces. The experimental parameters, such as pulse lengths, flip angles, magnetic field positions, pump and probe frequencies were chosen to be the same as in the experiment. All equations, which are necessary for the PELDOR data simulation, can be found in chapter 4.3.1.3 and in the following references.[95, 97, 109, 135]

Step 2:

In the second step, the library of time traces was used to fit the experimental time traces. For this purpose, an extended version of the search algorithm developed by Dr. Andriy Marko[95] was applied to select from the library a small subset of pre-simulated PELDOR time traces that reconstruct all experimental time traces recorded at X-band frequencies from the three spin-labeled samples simultaneously. The iterative fitting algorithm searches for signals in the library that minimize the error function Err_n (eq. 37 in chapter 4.3.1.3) between the experimental and the sum of selected simulated signals. The sum of selected simulated

signals is directly correlated to an ensemble of structures from the structure library. This ensemble consists of 100 structures with possible multiple occurrence of one structure, since 100 iterative fitting steps were performed and each conformer can be selected several times. Thereby, the resulting structures ensured a simultaneous fit to the experimental X-band PELDOR time traces. Thus, the relative spin label orientations, distances and the statistical weight of each conformation is implicitly derived by the fit. During the fitting procedure, the deviation between the selected pre-simulated and experimental time traces decreased drastically within a few iterative steps resulting in an almost perfect fit to the experimental data.

The fitting algorithm searches for a combination of time traces whose modulation frequency and damping describes the experimental PELDOR time traces, since a variation in the modulation depth can be due to incomplete excitation of the pumped spins. However, in the case of two rigid spin labels, the modulation depth can also depend on their relative orientation. Thus, variation in the modulation depth of 5–10% was allowed, which is the error of reproducibility from experiment to experiment (at X-band frequencies, if the experiments are recorded under the same conditions).[130]

5.1.2.3 Characterization of the structural ensemble

As a result, the structures corresponding to the selected time traces represent a structure bundle that is in accordance with the experimental NMR and PELDOR data. Further analysis of the selected structural ensemble reveals a detailed picture of both the structure and the conformational dynamics of the bent DNA. The bundle of structures obtained by this approach reproduces the experimental PELDOR time traces, which can be seen in Figure 30. Especially, the damping of the oscillations and oscillation pattern agrees very well with the experimental PELDOR data set.

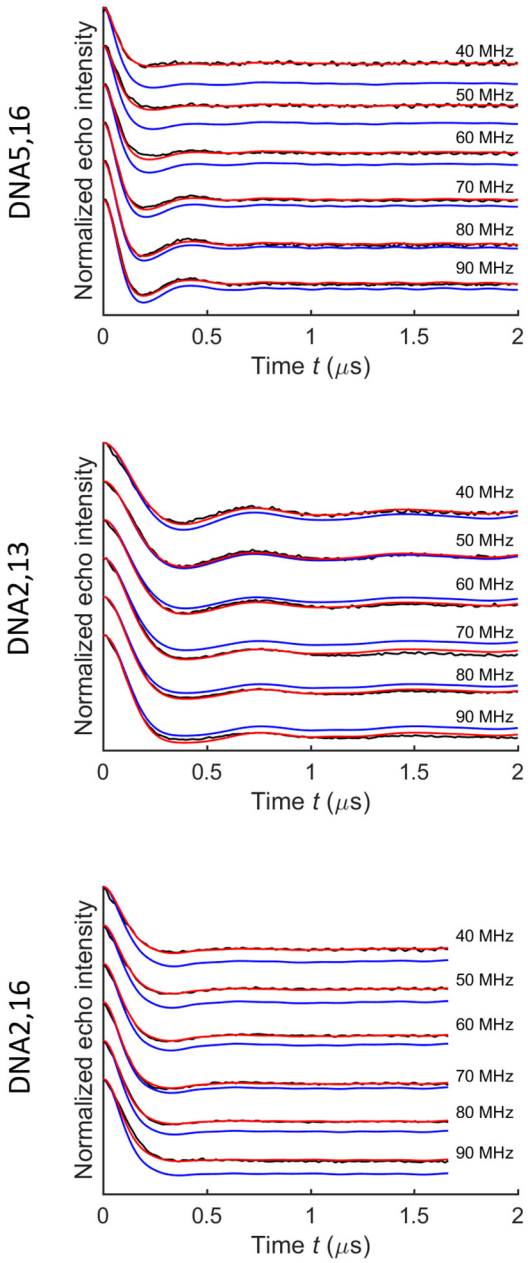

Figure 30: Fitted X-band PELDOR time traces obtained by the combined NMR/EPR approach. Comparison of experimental (black) and simultaneously fitted (red rescaled, blue not rescaled) X-band PELDOR time traces for different frequency offsets $\Delta\nu$ for **DNA5,16**, **DNA2,13** and **DNA2,16**. Fitted PELDOR time traces were obtained by the combined EPR/NMR approach for biomolecular structure determination. The simulated PELDOR traces (red) have been adjusted to the experimental traces for $t_{max} = 2.0$ µs for better comparison. The time traces have been shifted in the direction of the y-axis for an easier visual inspection.

The corresponding structural ensemble, in which helix II is aligned for all structures is shown in Figure 31. The weights of the selected, simulated time traces correspond to the number of structures within the ensemble, which is called 'statistical ensemble'.[119] In this figure, the

color saturation and transparency represent the occurrence of the individual structures within the ensemble: the darker the color, the higher the statistical weight of the structure. Figure 31 gives a description of the dynamical behavior of the considered DNA construct. The helices are shown as boxes in Figure 31A to visualize their relative orientation. An atomistic representation is shown in Figure 31B. The dynamics of the DNA molecule is characterized essentially by a broad continuum of conformers with a narrow region of higher population.

The kink angle φ and the twist angle θ between the two helical parts (Figure 21) were quantitatively determined from the resulting structural ensemble, represented in Figure 31 (Figure 32). The calculation of the helix angles was the same as in Woźniak *et al.*. The helix axes were obtained by calculation of the first principle component of the heavy atoms involved in base-pairing hydrogen bonds.

Figure 32 shows density plots that compare the population of θ, φ pairs between the structure library (step 1, Figure 32A) and the structures that were selected from the library using the protocol depicted in Figure 28 (step 2, Figure 32B). The density plot for the structure library (Figure 32A) shows that the distribution of twist and kink angles is broad and has some correlation between them. As it depends on both helix angles, this density plot clearly shows topological restrictions and topologically preferred inter-helical orientations.[136] This was expected since the structure library was calculated based on NMR restraints and repulsive van der Waals interactions. The distribution of the φ and Θ angle of the structure library in step 1 of the two-step procedure (Figure 32A) has different weights compared to the structures selected in the procedure of step 2 (Figure 32B). This indicates that the selection of the structures in step 2 does not depend on the frequency of occurrence of a structure within the structure library obtained in step 1.

The θ, φ pairs for the published NMR structures[121] of this DNA were in the high-populated region of the structure landscape derived from the structure library (Figure 32A and B, black points). As expected, the broader conformational ensemble, derived from the combined EPR/NMR approach, agrees with the published NMR structure bundle (Figure 32B). On the other hand the mean kink angle $\varphi = 90 \pm 20°$, which was obtained by the PELDOR approach, differs from the mean kink angle of $73 \pm 11°$ obtained by the NMR study[121]. The distributions are visibly shifted but still within their error range. However, the structures with the third and the fourth lowest target function value of the published NMR structures agree with the most populated structures found by this approach (marked by 3 and 4 in Figure 32, respectively).

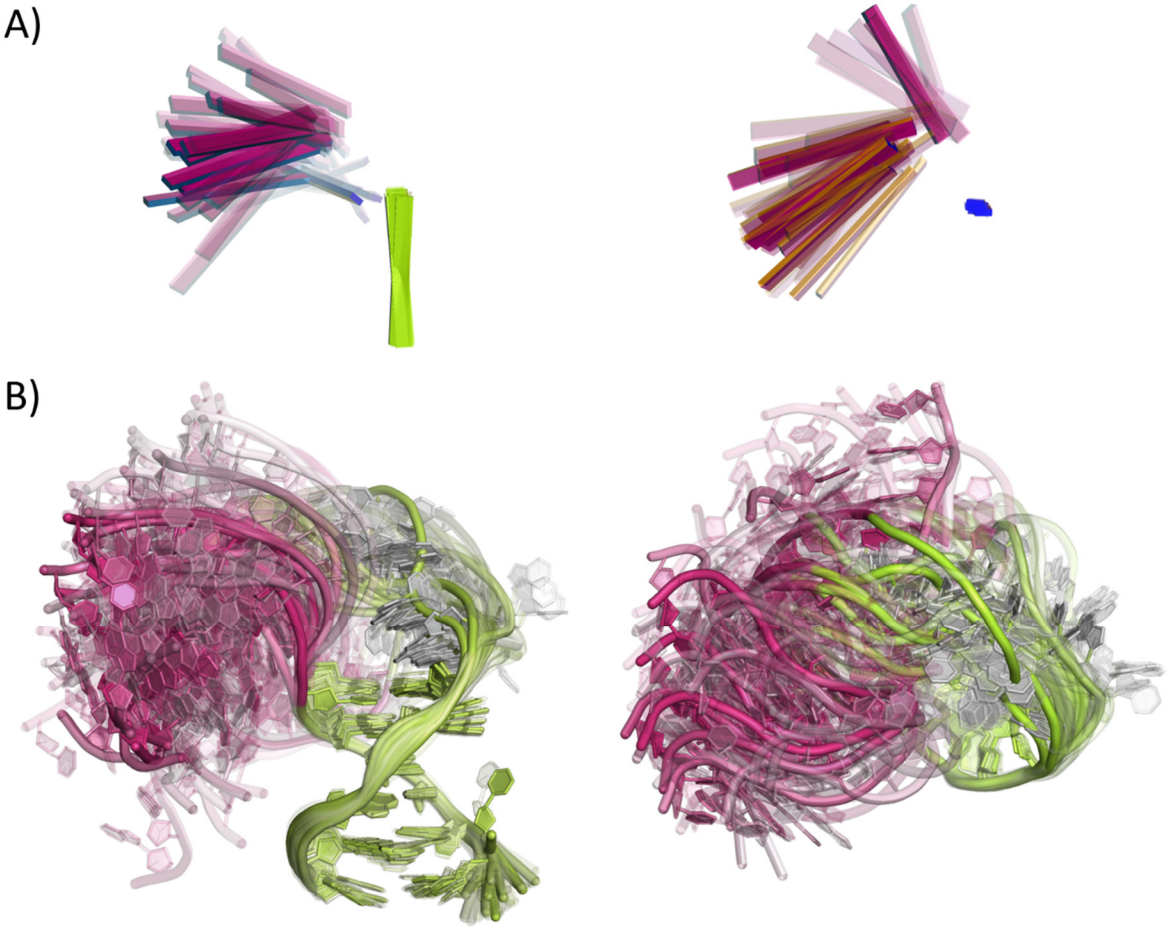

Figure 31: Structural ensemble derived from the two-step approach. (A) The structures were aligned on helix II, whose helix axes are indicated as boxes. To visualize the rotation of the helices relative to each other, the sides of the boxes are differently colored. The population of the individual structures within the ensemble is represented by the color saturation and transparency. Viewing directions are shown from the side (left) and from the top (right) of helix II. (B) Atomistic model of the structural ensemble from the side and the top of helix II. The color saturation and transparency represent the population of each structure within the ensemble. The structures were overlaid by helix II, in which helix II and the bulge are colored in green. The graphical representation was done by Dr. Sina Kazemi. For comparison with the original published NMR bundle see Dornberger *et al.*.[20]

A similar DNA containing five adenines (5A) in the bulge has also been studied by FRET.[20] The base sequences differ for the DNA helices, however the kink and twist angles depend predominantly on the five-adenine bulge. The mean kink angle $\varphi = 90 \pm 20°$, which we obtained by the PELDOR approach, differs from the kink angle around 73° obtained by the FRET-based models.[20] The FRET experiments have also shown a much broader conformational space compared to NMR similar to the structures from the EPR/NMR approach (Figure 32B, green circles).[20] The phase of the twist angle θ cannot be compared

with the twist angles obtained by FRET since the base sequence differs for the DNA helices used in the FRET and in the presented study. The phase of the θ angle depends on an arbitrarily selected reference atom defining the x-axis of the coordinate system on which the second helix axis is projected and thus is reliant on the base sequence of the considered structure. Nevertheless, the distributions of both ensembles conform in shape and width (Figure 32B, Supporting Information of Woźniak *et al.*[20]).

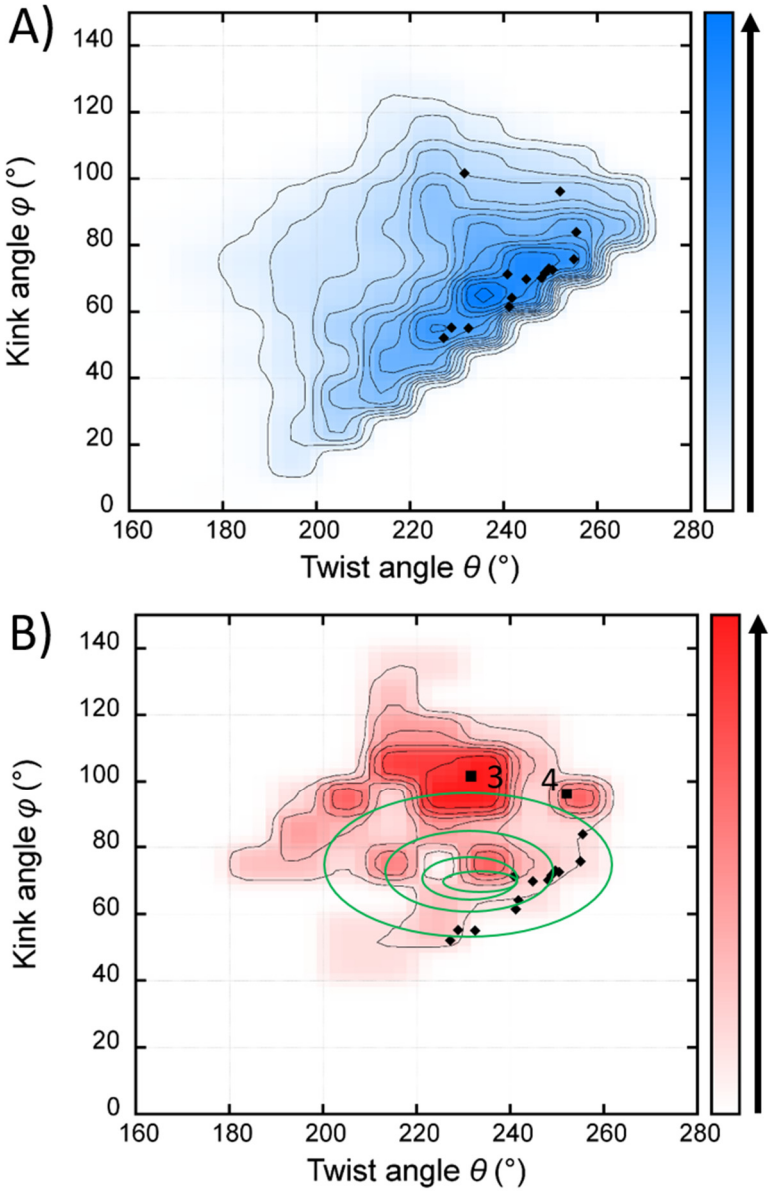

Figure 32: Density plot of twist θ and kink φ angles for all structures in the structure library, for the selected structural ensemble and comparison with FRET and NMR studies. (A) Density plot of θ against φ plotted for all structures in the structure library. The structures from the published NMR structure bundle are highlighted with black diamonds and squares in (A) and (B).[121] (B) θ, φ density plot for the structural ensemble selected out of the structure library by the fit procedure in step 2 of the EPR/NMR approach. The resolution of each density plots was 10° and the data points were smoothed by Gaussians. The structures with the third and the fourth lowest target function value of the published NMR structures are the two squares labeled with 3 and 4, respectively. The height represented by contour lines and the color (red in (A) and blue in (B)) are normalized for both density plots separately and indicate the density occurrence of the structures within the ensemble. The green circles, representing the FRET structure bundle, were extracted visually from the publication of Wozniak and coworkers[20]. The phase of the twist angle θ was chosen arbitrarily since the base sequence of the FRET and the presented studies is not the same.

6 Discussion - Accuracy in obtaining structural ensembles by orientation-selective PELDOR

PELDOR data only provide distance information in a conventional PELDOR experiment using flexible spin labels. However, accurate structure modelling requires multiple distance restraints.[114] In this respect, the additional orientational information of the rigid spin label used in this thesis strongly reduces the total number of spin-labeled samples that are required to give a sufficient number of structural restraints. In principle, these structural restraints give the complete description of a relative orientation of two molecular frames each containing a **Ç-**label and thereby of possible inter-helical orientations. This implies that the **Ç**-label has to be incorporated in a double-stranded helical part of the nucleic acid and is therefore rigidly embedded relative to the three-dimensional bimolecular structure of the studied nucleic acid. However, in the case of flexible systems the number of possible solutions by fitting the experimental orientation-selective PELDOR data gets ambiguous, since different ensembles of spin label conformations or structures might represent the same orientation-selective PELDOR data. At X-band frequencies, the angles γ_1 and γ_2 (Figure 13) cannot be determined, due to the small and equal values of A_{xx} and A_{yy} giving almost no asymmetry in x- and y-directions. This implies that the twist angles θ and ψ of one helix relative to the other cannot be determined, while it is possible to obtain the kink angle φ between both helices; this is shown for the case of the cocaine aptamer. This ambiguity can be solved by orientation-selective PELDOR experiments at high magnetic fields, where more orientational information can be achieved. Nevertheless, the indistinguishability of two nitroxide spin labels remains, since they are spectroscopically identical. The spectra are furthermore insensitive to an inversion of the magnetic field $\vec{B}$, yielding even more possible symmetry-related solutions.[115] In the case of the bent DNA project, thanks to the combination with a specific structural knowledge and labeling scheme (3 spin label pairs in the case of the bent DNA), the degeneracy of the aforementioned symmetry-related solutions should be removed. Consequently, the high-field PELDOR data depend strongly on the inter-helical orientations. There are several ways to validate the uniqueness of the obtained structural ensemble. In the case of the cocaine aptamer project, the range of spin label conformation which were found by using the fitting procedure were removed from the spin label conformation library. The

resulting restricted library was used to fit once again the experimental X-band PELDOR data set. This approach tests whether the conformations selected by the fitting algorithm are essential for the description of the PELDOR data. In contrast, for the bent DNA project orientation-selective PELDOR data at different magnetic field strengths and for three different positions of the **Ç**-labels were recorded, which could be used either for the selection of conformations from a structure library or for the validation of the obtained structural ensemble. The structural ensemble was used to predict high-field PELDOR data and for a global fit.

6.1 Flexibility and conformation of the cocaine aptamer studied by PELDOR

6.1.1 The limit of angular resolution from orientation-selective PELDOR data at X-band frequencies

A pronounced change in the modulation depth of the PELDOR signals depending on the probe frequency offset $\Delta\nu$ after cocaine binds to aptamer **1** was observed. In contrast, in the absence of cocaine no such dependence could be observed (Figure 15). This can be interpreted as non-random orientations between both spin labels in the cocaine-bound state. However, as mentioned in chapter 4.3.1, the modulation depth parameter is also sensitive to experimental parameters. It was shown that the modulation depth is reproducible by less than 10% error from experiment to experiment for our X-band spectrometer setup, if the experiments are performed under the same experimental conditions.[130] This error will be even lower within an orientation-selective PELDOR data set, if each offset measurement is performed in the same experimental session. Therefore, the variations of the modulation depth as a function of the frequency offset in these experiments (Figure 15B-D) reflect different distributions of the relative orientations between the two spin labels and cannot be disregarded as experimental errors. This is in contrast with the experimental PELDOR time traces of the aptamer **1** without cocaine (Figure 15A), where the modulation depth differs within the experimental accuracy of 10%. This confirms that the cocaine aptamer in the absence of cocaine is a rather flexible junction. In this case no angular correlations are visible in the experimental orientation-selective PELDOR data and no changes were observed in the oscillation frequency or damping for different frequency offsets. This was also confirmed by fitting those data using different

spin-spin orientations (Figure 19).

Due to the rigidity of the **Ç**-label, the estimation of the relative orientation of such moieties, and thereby of the two helices of the aptamer where they reside, is possible. An iterative fitting procedure of the orientation-selective PELDOR data recorded at X-band frequencies has determined the distance R and the three angles $(\alpha_2, \beta_1, \beta_2)$ describing the relative orientation of the two spin labels **Ç₁** and **Ç₂**. The angles γ_1 and γ_2 cannot be determined from X-band PELDOR measurements due to small values of A_{xx} and A_{yy}, such that the asymmetry in x- and y-directions cannot be determined (see also chapter 4.3.1). It should be pointed out that these angles are required for a complete description of the relative geometry between both **Ç**-labels. This implies that the twist angle θ of one helix relative to the other cannot be determined, while it is possible to obtain the kink angle φ between both helices from the X-band orientation-selective PELDOR data sets. Therefore, it is not possible to get a unique solution for the relative orientation of both helices out of this experimental orientation-selective PELDOR data recorded at X-band frequencies. This limitation could in principle be circumvented by performing orientation-selective PELDOR measurements at higher magnetic fields, where the x- and y-component of the anisotropic g-tensor are spectrally resolved. A frequency of 95 GHz or above would be needed to achieve a sufficient resolution in the x- and y-directions. Moreover, two nitroxide spin labels are generally indistinguishable and the spectra are insensitive to an inversion of the magnetic field $\vec{B}$ (for instance, the nitroxide radical normal ($\vec{A}_{zz}$) of each **Ç**-label can point up or down, which turns the helix upside down).[115] This yields a family of symmetry-related solutions. However, in most cases *a priori* knowledge about the biomolecule can help to obtain a consistent description of its conformational flexibility. In the specific instance, the additional geometrical knowledge about the helices restricts the conformational space of possible helix orientations and provides further refinement of the simulation.

6.1.2 Validation of the structural model by excluding spin-spin orientations during the fitting procedure

The geometrical parameters resulting from the fit algorithm of the PELDOR data might not be the only parameter set which leads to fits with a comparable agreement with the experimental data. This is especially the case for rather flexible systems.[95] In order to test for this hypothesis the spin label conformations, which were essential to fit the experimental data (Figure 33B, blue squared region) were removed from the library. This restricted library was used to fit the experimental PELDOR data set in order to test the robustness of the fit solution. The fit gets significantly worse, as can be seen in Figure 33A. Interestingly, the new found spin label conformers border on the edges of the cutregion (Figure 33B), next to the missing spin label conformations. These results confirm that the found spin label conformations from the fit with the complete library (Figure 19) are essential and not a solution replaceable by other ensembles of spin label conformations.

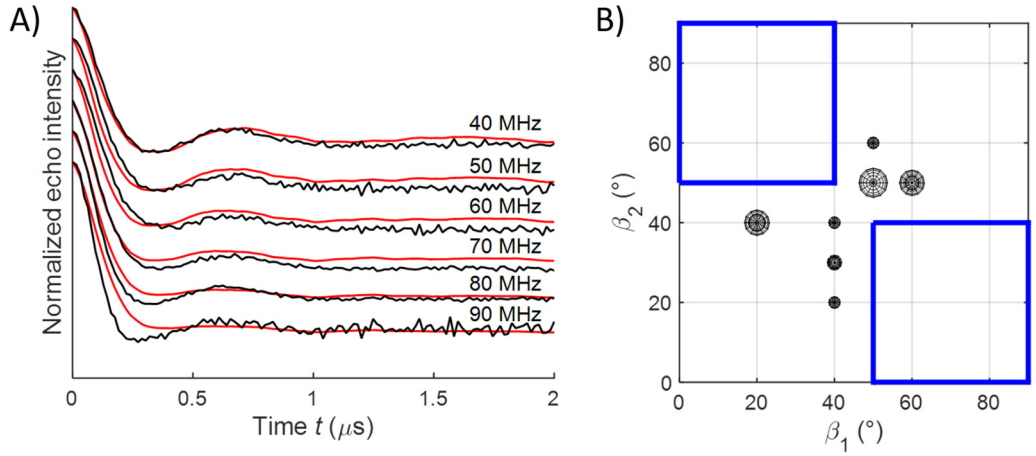

Figure 33: Fit by an ensemble of spin label conformers from a restricted spin label conformer library. (A) Experimental X-band orientation-selective PELDOR data set for the cocaine-bound aptamer **1** in the presence of cocaine (black) and fit by an ensemble of spin label conformers (red) from a restricted spin label conformer library. The time traces have been shifted in the direction of the y-axis for an easier visual inspection. (B) Angles β_1 and β_2 of the new spin label conformers found to best fit the experimental orientation-selective PELDOR data set. A spin label conformer is represented by a circle whose radius corresponds to the weight of the conformer in the fit. The blue-squared regions represent the spin label orientations that were removed from the spin label conformation library. For comparison with the fit to the complete spin label conformation library, see also Figure 19.

6.2 A combined EPR/NMR approach for ensemble determination of a bent DNA molecule

6.2.1 Validation on high-field orientation-selective PELDOR data

As was shown in the previous chapter for the cocaine aptamer, only the kink angle between the two helices can be described by using X-band PELDOR data, whereas the twist angles of one helix relative to the other cannot be determined from only one spin label pair.[117] This is due to the x- and y-components of the hyperfine tensor not being spectrally resolved at X-band frequencies. This is especially an issue for rather flexible systems, where the solutions from data on one **Ç**-labeled sample alone might not be unique (as this fitting is an ill-posed problem). For the considered system, a bent DNA, the structures were selected from the structure library such that the corresponding simulated time traces agree simultaneously with all X-band time traces from the three different **Ç**-labeled samples. An ensemble in agreement with the data of all three DNA samples is expected to be much less ambiguous, in spite of the fact that a fit to the time traces of the individual spin label pairs shows many possible solutions.

The validity of the results was checked using orientation-selective measurements at higher magnetic fields, where the x- and y-component of the anisotropic *g*-tensor become spectrally resolved. The resulting structural bundle from the fit based on the experimental X-band PELDOR data was used to predict high-field data recorded at Q- and G-band frequencies. These PELDOR data had not been used for the construction of the structure library or for the selection of the structures described above. The structural bundle reproduces the experimental G-band PELDOR data very well, except for the modulation depth (Figure 34). The discrepancy in the modulation depth was expected due to the limited reproducibility of this parameter at this frequency band, which is only 39 to 74% with a confidence of 95% using a Student's *t*-distribution. Further information regarding the reproducibility of PELDOR time traces at G-band frequencies can be found in the appendix chapter 10.2.5. The discrepancy in the modulation depth roots in the variations of the experimental conditions. More in detail the B_1-field was not always consistent and reproducible. For this reason, the modulation depth was neglected for the analysis of these data.

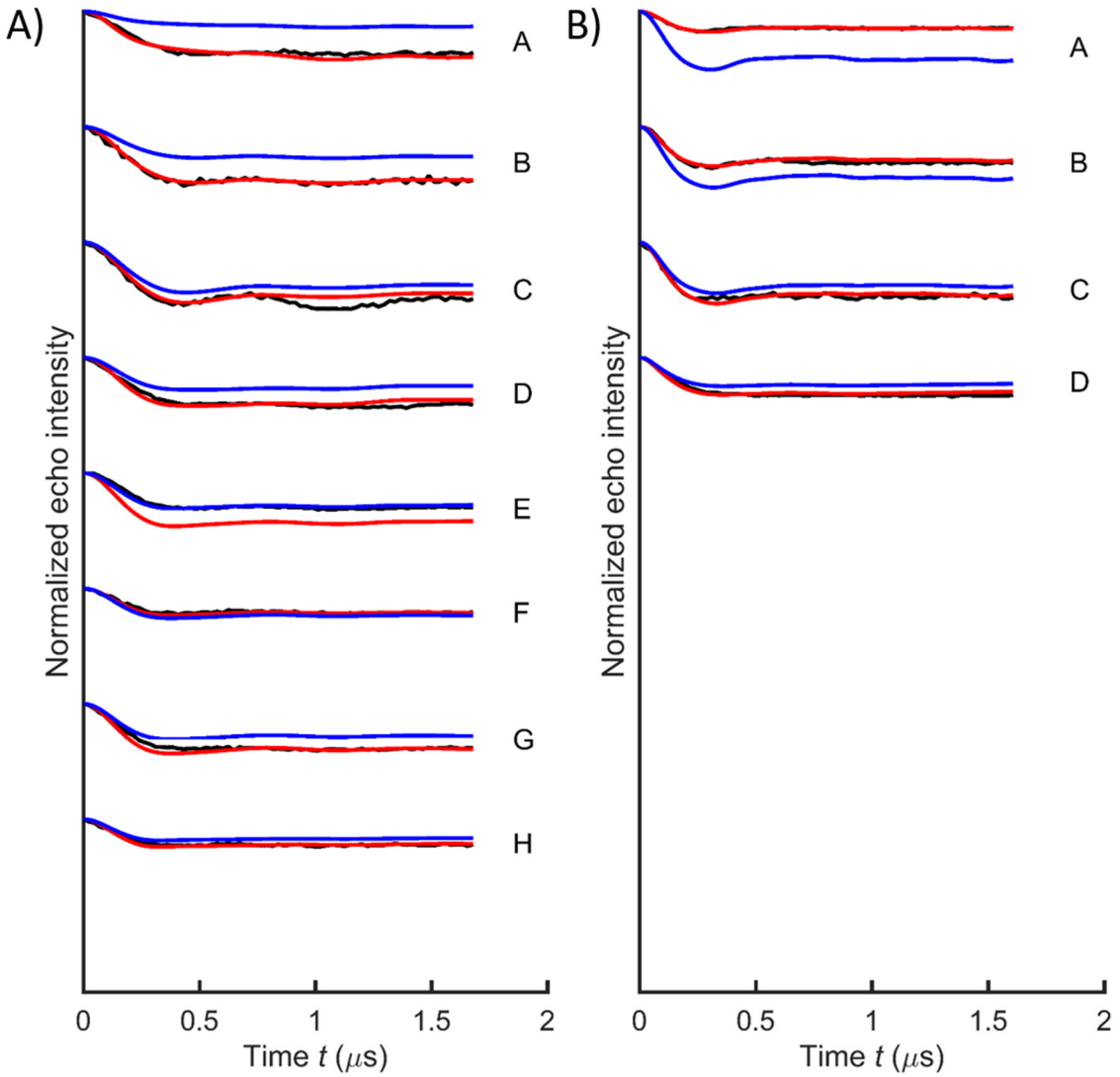

Figure 34: Prediction of orientation-selective PELDOR time traces recorded at G-band frequencies. Experimental G-Band PELDOR time traces (black) and predicted orientation-selective G-band PELDOR time traces of **DNA2,13** and **DNA2,16** from the structural ensemble fitting the experimental X-band PELDOR data (blue) at several magnetic field positions. The field positions A-H are marked in Figure A2C. The predicted PELDOR traces (red) have been adjusted to the experimental traces for better comparison. The time traces have been shifted in the direction of the y-axis for an easier visual inspection.

In addition the structural ensemble from the fit based on the experimental X-band PELDOR data was used to predict the Q-band PELDOR time traces. The prediction reproduced well the damping and the dipolar oscillation frequency of the experimental time traces (Figure 35).

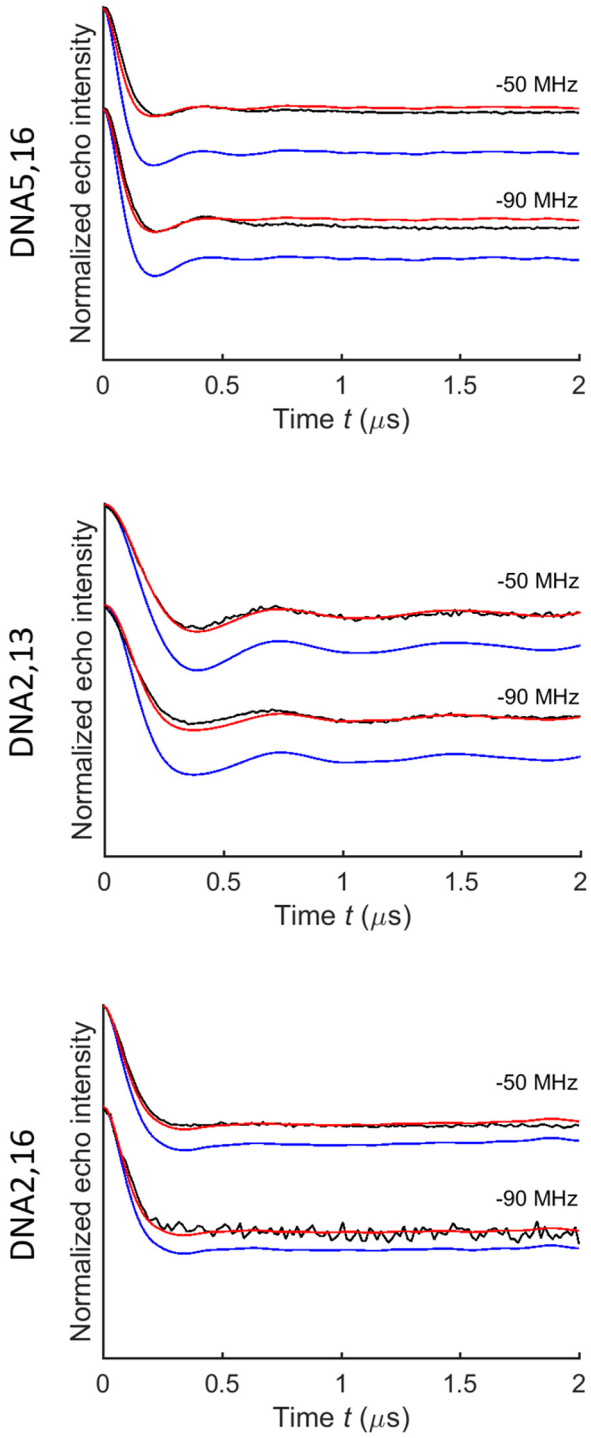

Figure 35: Prediction of orientation-selective PELDOR time traces recorded at Q-band frequencies. Experimental Q-Band PELDOR time traces (black) and predicted Q-Band PELDOR time traces from the structural ensemble fitting the experimental X-band PELDOR data of all DNA samples (blue). The predicted PELDOR traces (red) have been adjusted to the experimental traces for better comparison. The time traces have been shifted in the direction of the y-axis for an easier visual inspection.

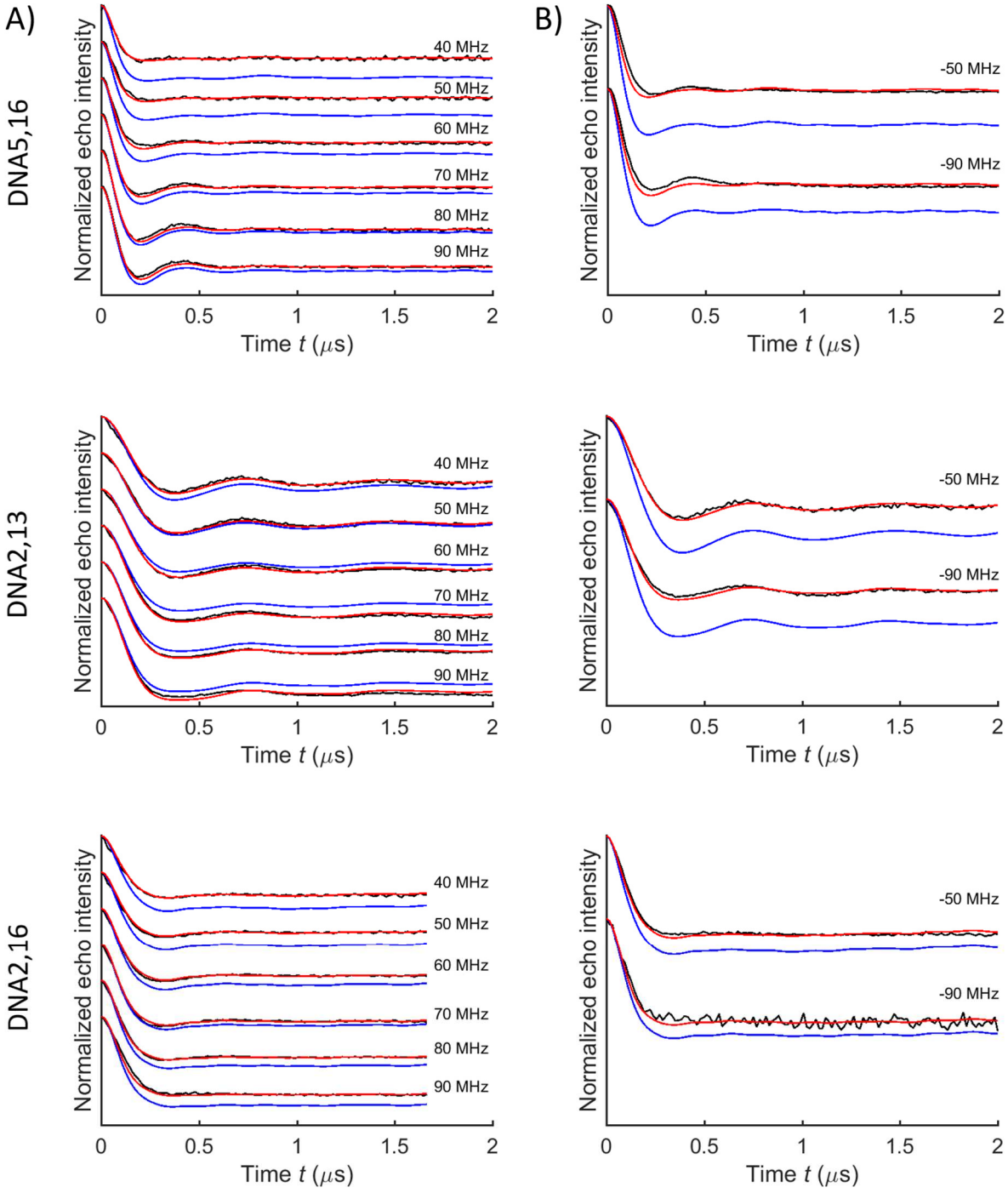
A)
B)
DNA5,16
DNA2,13
DNA2,16
Normalized echo intensity
Time t (μs)
40 MHz
50 MHz
60 MHz
70 MHz
80 MHz
90 MHz
-50 MHz
-90 MHz
0
0.5
1
1.5
2

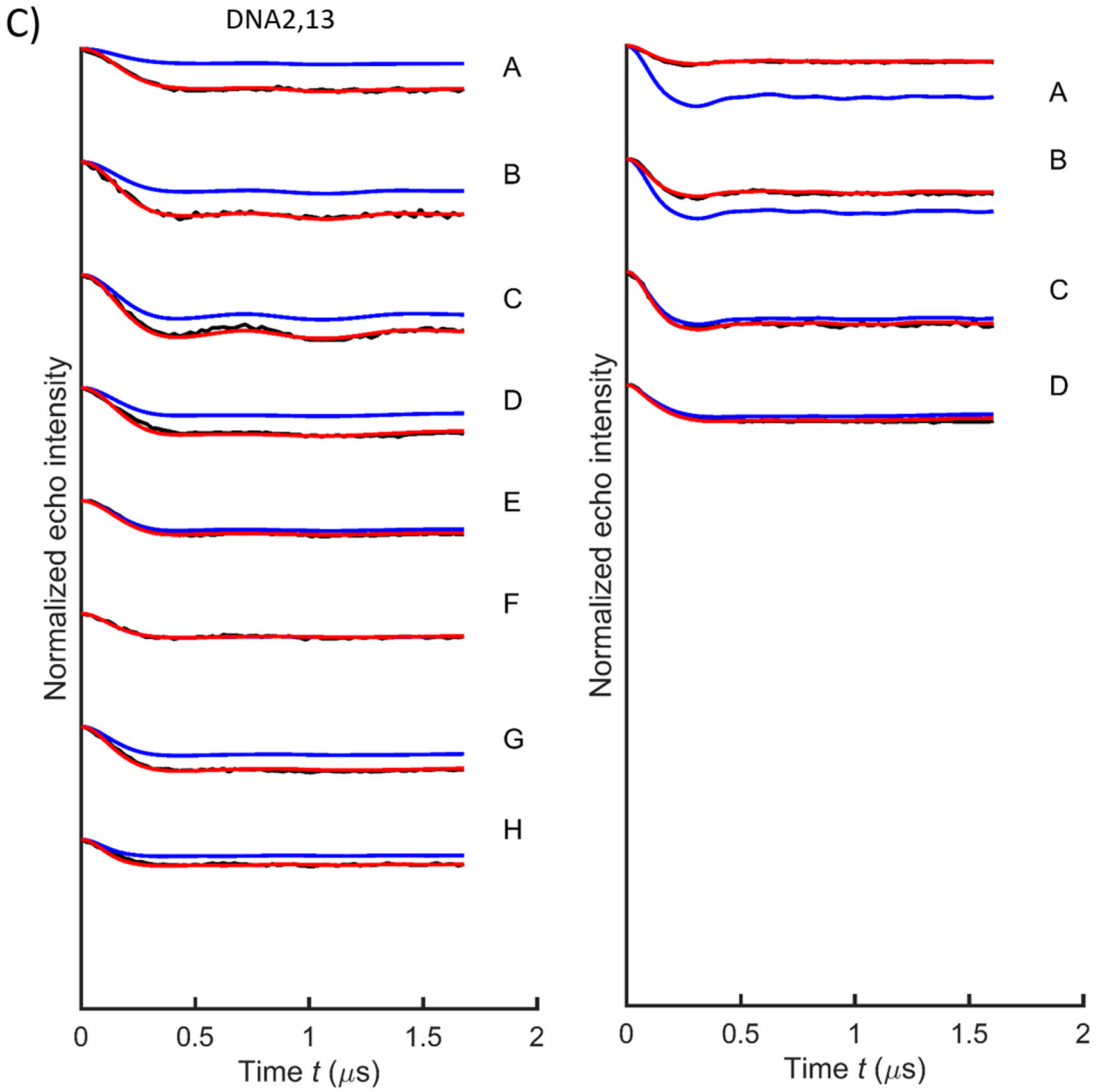

Figure 36: Global fit of all the experimental orientation-selective PELDOR data obtained by the combined NMR/EPR approach. Comparison between the experimental PELDOR time traces (black) and the globally fitted PELDOR time traces (blue) at (A) X-band (B) Q-band and (C) G-band frequencies. The predicted PELDOR traces (red) have been adjusted to the experimental traces for better comparison. The magnetic field positions A-H are marked in Figure A2C. The time traces have been shifted in the direction of the y-axis for an easier visual inspection.

All the experimental PELDOR time traces, including the Q- and G-band data, were used for a global fit to test the robustness of our protocol. The reproducibility of the modulation depth at G-band frequencies is within 39-74% (Figure A6). Therefore, the modulation depth was completely neglected during the fitting process. Due to the small modulation depth of the time traces recorded at G-band frequencies (maximal 5%) in comparison to the X-band (about 40%) or Q-band (about 20-30%) data, the deviation of experimental and simulated time traces Err_n

(eq. 37) could be large. Therefore, we consider the error function Err_n of the time traces recorded at G-band frequencies 20 times more than the time traces recorded at X- or Q-band frequencies. The fit gets considerably better, especially for position C. Here the modulation frequency is even better described.

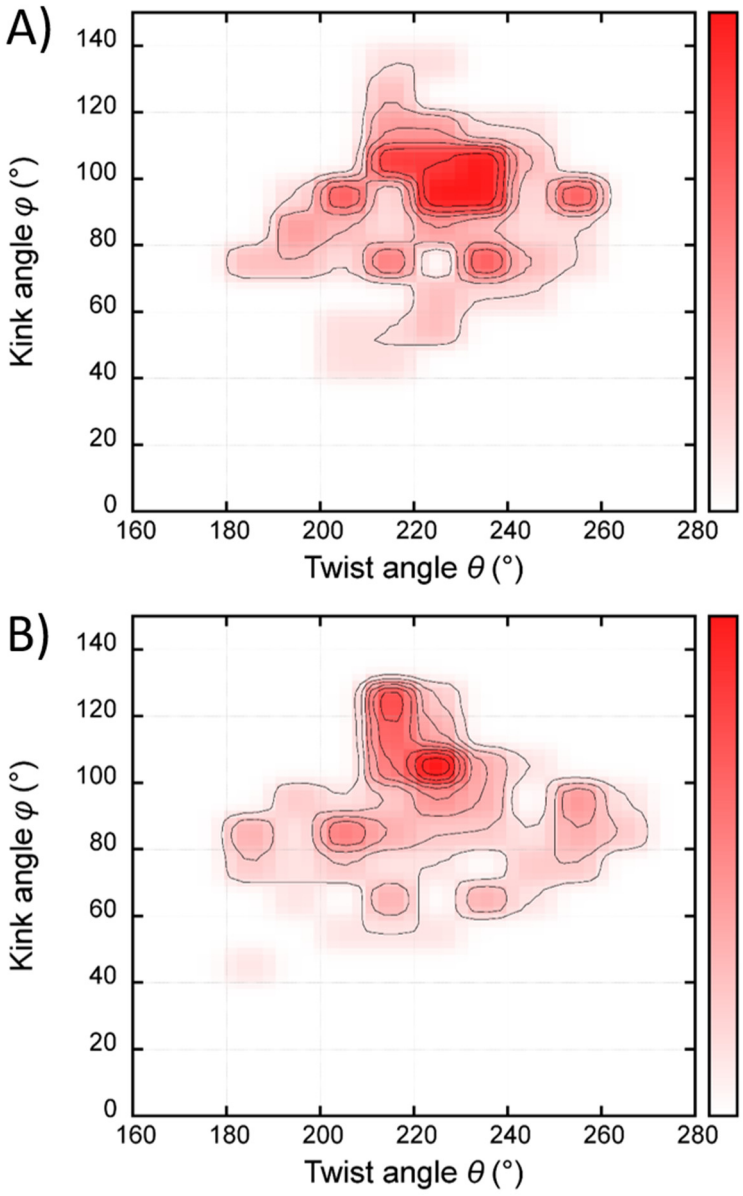

Figure 37: Density plot of twist and kink angles for the selected structure bundle from the fit on X-band PELDOR data and the global fit. (A) θ, φ density plot for the structure bundle selected out of the structure library obtained by the fit procedure in step 2 of the EPR/NMR approach (see Figure 32B). (B) Density plot of twist angle against kink angle of the structures selected by a global fit to all experimental data recorded at multiple magnetic field strengths including X-, Q- and G-band data. The height represented by contour lines and the color are normalized for both density plots separately.

The conformational spaces from the X-band fit and the global fit are similar. This indicates that the X-band data already comprise sufficient information to construct a meaningful structural ensemble.

NMR and FRET experiments are usually performed near room temperature in liquid solution, which is close to physiological conditions for biomolecules. However, PELDOR experiments have to be performed in a state where the biomolecule is immobilized (*e.g.* frozen state) to slow down the fast electron spin relaxation and to avoid averaging of the dipolar coupling due to movements of the molecules. This could be important because freezing might restrict the accessible conformational space of biomolecules.[51, 137] However, in the case of double-stranded DNA, DQC data recorded at room temperature were shown to be in agreement with PELDOR and DQC data recorded at low temperatures; this was shown for a double-stranded DNA molecule labeled using triarylmethyl-based spin tags immobilized on NucleosilDMA particles.[138] Interestingly, the bent DNA shows a larger conformational flexibility in the PELDOR experiments than reported in the earlier NMR study (*vide infra*). However, we found that the NMR data also revealed a relatively high mobility between the two helices (Figure 29). In fact, the broad distribution of conformations is in agreement with the NMR data. Thus, more information on the structural and notably dynamic properties of the nucleic acid molecule could be gained with a combination of NMR and PELDOR. The results show that the bent DNA molecule exists in multiple conformational states, which need to be considered for an accurate simulation of the experimental PELDOR data.

6.2.2 Comparison between the published NMR structures and the PELDOR results

The distance distributions for the three spin-labeled DNAs (Figure 25B) were compared with the published NMR structures[121] (Figure 38B). For comparison of the PELDOR distances with the corresponding distance distributions of the published NMR structure bundle,[121] the rigid **Ç**-label was modelled into these structures by a rigid superposition of the equivalent atoms of **Ç** and C at the labeled positions and their interspin distances were measured. The results are summarized in Table 2.

The results from PELDOR show similar average distances between **Ç**5 and **Ç**16, as well as **Ç**2 and **Ç**13, but quite a different average distance between the two bases **Ç**2 and **Ç**16 compared to the NMR bundle.[121] Moreover, narrower distance distributions were observed in

the NMR bundle.[121]

In addition to the comparison of the distances obtained from PELDOR to those obtained by NMR, we simulated the PELDOR data at X-band frequencies for all DNA samples based on the published NMR structure bundle. In Figure 38A, the experimental data are overlaid with these simulations. The oscillation frequency is similar in the experiment and the simulation besides **DNA2,16**, whereas the PELDOR oscillations are much less damped in the simulations compared to the experimental time traces. Stronger damping of the oscillation is correlated with a broader width of the distance distribution and thus an increased conformational flexibility of the biomolecule. From this, we infer that the experimental PELDOR data indicate a higher flexibility than exhibited by the relatively tight NMR[121] structure bundle. However, a very clear distinction needs to be made at this point, since the NMR bundle represents multiple models of a given state, which is called 'uncertainty ensemble'.[119] These multiple models might reflect the limited information available on the studied system in addition to an intrinsic conformational flexibility of the studied system. The published NMR restraints consist only of distance restraints from ^{1}H-^{1}H NOEs and angular restraints, which may not be sufficient to precisely describe the tertiary structure and especially the conformational flexibility of the DNA. The structural ensemble obtained by the combined EPR/NMR approach results in a set of conformations and corresponding weights, which is a 'statistical ensemble'. Therefore, it was not surprising that this ensemble reproduces the experimental PELDOR time traces much better than the published NMR structures.[121]

Table 2: Comparison between the distance distributions obtained by PELDOR (see also Figure 25) and from the published NMR structure bundle.[121]

	DNA5,16	**DNA2,13**	**DNA2,16**
PELDOR *R* (nm)[#]	2.66 ± 0.26	3.26 ± 0.26	3.00 ± 0.45
NMR *R* (nm)[*]	2.50 ± 0.18	3.38 ± 0.15	3.89 ± 0.33

[#]PELDOR mean interspin distance and half width at half maximum obtained from the PELDOR distance distributions by Tikhonov regularization for all DNA samples.

[*]Spin-spin mean distance and standard deviation determined from the published NMR structure bundle,[121] where the **Ç**-label was introduced by aligning to the corresponding C.

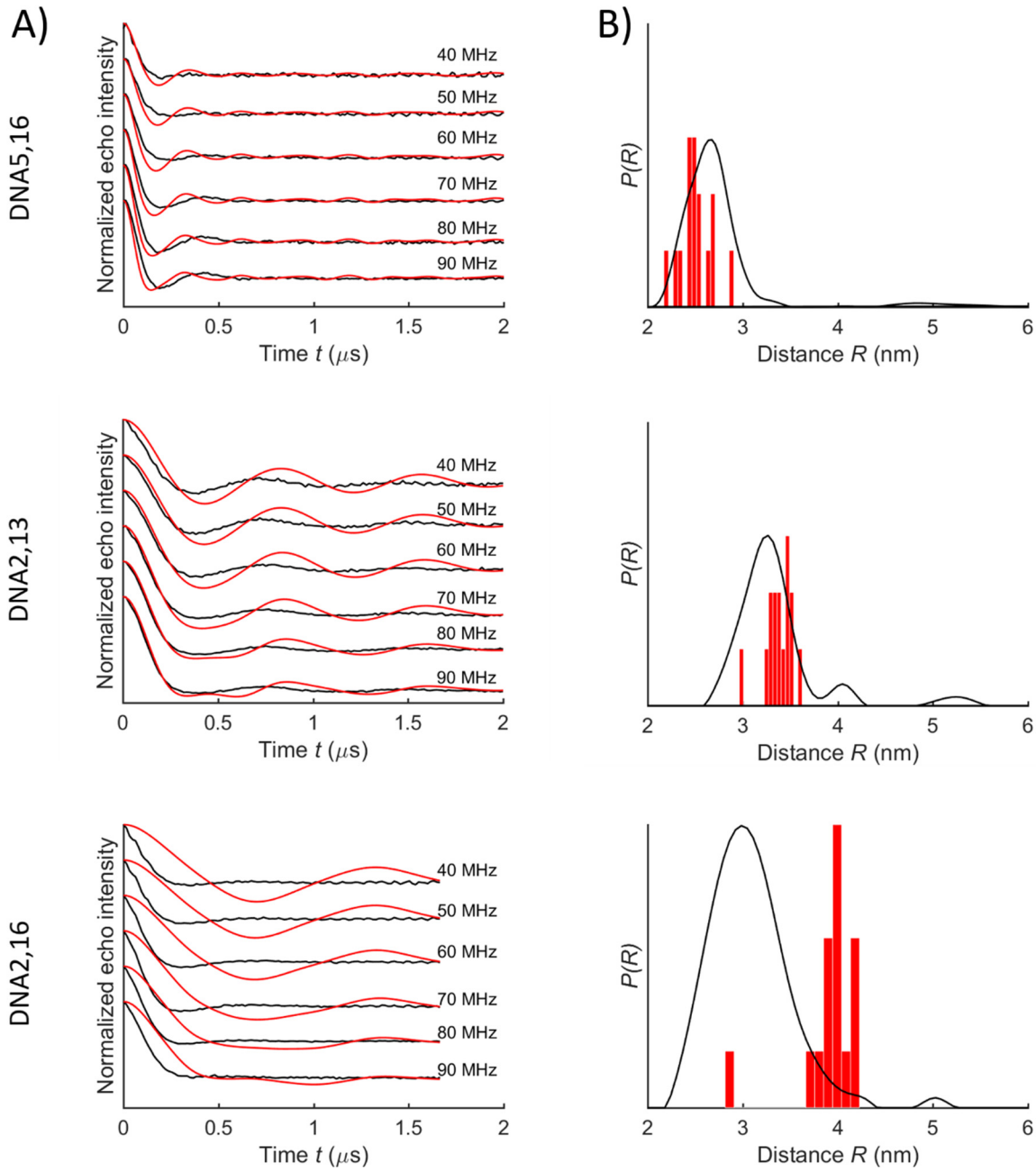

Figure 38: Comparison between the published NMR structures and the experimental PELDOR data on the basis of the PELDOR time traces and corresponding distance distributions. (A) Comparison of experimental (black) and simulated (red) X-band PELDOR time traces for different frequency offsets $\Delta\nu$ for **DNA5,16**, **DNA2,13** and **DNA2,16**. Simulated PELDOR time traces were obtained by superposition of the results from the 15 published NMR structures. The modulation depth of the PELDOR traces of the simulation has been adjusted to the experimental traces for better comparison. (B) Distance distributions based on a Tikhonov regularization of the X-band PELDOR data averaged over all measured frequency offsets $\Delta\nu$ (black line) and distance histogram of the published NMR structures shown in red. The experimental distribution was scaled to the maximum of the histogram obtained by the NMR structures.

7 Summary

Beyond the original scope of classical PELDOR experiments for structural determination *via* distance measurements; this thesis demonstrates the advancement of PELDOR spectroscopy to determine the structural ensembles of highly flexible nucleic acid molecules. The rigid spin label **Ç**, which contains a nitroxide rigidly fused to the nucleobase, was used to accomplish this goal. The motion of the spin label **Ç** is firmly connected to the motion of the base and thereby to the motion of the helix where this latter resides, when **Ç** is paired with guanine in a duplex region. The lack of spin label motion independent of the one of the nucleic acid helix provides an opportunity to monitor the bending and twisting of two **Ç**-labeled helical parts. A description of the conformational dynamics of nucleic acid molecules instead of static structures is urgently needed since many nucleic acids and their complexes with proteins or small molecules are dynamic in nature and thus determines their biological function.

In this thesis, the determination of the structural ensembles of highly flexible DNA motifs upon **Ç**-labeling was demonstrated on two examples: a cocaine aptamer in the presence of cocaine and a bent DNA. The relative orientation between pairs of rigid spin labels, encoded in the orientation-selective PELDOR data, was used to model the conformational flexibility.

In spite of no available atomic resolution structure of the investigated cocaine aptamer in its cocaine-bound state, a molecular model was obtained which describes the global folding and flexibility of the system. Here, the helices were described as rigid bodies and further *a priori* structural assumptions from the secondary structure were used to define the topology of the **Ç**-labeled helical parts of the cocaine aptamer. This yielded conclusive information on the structure and conformational flexibility from a single pair of spin labels and the corresponding orientation-selective PELDOR data recorded at X-band frequencies. In addition, it could be shown, that despite the large flexibility of the cocaine-bound aptamer, the kink angle φ between helices II and III is well-defined to be 85 ± 20°.

The conformational changes of the cocaine aptamer upon cocaine binding were furthermore investigated by PELDOR spectroscopy; for this purpose an additional construct was also considered. A lack of orientation dependence in the PELDOR experiments on the aptamer **1**, with a short helix I, in the absence of cocaine and a strong damping of the PELDOR oscillations showed that the aptamer is fairly flexible. This is consistent with the observed

changes in the global conformation of the aptamer upon cocaine binding, namely a reduced flexibility and a small shift in the mean distance.

Investigation on the conformational dynamics of the bent DNA could show that distance and angular information from pulsed EPR using the rigid spin label **Ç** and short distance and angular restraints from NMR are useful to derive information about the global structure and the conformational space of flexible nucleic acid molecules. A similar approach has previously been used for proteins[124-125] and for RNA[126] using flexible nitroxide spin labels. However, in this thesis rigid spin labels were utilized and their advantage demonstrated. A detailed ensemble determination protocol consisting of two steps was developed, including the fit to orientation-selective PELDOR data at multiple frequencies from three different **Ç**-labeled samples differing in the labeling scheme. The obtained structural ensemble was compared with published structural bundles obtained by NMR[121] and FRET[20] spectroscopy. Our results show that the flexibility of the bent DNA molecule is comparable in shape and width with previously reported FRET studies of a similar DNA.[20] The resulting structural ensemble is broader than the published NMR bundle, but is in complete agreement with the same NMR restraints.[121] Finally, a surprising finding was that the conformation deduced from X-band PELDOR data could also be used to reproduce high-field EPR data despite the fact that the high-field EPR data are additionally sensitive to orientations in the x/y-plane of the nitroxide spin label. Our data support the conclusion that indeed a defined structural ensemble can be extracted by the presented two-step procedure.

The results from both examples clearly show the advantage of using rigid spin labels to investigate the conformational flexibility of such systems, since no internal degree of freedom of the spin label itself has to be considered. PELDOR has no size limit of macromolecules, hence also larger DNA or RNA molecules (using **Çm**, the RNA analogue of **Ç**, in conjunction with ligation techniques[23]) and their complexes with proteins or other molecules should be accessible by this methodology. This work lays the foundation for further studies to understand the global dynamics of nucleic acids and could provide essential knowledge for the mechanisms involved in DNA/RNA-protein recognition, which are important for many processes in cells.

8 Outlook

The methods presented in this thesis together with other spectroscopic methods will strengthen PELDOR as a complementary method to study structures and conformational dynamics of highly flexible nucleic acid molecules.

PELDOR restraints alone or in combination with NMR restraints from NOESY-type experiments and from J-coupling measurements can be used to get insight into the conformational space of highly flexible DNA model systems, as shown in this thesis. Yet, there are other methods like MD or state-of-the-art NMR techniques, which can be included in the analysis of orientation-selective PELDOR data. For example, structures from a MD trajectory or NMR structures refined with RDC or PRE restraints could be used to simulate the PELDOR data directly, or conformational spaces estimated from such structures could be compared with the conformational space from the approach presented here.

In addition, on the one hand restraints from other structural methods, *e.g.* FRET, RDCs, PREs … could be included in the first step of the presented procedure, in which a library of spin label conformations or structures is generated instead of using structures obtained by EPR restraints alone or by combining EPR and NMR restraints. On the other hand, structures from an MD trajectory could be selected directly to fit the experimental PELDOR data.

Besides the applications to small nucleic acids designed as model systems, it would be interesting to investigate large DNA/RNA-protein complexes. For example, conformational changes upon binding of a nucleic acid onto a protein could be registered by a change in the relative orientation of two rigidly incorporated spin labels even if the interspin distance does not change. A step in that direction is currently under investigation: the conformational rearrangement of the neomycin-responsive riboswitch upon binding of neomycin using PELDOR spectroscopy in combination with the rigid **Çm-**label is studied. This project is a cooperation with the research groups headed by Prof. Dr. Sigurdsson (University of Island), Prof. Dr. Höbartner (Max-Planck Institute, Göttingen) and Prof. Dr. Suess (Technische University Darmstadt). The engineered RNA aptamer, the neomycin-responsive riboswitch, which is a functional synthetic riboswitch, was identified via *in vitro* selection and *in vivo* screening by Weigand *et al*..[139] The aptamer exhibits regulation of gene expression by interfering with translation initiation upon binding of the ligand neomycin B, which is a broad-spectrum aminoglycoside antibiotic with activity against Gram-positive and Gram-

negative bacteria. Under native conditions, neomycin blocks the protein biosynthesis of sensitive bacteria during binding to the ribosomal A-site. The riboswitch adopts a global stem-loop structure with a terminal and an internal asymmetric loop (Figure 39A). The binding pocket for neomycin is placed in the center of the RNA riboswitch. The terminal loop contains the UUAA sequence, a well understood RNA motif called U-turn containing the consensus sequence UNRN (N: any nucleotide, R: any purine). Hydrogen bonds between the imino proton of U1 and the phosphate oxygen of the last nucleotide in the motif and between 2'-OH of U1 and N7 in the purine base stabilize the conformation of this motif.
Wöhnert and coworkers have solved the atomic resolution structure of the riboswitch-neomycin complex (pdb-code: 2kxm), in which the two helical regions are coaxially stacked.[140] Moreover, they reported a temperature-dependent conformational equilibrium of the riboswitch in absence of neomycin between a less-structured open form and a compact, highly structured conformation. The compact form resembles the structure of the riboswitch-neomycin complex. From that, they have proposed a conformational capture ligand binding mechanism.[137]

Recently, Krstić *et al.* have shown that PELDOR measurements at low temperatures on neomycin-responsive riboswitch using the TPA spin label do not display a significant change in the mobility or in the structure upon binding of neomycin.[51] This indicates the existence of a prearranged tertiary structure of the RNA aptamer in the absence of neomycin.

In comparison to the TPA spin label, which is reported to give well-defined and narrow distance distribution functions, the rigid **Çm-**label enables the additional determination of angular information.[68-69] Therefore, we are going to study the conformational rearrangement of the neomycin-responsive riboswitch upon binding of neomycin using the rigid **Çm-**label. Our first orientation-selective PELDOR experiments at X-band frequency of the RNA aptamer in absence and presence of neomycin indicate a conformational change upon binding of neomycin (Figure 39B). In contrast to the previous study using the TPA-spin label, we clearly observe a frequency shift in our PELDOR data upon neomycin binding. Moreover, changes in oscillation frequency, modulation depth and damping of the PELDOR signals in dependence of the frequency offsets could be detected in the orientation-selective PELDOR data, which is a sign of orientational correlation. This will allow to determine the mutual orientation between two **Çm-**labels. A quantitative analysis of these experimental orientation-selective PELDOR data is ongoing.

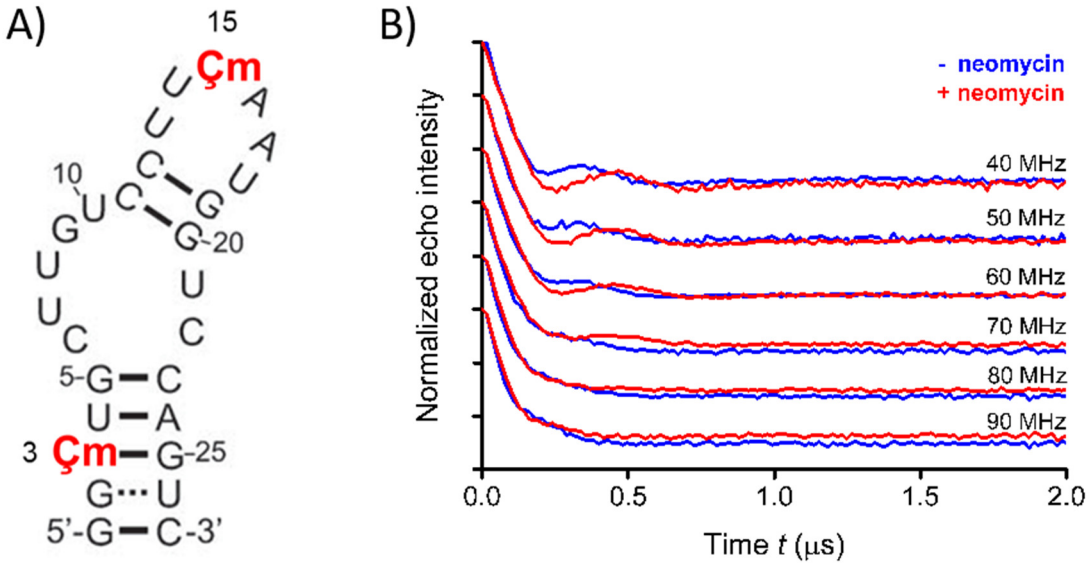

Figure 39: Çm-labeled neomycin-responsive riboswitch and experimental PELDOR data recorded at X-band frequencies in the absence and presence of neomycin. (A) 27-mer RNA secondary structure of the neomycin-responsive riboswitch and **Çm-**label positions at C3 and U15 marked in red. The binding pocket of the neomycin covers the complete internal loop and half of the terminal loop. (B) Experimental orientation-selective X-band PELDOR time traces for different frequency offsets between probe and pump pulses, which were varied ranging from 40 to 90 MHz, in the absence (blue) and presence (red) of the ligand neomycin. The time traces have been shifted in the direction of the y-axis for an easier visual inspection.

9 Deutsche Zusammenfassung

Gepulste Elektron-Elektron Doppel Resonanz (PELDOR), auch Doppel Elektron-Elektron Resonanz (DEER) genannt, ist eine gepulste EPR-Methode. Durch Messung der dipolaren Kopplung zwischen zwei paramagnetischen Zentren, welche an einem Biomolekül (Proteine oder Nukleinsäuremoleküle) kovalent angebracht sind, können Abstände von 1,5 bis 10 nm bestimmt werden. Solche langreichweitigen Abstände geben wiederrum strukturelle Rückschlüsse auf das zu untersuchende Biomolekül ergänzend zu anderen Strukturbestimmungsmethoden.

Wenn der starre **Ç**-Spinmarker paarweise in DNS- oder RNS-Moleküle eingebaut wird, kann nicht nur der Abstand, sondern auch die relative Orientierung zwischen zwei **Ç**-Spinmarkern durch orientierungsselektive PELDOR Daten aus verschiedenen Frequenzbändern (X-, Q- und G-Band Frequenzen) bestimmt werden. Somit kann die Information über die Orientierung von Sekundärstrukturelementen der Nukleinsäuren ermittelt und als zusätzliche Orientierungsinformation zu ihrer Strukturbestimmung verwendet werden. Da der **Ç**-Spinmarker keine Bewegung unabhängig von der Helix besitzt, in der dieser eingebaut ist, kann die Konformationsflexibilität des Nukleinsäuremoleküls direkt bestimmt und deren Biege- und Verwindungsbewegung analysiert werden.

Diese Arbeit zeigt die Weiterentwicklung der PELDOR Spektroskopie über ihren ursprünglichen Anwendungsbereich hinaus zur Charakterisierung des Konformationsraums von stark flexiblen Nukleinsäuremolekülen. Die Beschreibung flexibler statt starrer Strukturen, ist wesentlich, da viele Nukleinsäuren und deren Komplexe mit Proteinen oder kleinen Molekülen in der Natur dynamisch sind und die Dynamik deren biologische Funktion bestimmen. Im Rahmen dieser Arbeit werden Anwendungen der dargestellten Methodik auf zwei Systeme vorgestellt: Eine Dreifachgabelung, ein Kokain-Aptamer in seinem gebundenen Zustand und eine Zweifachgabelung, ein gebogenes DNS Molekül. Die relative Orientierung zwischen zwei starr angebrachten Spinmarkern, die in den orientierungsselektiven PELDOR Daten kodiert ist, wurde verwendet um die Konformationsflexibilität des Nukleinsäuremoleküls zu modellieren.

Die Extrahierung von Winkelinformationen aus orientierungsselektiven PELDOR Daten ist nicht immer eindeutig. Es könnten unterschiedliche Strukturbündel die gleiche

orientierungsselektive PELDOR Zeitspuren besitzen.[95] Dies gilt insbesondere für die Untersuchung von flexiblen Systemen, bei denen viele Konformere der Nukleinsäuremoleküle nebeneinander existieren. Dies stellt für die Bestimmung des zugehörigen strukturellen Ensembles mit Hilfe der PELDOR Spektroskopie eine besondere Herausforderung dar. Allerdings können experimentelle PELDOR Zeitspuren in einem zweistufigen Ansatz, der in unserem Arbeitskreis entwickelt wurde, rekonstruiert werden. Im ersten Schritt wird eine Datenbank aus möglichen Spin-Spin-Orientierungen erstellt und die dazugehörigen orientierungsselektiven PELDOR Zeitspuren simuliert. Im zweiten Schritt wird aus diesen vorher simulierten Zeitspuren eine Teilmenge selektiert, die die experimentellen Daten rekonstruieren. Dieser Ansatz berücksichtigt nur zwei starre Nitroxid-Spinmarker ohne eine biomolekulare Struktur dazwischen. Das Biomolekül beschränkt jedoch die Bereiche möglicher Winkel und Abstände zwischen zwei Spinmarkern. An diesem Punkt stellt sich die Frage, ob physiologisch sinnvolle Strukturen von Spin-markierten DNS Molekülen existieren, die mit den gefundenen Spinmarker-Konformationen übereinstimmen. Aus diesem Grund wurde in dieser Arbeit eine andere Strategie gewählt, um die Konformationsräume der hochflexiblen DNS-Motive zu charakterisieren. Es wurde eine PELDOR Daten geführte Selektion von Konformeren aus einer Spinmarkerkonformationsdatenbank beziehungsweise einer Strukturdatenbank verwendet, die den physiologischen Gegebenheiten genügt.

Die Untersuchung der relativen Orientierung zwischen den beiden Spin-markierten Helices des Kokain-Aptamers zeigte strukturelle Einblicke in die konformationelle Dynamik des Kokain-gebundenen Zustands. Obwohl keine NMR oder Kristallstruktur des untersuchten Kokain-Aptamers weder im gebundenen noch im ungebundenen Zustands in atomarer Auflösung verfügbar war, konnte ein molekulares Model des gebundenen Zustands entwickelt werden, welche seine globale Faltung und seine Konformationsflexibilität beschreibt. Hierbei wurde zunächst der klassische zweistufige Ansatz verwendet, um mögliche Spinmarkerkonformationen zu selektieren, die die experimentellen orientierungsselektiven X-Band PELDOR Daten rekonstruieren. Um topologisch erlaubte interhelikale Orientierungen aus den gefundenen Spinmarkerkonformationen zu erzeugen wurden die Helices als starre Körper beschrieben und weitere *a priori*-Kenntnisse über die Sekundärstruktur verwendet, die die Topologie der **Ç**-markierten Helices des Kokain-Aptamers definieren. Dies lieferte schlüssige Informationen über die Struktur und Flexibilität eines Aptamers aus einem einzigen Paar von Spinmarkern und den

dazugehörigen orientierungsselektiven PELDOR Daten, die bei X-Band Frequenzen aufgezeichnet wurden. Darüber hinaus konnte gezeigt werden, dass trotz der großen Flexibilität des Kokain-gebundenen Zustands der Knickwinkel φ zwischen Helix II und III gut definiert ist, 85±20°. Im Gegensatz dazu können die Drehwinkel θ und ψ einer Helix relativ zu einer anderen Helix aus experimentellen X-band PELDOR Daten nicht bestimmt werden.

Die Eindeutigkeit des strukturellen Ensembles wurde durch eine Validierung überprüft. Die Spinmarkerkonformationsregion, die unter Verwendung des *Fit*-Verfahrens gefunden wurde, wurde aus der Spinmarkerkonformationsdatenbank entfernt. Anschließend wurde diese eingeschränkte Datenbank verwendet, um erneut den experimentellen X-Band PELDOR Datensatz zu reproduzieren. Dies ermöglicht die Überprüfung der Wichtigkeit der zuvor selektierten Spinmarkerkonformationen im Ensemble um die PELDOR Daten zu beschrieben. Der *Fit* wird deutlich schlechter, wobei die neu gefundenen Spinmarkerkonformationen sich an den Grenzen der entfernten Spinmarkerkonformationensregion ansiedeln. Diese Ergebnisse bestätigen, dass unsere gefundenen Spinmarkerkonformationen aus dem *Fit* mit der vollständigen Spinmarkerkonformationsdatenbank essentiell sind und keine Lösung darstellen, die durch andere Ensembles von Spinmarkerkonformationen ersetzt werden kann.

Darüber hinaus wurden die Konformationsänderungen des Kokain-Aptamers, welche durch die Bindung von Kokain induziert wurden, durch eine Analyse der Abstandsverteilungen untersucht. Aus diesem Grund wurde durch Aufsummieren der Zeitspuren, die bei verschiedenen Frequenzdifferenzen zwischen gepumpter und detektierter Frequenz aufgenommen wurden, eine orientierungs-gemittelte Zeitspur generiert. Aus dieser wurde jeweils eine Abstandsverteilung ohne Orientierungsinformationen mithilfe einer Tikhonov Regularisierung berechnet. Bereits der Mangel an Orientierungsabhängigkeit im PELDOR Experiment von Aptamer **1** mit einer kurzen Helix I in Abwesenheit von Kokain und einer starken Dämpfung der PELDOR Oszillationen zeigte, dass das Kokain-Aptamer sehr flexibel ist. Nach Zugabe von Kokain tauchte in den PELDOR Zeitspuren eine ausgeprägte Oszillation auf, welche auf eine Abnahme der konformationellen Flexibilität in Gegenwart des Liganden schließen lässt. Des Weiteren zeigen die Abstandsverteilungen eine kleine Verschiebung des mittleren Abstands zwischen den beiden Spinmarkern, hervorgerufen durch die Bindung des Kokains. Dies deutet auf eine Liganden-induzierte Konformationsänderung hin, die vermutlich an der Gabelung entsteht, an der das Kokain bindet.

Im Gegensatz zum Kokain-Aptamer Projekt waren für das zweite System, die gebogene DNS, welches aus einer Wölbung von fünf Adeninen und benachbarten kurzen Helices aufgebaut ist, spektroskopische NMR Daten verfügbar. Dornberger *et al.* haben die dreidimensionale Struktur dieser DNS gelöst (PDB-Eintrag: 1QSK).[121] Die gleichen Abstands- und Winkel*restraints*, die aus NOESY-Experimenten und aus J-Kopplungsmessungen abgeleitet wurden, wurden in dieser Arbeit mit Abstandsbereichen aus PELDOR kombiniert um ein strukturelles Ensemble zu erzeugen, welches die konformationelle Flexibilität der gebogenen DNS beschreibt.

Eine hohe konformationelle Flexibilität des gebogenen DNS-Moleküls zeigte sich in den experimentellen orientierungsselektiven PELDOR Daten durch eine starke Dämpfung der Zeitspuren. Aus den orientierungsselektiven PELDOR Zeitspuren wurde eine orientierungs-gemittelte Zeitspur generiert, aus der jeweils eine Abstandsverteilung von **DNA5,16**, **DNA2,13** und **DNA2,16** mithilfe einer Tikhonov Regularisierung berechnet wurde. In allen Fällen konnte eine breite Abstandsverteilung ermittelt werden, insbesondere für **DNA2,16**, die an den jeweiligen Enden beider Helices spinmarkiert ist. Die Spinmarker, der in der Helix zwischen benachbarten Basen geschichtet vorliegt, zeigt keine von der Helix unabhängige Flexibilität. Daher ist die hier beobachtete höhere Flexibilität ein direktes Ergebnis der Flexibilität des DNS-Moleküls.

Um die konformationelle Flexibilität des gebogenen DNS-Moleküls zu untersuchen, wird in dieser Arbeit ein zweistufiges Protokoll vorgeschlagen. Im ersten Schritt wird eine Datenbank bestehend aus einer breiten Variation an Konformeren erstellt, die mit topologischen *Constraint*s, NMR-*Restraints* und Abstandsbereiche, die aus PELDOR abgeleitet wurden, im Einklang sind. Im zweiten Schritt wird ein gewichtetes Ensemble dieser Konformere so gewählt, dass dieses Ensemble gleichzeitig alle experimentellen orientierungsselektiven PELDOR Zeitspuren der drei doppelt **Ç**-markierten Proben beschreibt.

Für das untersuchte gebogene DNS-Molekül reichen die ^{1}H-^{1}H-NOEs und die Winkel-*Restraints* aus dem NMR-Datensatz aus, um präzise die Struktur der Helices und eine zusätzliche Restriktion der Struktur aufgrund der Wölbung zu beschreiben, die die Topologie der untersuchten DNS definiert. Die Verwendung der verfügbaren NMR-Daten für die gebogene DNS ermöglicht die Bestimmung hochauflösender atomarer Strukturen und erleichtert die Modellierung der kurzen Helices. Die langreichweitigen PELDOR Abstände sind wiederrum nützlich, um den Konformationsraum zu beschränken, der die globale Anordnung der zwei Helices relativ zueinander beschreibt. So spiegelt das

resultierende Strukturbündel die dynamische Natur dieses gebogenen DNS-Moleküls wieder.
Zusätzlich wurden die Knick- und Drehwinkel Paare quantitativ bestimmt. Die Knick- und Drehwinkel Paare der Strukturdatenbank sind korreliert, zeigen topologische Restriktionen und bevorzugte interhelikale Orientierungen. Das resultierende, strukturelle Ensemble wurde mit den Konformationsräumen aus FRET Experimenten[20] und mit den NMR-Strukturen[121] verglichen.
Die Eindeutigkeit des erhaltenen strukturellen Ensembles aus X-Band PELDOR Daten wurde durch die Vorhersage eines unabhängigen PELDOR Datensatzes, der bei hohen Magnetfeldstärken aufgenommen wurde, validiert. Die Prozedur, unter Verwendung der X-Band Daten und der NMR Restriktionen, beschreibt einen Konformationsraum der auch mit den gemessenen Hochfelddaten übereinstimmt, welches nicht für die Selektion der Strukturen im zweiten Schritt des zweistufigen Protokolls verwendet wurde. Darüber hinaus konnte durch einen *Fit* an allen PELDOR Daten gleichzeitig gezeigt werden, dass die Konformationsräume aus dem *Fit* an X-Band Daten alleine und dem *Fit* an aller zur Verfügung stehender, experimenteller PELDOR Zeitspuren vergleichbar sind.

Zusammenfassend zeigt diese Arbeit das Potenzial von PELDOR Spektroskopie in Kombination mit starren Spinmarkern zur Strukturbestimmung von Nukleinsäuren: Die relative Orientierung zwischen zwei Helices, die konformationelle Flexibilität und die Konformationsänderungen von Nukleinsäuremolekülen bei der Substratbindung wurden bestimmt.

In Zukunft wird es neben der Anwendung von kleinen Nukleinsäuren, die als Modellsysteme konzipiert wurden, äußerst interessant sein, große Protein-RNA/DNA-Komplexe zu untersuchen. Beispielsweise könnten Konformationsänderungen bei der Bindung einer Nukleinsäure an ein Protein durch eine Änderung der relativen Orientierung von zwei starr eingebauten Spinmarkern untersucht werden, auch wenn sich der Abstand zwischen den Spinmarkern nicht ändern sollte. Ein Schritt in diese Richtung ist die Untersuchung der Konformationsänderungen des Neomycin-responsiven Riboswitches bei der Bindung von Neomycin mithilfe von PELDOR Spektroskopie in Kombination mit dem starren **Çm**-Marker. Die ersten orientierungsselektiven PELDOR Untersuchungen aufgenommen bei X-Band Frequenzen zeigten eine Verschiebung des mittleren Abstandes nach Bindung von Neomycin, welches in vorherigen Untersuchung unter Zuhilfenahme des TPA-Spinmarkers

nicht beobachtet werden konnte.[51] Dies weist auf eine Konformationsänderung bei der Bindung von Neomycin hin. Darüber hinaus ändert sich die Modulationsfrequenz, die Modulationstiefe und die Dämpfung der PELDOR Signale in Abhängigkeit von den Frequenzdifferenzen, welches uns erlaubt Winkelinformationen aus diesen orientierungsselektiven PELDOR Daten zu bestimmen und so auf die relative Orientierung zweier **Çm**-Spinmarker rückzuschließen. Eine quantitative Analyse dieser orientierungsselektiven PELDOR Daten ist derzeit in Bearbeitung.

10 Appendix

10.1 DNA constructs and sample preparation

For the EPR experiments, the rigid spin label **Ç** was incorporated pairwise into helices II and III of the cocaine aptamer DNA (Figure 14). Two aptamer constructs were prepared, each containing two **Ç-**labels on the same position, but differing in the length of helix I. Aptamer **1** (Table A1) consists of a 13-mer with the sequence 5'-d(GACAAGAAG**Ç**GAC)-3' which is paired with a 24-mer with the sequence 5'-d(GTCGCTTCTTCAA**Ç**GAAGTGGGTC)-3'. Aptamer **2** contains a longer helix I (seven base pairs instead of three, Figure 14). A GT-mismatch in helix III of the original construct[66] was substituted by a Watson-Crick base pair G**Ç**, which results in a tighter binding of cocaine.[141] With respect to the original construct helix II, which is known to form in the absence of cocaine,[66] was elongated to enable the spin labels residing in it to be incorporated further away from the junction. A two-strand construct was used to give more flexibility in the preparation of the spin-labeled oligonucleotides and higher yields.

The bent DNA molecule consists of a 17-mer with the sequence 5'-d(GCATCGAAAAAGCTACG)-3', which is paired with a 12-mer with the sequence 5'-d(CGTAGCGATGC)-3'. The flexible 5-nucleotide bulge with the sequence dAAAAA (dA-bulge) (Figure 24) is located between two double-stranded regions. **Ç**-labels are introduced pairwise, each in one of the double-stranded regions (Table A1).

All the spin-labeled oligonucleotides were synthesized as previously described by automated chemical synthesis, using the phosphoramidite derivative of **Ç**.[59, 61] After purification by denaturing polyacrylamide gel electrophoresis, 10 nmol of spin-labeled DNA duplex samples were annealed in 100 µl of 10 mM phosphate buffer (pH = 7), 100 mM NaCl and 0.1 mM EDTA, followed by evaporation of the solvent. Afterwards, each sample was dissolved in 100 µl of 20% non-deuterated ethylene glycol/water mixture. Ethylene glycol was used as a cryoprotectant. For the cocaine aptamer, samples with deuterated solvent, a 20% deuterated ethylene glycol / D_2O mixture, were prepared additionally. The aptamer samples with the cocaine ligand (5 mM) were prepared in a similar manner. It should be noted that the sample preparations for the bent DNA samples were very similar to the ones used in the published NMR experiments[121] with respect to buffer conditions, DNA concentration, pH value and metal ion concentration. Before the PELDOR experiments the spin-labeled samples were

filled in EPR tubes and frozen in liquid nitrogen.

Table A1: Samples for the cocaine aptamer and the bent DNA system. The synthesis of the spin label and all DNA samples used in this thesis were performed by Dr. Cekan a former group member of the research group of Prof. Dr. Sigurdsson from the University of Island.

Sample	Sequence
Aptamer **1**	13-mer: 5'-d(GACAAGAAG**Ç**GAC)-3'
	24-mer: 5'-d(GTCGCTTCTTCAA**Ç**GAAGTGGGTC)-3'
Aptamer **2**	17-mer: 5'-d(CGGCGACAAGAAG**Ç**GAC)-3'
	28-mer: 5'-d(GTCGCTTCTTCAA**Ç**GAAGTGGGTCGACG)-3'
DNA5,16	17-mer: 5'-d(GCAT**Ç**GAAAAAGCTA**Ç**G)-3'
	12-mer: 5'-d(CGTAGCCGATGC)-3'
DNA2,13	17-mer: 5'-d(G**Ç**ATCGAAAAAG**Ç**TACG)-3'
	12-mer: 5'-d(CGTAGCCGATGC)-3'
DNA2,16	17-mer: 5'-d(G**Ç**ATCGAATAAGCTA**Ç**G)-3'
	12-mer: 5'-d(CGTAGCCGATGC)-3'

10.2 PELDOR experiments

The dead-time-free 4-pulse ELDOR sequence was used for all PELDOR experiments:

$$\pi/2(\nu_A) \; - \; \tau_1 \; - \; \pi(\nu_A) \; - \; (\tau_1 + t) \; - \; \pi(\nu_B) \; - \; (\tau_2 - t) \; - \; \pi(\nu_A) \; - \; \tau_2 \; - \; \text{echo signal}$$

These experiments were carried out in frozen aqueous buffer solution with a DNA duplex concentration of 100 µM at a temperature of 40 K (bent DNA) or 50 K (cocaine aptamer).

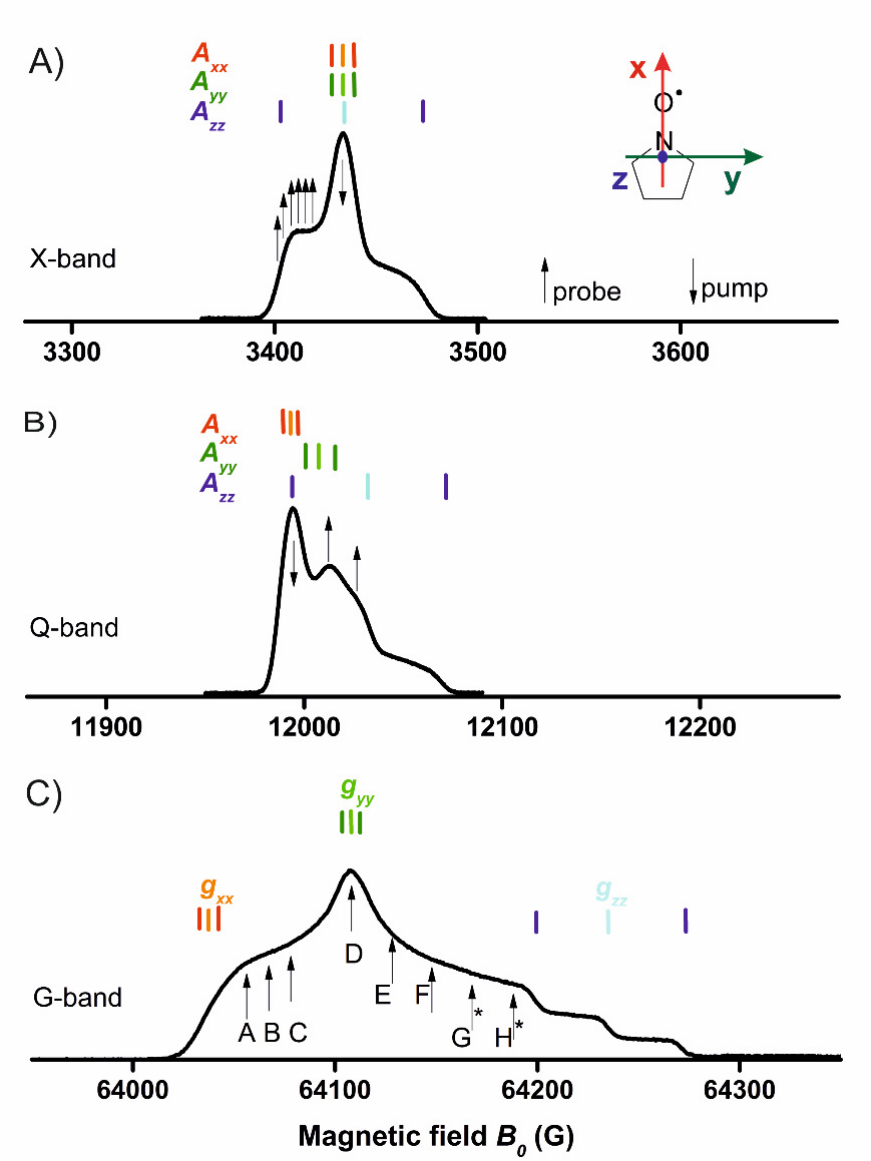

Figure A1: Echo-detected field swept EPR spectra of the **Ç**-labeled bent DNA recorded at 40 K and corresponding ^{14}N stick diagram for (A) X-, (B) Q- and (C) G-band frequencies, respectively. Arrows indicate pump and probe frequencies, where the offset between the detection and the pump frequencies $\Delta\nu$ was varied from 40 to 90 MHz at X-band frequencies. At Q-band frequencies, the pump pulse was set to the maximum absorption position and the probe pulses 50 and 90 MHz below. At G-band frequencies, arrows mark the detection positions. The pump frequency was set at a constant offset $\Delta\nu$ of 60 MHz below or above (at positions G and H, marked with *) the detection frequency. The magnetic field was not calibrated.

10.2.1 Orientation-selective PELDOR experiments at X-band frequencies

Before the measurements 100 µl of the spin-labeled samples **DNA5,16**, **DNA2,13** and **DNA2,16** were filled in EPR tubes (4 mm OD) and frozen in liquid nitrogen. 25 µl of the spin-labeled samples of aptamer **1** and **2** with non-deuterated solvent were filled in EPR tubes (2.8 mm OD). Orientation-selective PELDOR experiments at X-band frequencies were performed for all samples on a Bruker ELEXSYS E580 pulsed X-band EPR spectrometer. The spectrometer contains a standard Flexline probehead housing a dielectric ring resonator (MD5 W1) equipped with a continuous flow helium cryostat (CF935) and temperature control system (ITC 502), both purchased from Oxford instruments. For the cocaine aptamer samples, a splitring resonator (ER 4118X-MS3) was used. A commercially available setup (E580-400U) from Bruker was used to couple the second (not phase-stabilized) microwave source into the microwave bridge. All pulses were amplified via a pulsed travelling wave tube amplifier from Applied Systems Engineering (117X). The over-coupled resonator had a quality factor Q of about 100. The detection pulses ν_A were set to 32 ns for both π- and π/2-pulses. The length of the pump pulse ν_B was set to 12 ns. The pump pulse was situated at the maximum of the anisotropic powder spectra, selecting the nitrogen nuclear spin sublevel with $m_I = 0$ with random orientations of the nitroxide radical with respect to the external magnetic field (Figure A1A). The frequency of the pump pulse ν_B was set at the resonance frequency of the resonator. The amplitude of the pump pulse was optimized by the inversion of a Hahn-echo at the frequency ν_B. The frequency $\Delta\nu = \nu_A - \nu_B$ was varied from 40 to 90 MHz in steps of 10 MHz to select different orientations of the nitroxide radicals due to the anisotropic nitrogen hyperfine tensor, as explained in the Results and Discussion section. The probe pulse frequencies were slightly off-resonance to the cavity resonance, but still within the bandwidth of the microwave resonator to accomplish sufficient B_1 field strength. Proton ESEEM modulation was suppressed by averaging over 9 spectra with τ_1 from132 to 196 ns in steps $\Delta\tau_1$ of 8 ns. The time delay between the second and the third detection pulse ($\tau_1 + \tau_2$) was 2.5 µs. In order to eliminate receiver offsets, a two-step phase cycle on the π/2-pulse was applied (+(+x), -(-x)). The video amplifier bandwidth was 50 MHz. The spectra for **DNA5,16** and **DNA2,16** were recorded with a repetition time of 4 ms. For **DNA2,13** the repetition time was increased to 8 ms. For the cocaine aptamer, the spectra were recorded with a repetition time of the pulse sequence of 4 to 5 ms. Depending on the frequency offset $\Delta\nu$, the measurement time was about 2–3 h for 40 – 70 MHz and about 8 – 15 h for 80, 90 MHz.

10.2.2 PELDOR experiments at Q-band frequencies

For all samples a volume of 10 µl was filled in an EPR tube (1.6 mm OD) and frozen in liquid nitrogen before the measurement. The cocaine aptamer **1** samples in presence and absence of cocaine were solved in deuterated solvent, which allows elongating the dipolar evolution time to 5 µs for a better evaluation of the intermolecular contribution.[82]

The PELDOR experiments were performed at a temperature of 40 K for the bent DNA samples and 50 K for the aptamer samples, which was controlled by an Oxford continuous flow helium cryostat, on an ELEXSYS E580 (X-band) spectrometer equipped with Bruker ELEXSYS SuperQ-FT Q-band extension and a 10 W pulsed microwave solid state amplifier (HA8019). A Bruker EN5107D2 resonator was used. For the bent DNA samples, the detection pulses at the frequency ν_A were set to 48 ns for both π- and π/2-flip angles. The frequency ν_A was about 50 or 90 MHz lower than the resonance frequency of the microwave resonator. A length of 20 ns was chosen for the pump pulse with the frequency ν_B, which was set on-resonance with the microwave cavity. The delay time τ_1 between the first and the second detection pulse was set to an initial value of 132 ns and incremented in 8 steps of 2 ns to average proton ESEEM modulation. The pulse separation between the second and the third detection pulse ($\tau_1 + \tau_2$) was set to 3 µs. The shot repetition time was set to 4 ms. The total measurement time was approximately 4 h to achieve an optimal signal-to-noise ratio.

For the cocaine aptamer samples, the detection pulses at the frequency ν_A were set to 32 ns for the π- and $\pi/2$-flip angles. The frequency ν_A was about 50 MHz lower than the resonance frequency of the microwave resonator. Lengths of 20 and 26 ns were chosen for the pump pulse with frequency ν_B. The time delay τ_1 between the first and the second probe pulses was set to an initial value of 124 ns and incremented in 8 steps of 2 ns each to average deuterium ESEEM modulation. The pulse separation between the second and the third probe pulses ($\tau_1 + \tau_2$) was set to 5 µs.

10.2.3 Orientation-selective PELDOR experiments at G-band frequencies

Orientation-selective PELDOR experiments were performed for the samples **DNA2,13** and **DNA2,16** on a home-built pulsed-EPR spectrometer extended for two-frequency irradiation and controlled by the Specman4EPR software program[142]. The operating frequency was 180 GHz (G-band), corresponding to a static magnetic field of 6.422 T. The magnet consists of two superconductive coils, the main one creating a static magnetic field between 0 to 7 T. The second superconductive coil has a range between ± 0.08 T and is used to tune the magnetic field during an experiment. The cryostat, probe head and the microwave bridge were thermally equilibrated for 1–2 h to avoid shifts of the microwave phase during the long accumulation time. The microwave, with an applied power of approximately 60 mW, was coupled into a cylindrical resonator which operates in TE_{011} mode. The pump frequency was set at a constant offset $\Delta\nu$ of 60 MHz below or above (marked with a * in Figure A1) the detection frequency either to achieve a better signal-to-noise ratio (in the case of **DNA2,13**) or a more pronounced dipolar oscillation pattern (in the case of **DNA5,16**). The detection pulses were adjusted to approximately 45 and 75 ns delivered at the cavity resonance frequency and optimized for maximum echo intensity. The length of the pump pulse was about 75 ns and optimized for maximum modulation depth. 500 of the echo signal averages were performed to get an appropriate signal-to-noise ratio. A time window of maximally 2.2 µs (τ_2) between the second and third pulse, a pulse sequence repetition time of 5 ms and a temperature of 40 K were employed. Time traces, consisting of around 60 to 120 scans, were recorded at several field positions across the nitroxide EPR spectrum approximately from $B \parallel g_{xx}$, $B \parallel g_{yy}$ to $B \parallel g_{zz}$ to obtain the orientation dependence of the modulation frequency. The field positions are marked by A, B… in Figure A1C.

10.2.4 Original experimental PELDOR time traces

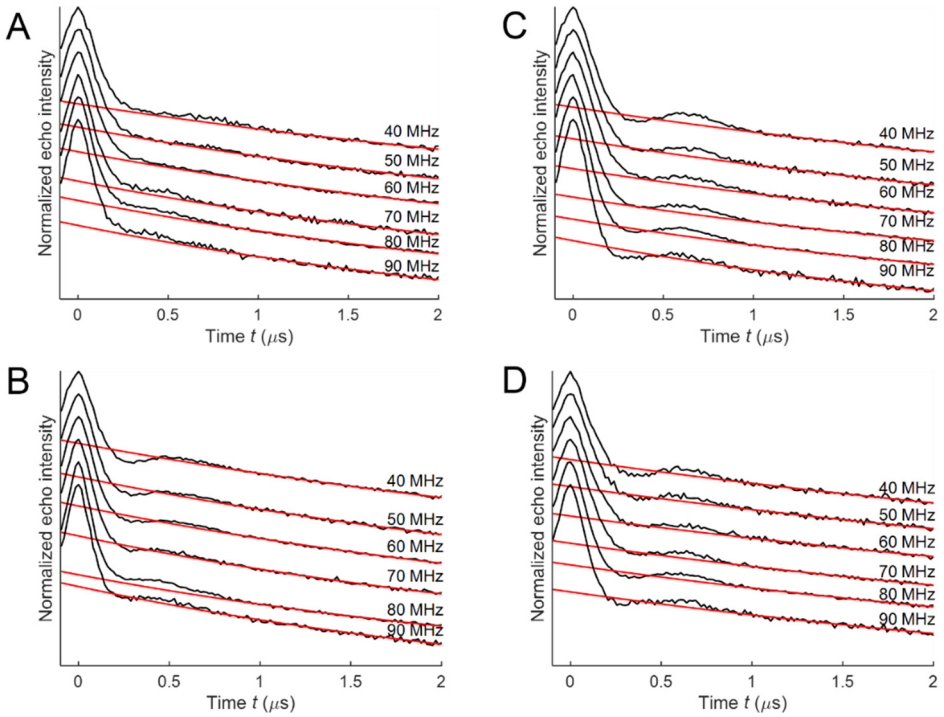

Figure A2: Experimental X-band PELDOR time traces measured at frequency offsets Δν from 40 to 90 MHz for spin-labeled aptamers **1** (A), (B) and 2 (C), (D) in the absence and presence of cocaine, respectively. The background function is shown in red.

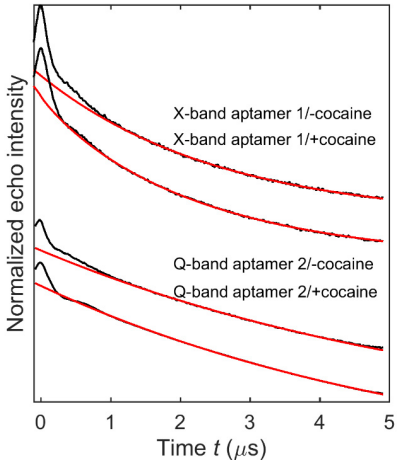

Figure A3: Experimental time traces of spin-labeled cocaine aptamer **1** in the presence and absence of cocaine in a deuterated solvent at Q-band with a maximum dipolar evolution time of 5 µs. Distance distributions were obtained by Tikhonov regularization. The background function is shown in red.

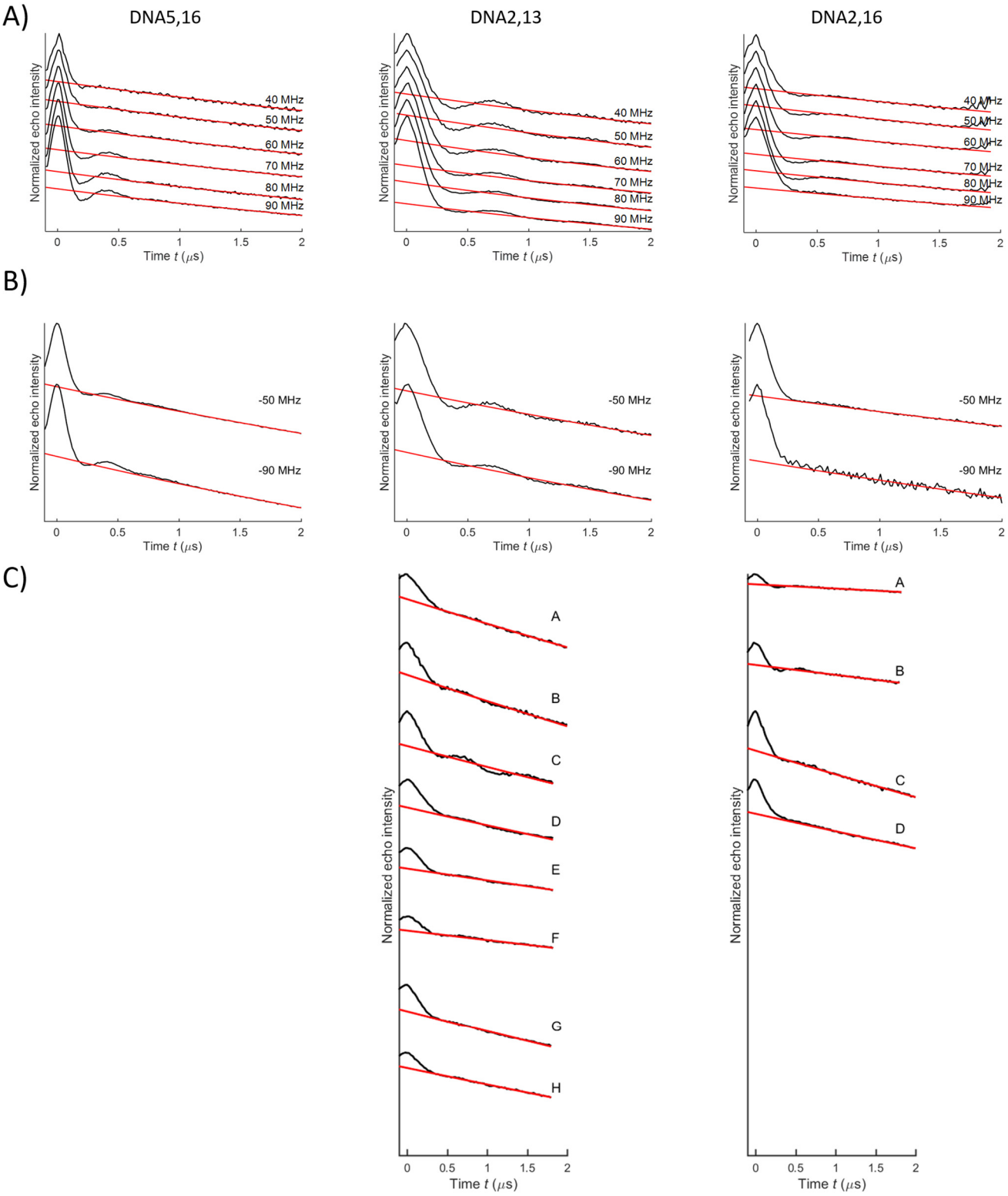

Figure A4: Experimental PELDOR time traces measured at frequency offsets $\Delta\nu$ from 40 to 90 MHz at (A) X-, (B) Q- and (C) G-band frequencies of **DNA5,16**, **DNA2,13** and **DNA2,16**. The background function is shown in red. The field positions A-H are marked in Figure A1C.

10.2.5 Data analysis with respect to distance distribution

For distance determination, a single orientation-averaged time trace was generated from the orientation-selective PELDOR data set by summing up all time traces collected at different frequency offsets $\Delta\nu$. Prior to summing up, an exponential background function was fitted to the last 2/3 of the PELDOR time traces; the PELDOR traces were then divided by this background function. Data points at the end of the time trace were cut to avoid artefacts at t_{max} caused by the overlap between the pump pulse and the second π-pulse of the probe channel. Tikhonov regularization of the averaged PELDOR signal was performed using the software DeerAnalysis2013[88] to obtain the distance information. The regularization parameter α was set to 100, which was estimated by using the L-curve criterion. For the bent DNA projects, the software packages DeerAnalysis2011 and DeerAnalysis2013 were used for the analysis of the time traces recorded at X-, Q- and at G-band frequencies, respectively. DeerAnalysis2013 was used for all the traces pertaining to the cocaine aptamer project.

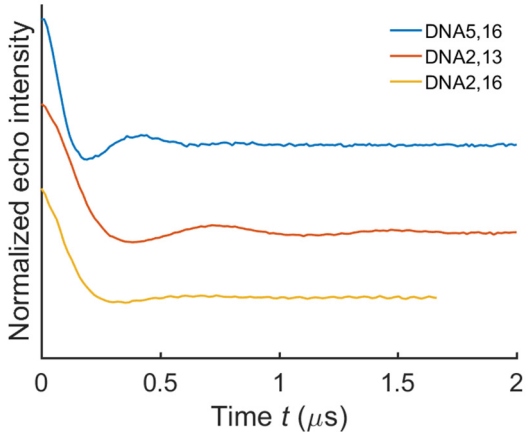

Figure A5: Averaged and background-divided time traces of **DNA5,16**, **DNA2,13** and **DNA2,16** at X-band frequencies. For better visualization, the time traces have been shifted in the vertical direction.

10.2.6 Reproducibility of the modulation depth at G-band frequencies

In order to perform orientation-selective PELDOR experiments, the microwave setup is usually optimized at one field position and the additional time traces are acquired in the same experimental session. The magnetic field is changed and the microwave setup is kept

untouched.[108] However, to achieve a good signal-to-noise ratio of the PELDOR time traces at G-band frequencies, it was not possible to record all time traces in one experimental session. For demonstration of the variance from experiment to experiment in the modulation depth of the PELDOR time traces recorded at G-band frequencies, experimental independently recorded PELDOR time traces were obtained under the same nominal conditions. Two different positions were measured: First, the detection was set at the maximum of the nitroxide spectra (position D in Figure A1C, Figure A6A). Second, the magnetic field position was set half way between the low field edge and the maximum of the EPR spectra (position C in Figure A1C, Figure A6B). The shapes of the PELDOR time traces are identical within the signal-to-noise ratio whereas the modulation depths vary from experiment to experiment.

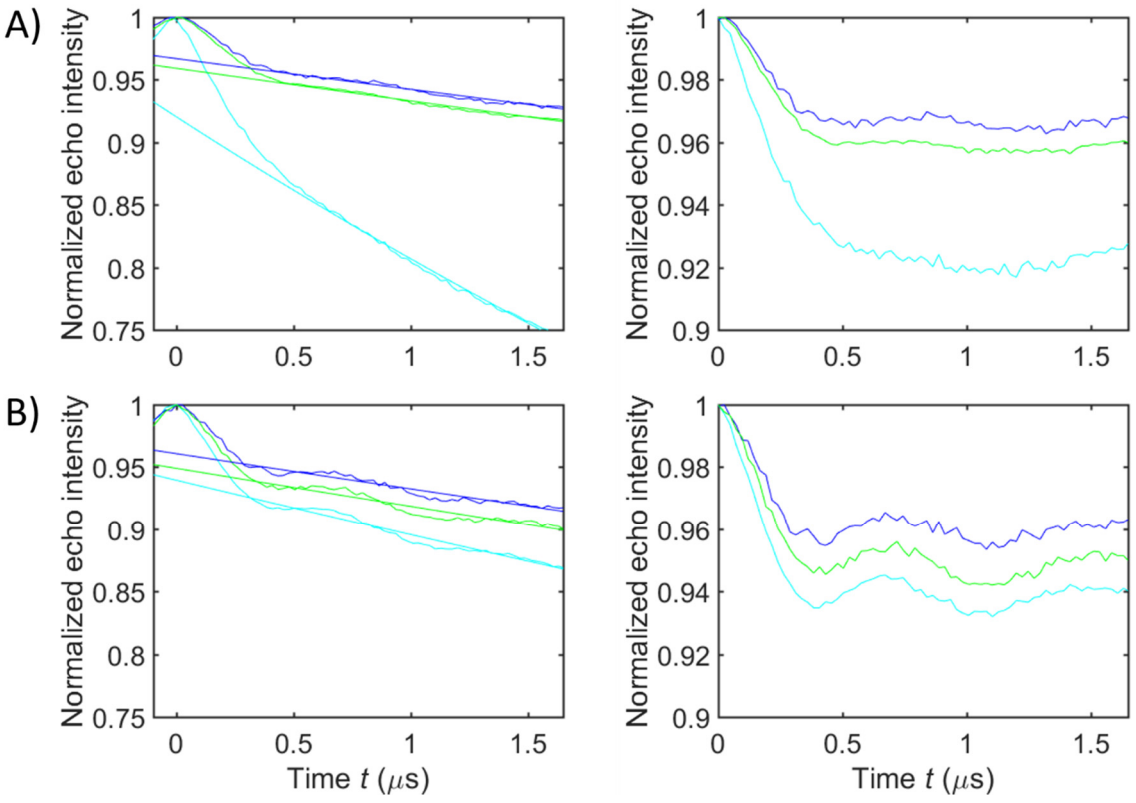

Figure A6: (A) Left: Experimental PELDOR time traces measured at the maximum of the nitroxide spectrum (position D in Figure A1C) and the corresponding background function for **DNA2,13**. Right: Experimental background-divided PELDOR time traces. (B) Left: Experimental PELDOR time traces measured -30 G away from the maximum of the nitroxide spectra (position C in Figure A1C) and the corresponding background function for **DNA2,13**. Right: Experimental background-divided PELDOR time traces.

For the calculation of the reproducibility of the modulation depth parameter λ the Student's t-distribution was used. The t-coefficient $t_{\alpha,\upsilon}$, with the degree of freedom $\upsilon = n - 1$ (n number

of measurement values) and the probability 1 - α, that the true measurement value will be less than $t_{\alpha,\upsilon}$, can be taken from a *t*-distribution quantiles table. In this study the measurements were repeated three times, resulting in $\upsilon = 2$. The errors were calculated with a 95% confidence. Therefore, the *t*-coefficient was $t_{0.95,2} = 2.92$. The confidence interval for the mean modulation depth parameter λ was calculated by using the formula $\bar{\lambda} \pm t_{\alpha,\upsilon}\frac{\sigma_\lambda}{\sqrt{n}}$. At 95% confidence, the true modulation depth parameter λ is expected to be within $\lambda = 0.005 \pm 0.0037$ (74%) (Figure A6A) and $\lambda_2 = 0.0049 \pm 0.0019$ (39%) (Figure A6B).

Table A2: Error estimation of the modulation depth parameter. Mean value $\bar{\lambda}$ and standard deviation σ_λ **(**with its percentage amount), mean value $\bar{\lambda}$ and standard deviation (with its percentage amount) under use of a Student's *t*-distribution.

time traces recorded at	$\bar{\lambda} \pm \sigma_\lambda$	$\sigma_\lambda/\bar{\lambda}$ (%)	$\bar{\lambda} \pm t_{0.95,2}\frac{\sigma_\lambda}{\sqrt{3}}$	$t_{0.95,2}\frac{S_3}{\sqrt{3}}/\bar{\lambda}$ (%)
Position D in Figure A1C	0.0050 ± 0.0022	44	0.0050 ± 0.0037	74
Position C in Figure A1C	0.0049 ± 0.0011	22	0.0049 ± 0.0019	39

The reproducibility of the modulation depth at this frequency band is only within 39–74% with a confidence of 95% using Student's t-distribution. This very large variability is due to variations in the experimental conditions. The B_1-field was not always consistent and reproducible. Therefore, the modulation depth was neglected for the analysis of this data.

10.3 Twist and kink angle calculation describing for the cocaine aptamer helices

For the calculation of the angles describing a kink of the DNA, two independent coordinate systems were defined for each helix (Figure 21). The nitroxide molecular frame of **Ç** attached to a helix represents its frame, which is provided by the design of the **Ç**-label. Thereby, the out of plane normal of the **Ç**-label is parallel to the helix axis.

The kink angle φ is calculated via the scalar product between the z-axes of the **Ç**-label attached to helix II $\vec{A}_{zz,II}$ and the z-axes of the **Ç** attached to helix III $\vec{A}_{zz,III}$.

$$\varphi[°] = \arccos\left(\vec{A}_{zz,II} \cdot \vec{A}_{zz,III}\right) \cdot \frac{180°}{\pi} \qquad \textbf{eq. A1}$$

For the twist angle θ calculation, $\vec{A}_{zz,III}$ is projected to the nitroxide plane which is defined by $\vec{A}_{xx,III}$ and $\vec{A}_{yy,III}$. The sum of the projections of $\vec{A}_{zz,II}$ in the $\vec{A}_{xx,III}$ direction ($\vec{A}_{xx,II} \cdot \vec{A}_{zz,III} = antx_{II}$) and in the $\vec{A}_{yy,III}$ direction ($\vec{A}_{yy,II} \cdot \vec{A}_{zz,III} = anty_{II}$) results in the vector $\vec{A}'_{zz,III}$.

$$\vec{A}'_{zz,III} = antx_{II} \cdot \vec{A}_{xx,II} + anty_{II} \cdot \vec{A}_{yy,II} \qquad \textbf{eq. A2}$$

For angle calculation within the interval [π, -π], $\vec{A}'_{zz,III}$ is defined as a complex number $antx_{II} + i \cdot anty_{II}$. The twist angle θ is then the phase angle of $\vec{A}_{zz,III}$

$$\theta[°] = \text{atan2}(anty_{II}, antx_{II}) \cdot \frac{180°}{\pi} \qquad \textbf{eq. A3}$$

where atan2 is in the Matlab function for the four-quadrant arctangent (see the Matlab documentation). To have the angles within the interval [0, 2π], θ is increased by 2π if negative. The twist angle ψ is calculated in an analog manner.

The weighted mean kink angle $\bar{\varphi}$ and its standard deviation $\sigma_{\bar{\varphi}}$ with the weight of the individual conformers w_i are calculated by

$$\bar{\varphi} = \frac{\sum_{i=1}^{N} \varphi_i \cdot w_i}{\sum_{i=1}^{N} w_i} \text{ and } \sigma_{\bar{\varphi}} = \sqrt{\frac{\sum_{i=1}^{N} (\varphi_i - \bar{\varphi})^2 \cdot w_i}{\sum_{i=1}^{N} w_i}} \qquad \textbf{eq. A4}$$

11 Bibliography

1. Dethoff, E. A.; Chugh, J.; Mustoe, A. M.; Al-Hashimi, H. M., Functional complexity and regulation through RNA dynamics. *Nature* **2012,** *482* (7385), 322-330.
2. Fuxreiter, M.; Simon, I.; Bondos, S., Dynamic protein-DNA recognition: beyond what can be seen. *Trends Biochem.Sci.* **2011,** *36* (8), 415-423.
3. Bischoff, G.; Hoffmann, S., DNA-binding of drugs used in medicinal therapies. *Curr. Med. Chem.* **2002,** *9* (3), 312-348.
4. Kennard, O.; Hunter, W. N., Single-Crystal X-Ray Diffraction Studies of Oligonucleotides and Oligonucleotide-Drug Complexes. *Angew. Chem. Int. Ed.* **1991,** *30* (10), 1254-1277.
5. Salmon, L.; Yang, S.; Al-Hashimi, H. M., Advances in the determination of nucleic acid conformational ensembles. *Annu. Rev. Phys. Chem.* **2014,** *65*, 293-316.
6. Glaeser, R. M., How good can cryo-EM become? *Nat. Methods* **2016,** *13* (1), 28-32.
7. Ernst, R. R., Nuclear magnetic resonance Fourier transform spectroscopy (Nobel Lecture). *Angew. Chem. Int. Ed.* **1992,** *31* (7), 805-823.
8. Bertini, I.; McGreevy, K. S.; Parigi, G., *NMR of Biomolecules: Towards Mechanistic Systems Biology*. Wiley-Blackwell: 2012.
9. Dominguez, C.; Schubert, M.; Duss, O.; Ravindranathan, S.; Allain, F. H. T., Structure determination and dynamics of protein-RNA complexes by NMR spectroscopy. *Prog. Nucl. Magn. Reson. Spectrosc.* **2011,** *58* (1-2), 1-61.
10. Bonvin, A.; Boelens, R.; Kaptein, R., NMR analysis of protein interactions. *Curr. Opin. Chem. Biol.* **2005,** *9* (5), 501-508.
11. Blackledge, M., Recent progress in the study of biomolecular structure and dynamics in solution from residual dipolar couplings. *Prog. Nucl. Magn. Reson. Spectrosc.* **2005,** *46* (1), 23-61.
12. Bailor, M. H.; Musselman, C.; Hansen, A. L.; Gulati, K.; Patel, D. J.; Al-Hashimi, H. M., Characterizing the relative orientation and dynamics of RNA A-form helices using NMR residual dipolar couplings. *Nat. Protoc.* **2007,** *2* (6), 1536-1546.
13. Nitsche, C.; Otting, G., Pseudocontact shifts in biomolecular NMR using paramagnetic metal tags. *Prog. Nucl. Magn. Reson. Spectrosc.* **2017,** *98-99*, 20-49.
14. Otting, G., Protein NMR Using Paramagnetic Ions. *Annu. Rev. Biophys. Biomolec. Struct.* **2010,** *39*, 387-405.
15. Clore, G. M.; Iwahara, J., Theory, Practice, and Applications of Paramagnetic Relaxation Enhancement for the Characterization of Transient Low-Population States of Biological Macromolecules and Their Complexes. *Chem. Rev.* **2009,** *109* (9), 4108-4139.
16. Zhang, Y.; Yamaguchi, T.; Kato, K., New NMR Tools for Characterizing the Dynamic Conformations and Interactions of Oligosaccharides. *Chem. Lett.* **2013,** *42* (12), 1455-1462.
17. Akke, M., NMR methods for characterizing microsecond to millisecond dynamics in recognition and catalysis. *Curr. Opin. Struct. Biol.* **2002,** *12* (5), 642-647.
18. Palmer, A. G.; Kroenke, C. D.; Loria, J. P., Nuclear magnetic resonance methods for quantifying microsecond-to-millisecond motions in biological macromolecules. *Methods Enzymol.* **2001,** *339*, 204-238.
19. Förster, T., Zwischenmolekulare Energiewanderung und Fluoreszenz. *Ann. Phys.-Berlin* **1948,** *2* (1-2), 55-75.
20. Woźniak, A. K.; Schröder, G. F.; Grubmüller, H.; Seidel, C. A. M.; Oesterhelt, F., Single-molecule FRET measures bends and kinks in DNA. *Proc. Natl. Acad. Sci. U. S. A.*

2008, *105*, 18337-18342.
21. Rabenstein, M. D.; Shin, Y. K., Determination of the distance between 2 spin labels attached to a macromolecule. *Proc. Natl. Acad. Sci. U. S. A.* **1995,** *92* (18), 8239-8243.
22. Macosko, J. C.; Pio, M. S.; Tinoco, I.; Shin, Y. K., A novel 5 ' displacement spin-labeling technique for electron paramagnetic resonance spectroscopy of RNA. *RNA-Publ. RNA Soc.* **1999,** *5* (9), 1158-1166.
23. Kim, N. K.; Murali, A.; DeRose, V. J., A distance ruler for RNA using EPR and site-directed spin labeling. *Chem. Biol.* **2004,** *11* (7), 939-948.
24. Milov, A. D.; Salikhov, K. M.; Shchirov, M. D., Application of the double resonance method to electron spin echo in a study of the spatial distribution of paramagnetic centers in solids. *Sov Phys Solid State* **1981,** *23*, 565-569.
25. Milov, A. D.; Ponomarev, A. B.; Tsvetkov, Y. D., Electron-electron double resonance in electron spin echo: model biradical systems and sensitized photolysis of decalin. *Chem. Phys. Lett.* **1984,** *110*, 67-72.
26. Sponer, J.; Krepl, M.; Banas, P.; Kuhrova, P.; Zgarbova, M.; Jurecka, P.; Havrila, M.; Otyepka, M., How to understand atomistic molecular dynamics simulations of RNA and protein-RNA complexes? *Wiley Interdiscip. Rev.-RNA* **2017,** *8* (3), 17.
27. Neidle, S., *Principles of nucleic acid structure*. Elsevier: 2008.
28. Lilley, D. M. J., Structures of helical junctions in nucleic acids. *Q. Rev. Biophys.* **2000,** *33* (2), 109-159.
29. J. D. Watson; Crick, F. H., Molecular structure of nucleic acids; a structure for deoxyribose nucleic acid. *Nature* **1953,** *171*, 4356.
30. G. M. Blackburn; M. J. Gait; D. Loakes; D. M. Williams, *Nucleic acids in chemistry and biology*. 3rd ed.; The Royal Society of Chemistry: Cambridge, 2006.
31. Nelson, D. L.; Cox, M. C., *Lehninger Principles of biochemistry*. 4 ed.; Palgrave Macmillan; Freeman.
32. Holliday, R., A mechanism for gene conversion in fungi. *Genet. Res.* **1964,** *5*, 282–304.
33. Forster, A. C.; Symons, R. H., Self-cleavage of plus and minus RNAs of a virusoid and a structural model for the active sites. *Cell* **1987,** *49*, 211–220.
34. Haseloff, J.; Gerlach, W. L., Simple RNA enzymes with new and highly specific endoribonuclease activities. *Nature* **1988,** *334* (6183), 585-591.
35. Duckett, D. R.; Lilley, D. M. J., The 3-way DNA junction is a Y-shaped molecule in which there is no helix helix stacking. *Embo J.* **1990,** *9* (5), 1659-1664.
36. Stuhmeier, F.; Welch, J. B.; Murchie, A. I. H.; Lilley, D. M. J.; Clegg, R. M., Global structure of three-way DNA junctions with and without additional unpaired bases: A fluorescence resonance energy transfer analysis. *Biochemistry* **1997,** *36* (44), 13530-13538.
37. Shlyakhtenko, L. S.; Potaman, V. N.; Sinden, R. R.; Gall, A. A.; Lyubchenko, Y. L., Structure and dynamics of three-way DNA junctions: atomic force microscopy studies. *Nucleic Acids Res.* **2000,** *28* (18), 3472-3477.
38. Thiviyanathan, V.; Luxon, B. A.; Leontis, N. B.; Illangasekare, N.; Donne, D. G.; Gorenstein, D. G., Hybrid-hybrid matrix structural refinement of a DNA three-way junction from 3D NOESY-NOESY. *J. Biomol. NMR* **1999,** *14* (3), 209-221.
39. Wu, B.; Girard, F.; van Buuren, B.; Schleucher, J.; Tessari, M.; Wijmenga, S., Global structure of a DNA three-way junction by solution NMR: towards prediction of 3H fold. *Nucleic Acids Res.* **2004,** *32* (10), 3228-3239.
40. Kaminker, I.; Bye, M.; Mendelman, N.; Gislason, K.; Sigurdsson, S. T.; Goldfarb, D., Distance measurements between manganese(II) and nitroxide spin-labels by DEER determine a binding site of Mn2+ in the HP92 loop of ribosomal RNA. *Phys. Chem. Chem.*

Phys. **2015,** *17* (23), 15098-15102.
41. Shelke, S. A.; Sigurdsson, S. T., Site-directed spin labelling of nucleic acids. *Eur. J. Org. Chem.* **2012,** (12), 2291-2301.
42. Sigurdsson, S. T., Nitroxides and nucleic acids: Chemistry and electron paramagnetic resonance (EPR) spectroscopy. *Pure Appl. Chem.* **2011,** *83* (3), 677-686.
43. Edwards, T. E.; Sigurdsson, S. T., Site-specific incorporation of nitroxide spin-labels into 2 '-positions of nucleic acids. *Nat. Protoc.* **2007,** *2* (8), 1954-1962.
44. Cai, Q.; Kusnetzow, A. K.; Hubbell, W. L.; Haworth, I. S.; Gacho, G. P. C.; Van Eps, N.; Hideg, K.; Chambers, E. J.; Qin, P. Z., Site-directed spin labeling measurements of nanometer distances in nucleic acids using a sequence-independent nitroxide probe. *Nucleic Acids Res.* **2006,** *34* (17), 4722-4730.
45. Spaltenstein, A.; Robinson, B. H.; Hopkins, P. B., A rigid and nonperturbting probe for duplex DNA motion *J. Am. Chem. Soc.* **1988,** *110* (4), 1299-1301.
46. Fischhaber, P. L.; Reese, A. W.; Nguyen, T.; Kirchner, J. J.; Hustedt, E. J.; Robinson, B. H.; Hopkins, P. B., Synthesis of duplex DNA containing a spin labeled analog of 2'-deoxycytidine. *Nucleosides Nucleotides* **1997,** *16* (4), 365-377.
47. Kamble, N. R.; Granz, M.; Prisner, T. F.; Sigurdsson, S. T., Noncovalent and site-directed spin labeling of duplex RNA. *Chem. Commun.* **2016,** *52* (100), 14442-14445.
48. Schiemann, O.; Piton, N.; Plackmeyer, J.; Bode, B. E.; Prisner, T. F.; Engels, J. W., Spin labeling of oligonucleotides with the nitroxide TPA and use of PELDOR, a pulse EPR method, to measure intramolecular distances. *Nat. Protoc.* **2007,** *2* (4), 904-923.
49. Schiemann, O.; Piton, N.; Mu, Y. G.; Stock, G.; Engels, J. W.; Prisner, T. F., A PELDOR-based nanometer distance ruler for oligonucleotides. *J. Am. Chem. Soc.* **2004,** *126* (18), 5722-5729.
50. Piton, N.; Mu, Y. G.; Stock, G.; Prisner, T. F.; Schiemann, O.; Engels, J. W., Base-specific spin-labeling of RNA for structure determination. *Nucleic Acids Res.* **2007,** *35* (9), 3128-3143.
51. Krstić, I.; Frolow, O.; Sezer, D.; Endeward, B.; Weigand, J. E.; Suess, B.; Engels, J. W.; Prisner, T. F., PELDOR spectroscopy reveals preorganization of the neomycin-responsive riboswitch tertiary structure. *J. Am. Chem. Soc.* **2010,** *132* (5), 1454-1455.
52. Krstic, I.; Hansel, R.; Romainczyk, O.; Engels, J. W.; Dotsch, V.; Prisner, T. F., Long-Range Distance Measurements on Nucleic Acids in Cells by Pulsed EPR Spectroscopy. *Angew. Chem. Int. Ed.* **2011,** *50* (22), 5070-5074.
53. Gannett, P. M.; Darian, E.; Powell, J. H.; Johnson, E. M., A short procedure for synthesis of 4-ethynyl-2,2,6,6-tetramethyl-3,4-dehydro-piperidine-1-oxyl nitroxide. *Synth. Commun.* **2001,** *31* (14), 2137-2141.
54. Gannett, P. M.; Powell, J. H.; Johnson, E. M.; Darian, E.; Dalal, N. S.; Norton, M. L.; Budil, D. E., Solid-phase DNA binding detection by EPR spectroscopy. *Tetrahedron Lett.* **2002,** *43* (11), 1931-1933.
55. Singh, V.; Azarkh, M.; Exner, T. E.; Hartig, J. S.; Drescher, M., Human Telomeric Quadruplex Conformations Studied by Pulsed EPR. *Angew. Chem. Int. Ed.* **2009,** *48* (51), 9728-9730.
56. Gophane, D. B.; Sigurdsson, S. T., Hydrogen-bonding controlled rigidity of an isoindoline-derived nitroxide spin label for nucleic acids. *Chem. Commun.* **2013,** *49* (10), 999-1001.
57. Erlenbach, N.; Endeward, B.; Schops, P.; Gophane, D. B.; Sigurdsson, S. T.; Prisner, T. F., Flexibilities of isoindoline-derived spin labels for nucleic acids by orientation selective PELDOR. *Phys. Chem. Chem. Phys.* **2016,** *18* (24), 16196-16201.
58. Gophane, D. B.; Endeward, B.; Prisner, T. F.; Sigurdsson, S. T., Conformationally Restricted Isoindoline-Derived Spin Labels in Duplex DNA: Distances and Rotational

Flexibility by Pulsed Electron-Electron Double Resonance Spectroscopy. *Chem.-Eur. J.* **2014,** *20* (48), 15913-15919.
59. Barhate, N.; Cekan, P.; Massey, A. P.; Sigurdsson, S. T., A nucleoside that contains a rigid nitroxide spin label: A fluorophore in disguise. *Angew. Chem. -Int. Ed.* **2007,** *46* (15), 2655-2658.
60. Cekan, P.; Sigurdsson, S. T., Conformation and dynamics of nucleotides in bulges and symmetric internal loops in duplex DNA studied by EPR and fluorescence spectroscopies. *Biochem. Biophys. Res. Commun.* **2012,** *420* (3), 656-661.
61. Cekan, P.; Smith, A. L.; Barhate, N.; Robinson, B. H.; Sigurdsson, S. T., Rigid spin-labeled nucleoside Ç: a nonperturbing EPR probe of nucleic acid conformation. *Nucleic Acids Res.* **2008,** *36* (18), 5946-5954.
62. Miller, T. R.; Hopkins, P. B., Toward the synthesis of a 2nd-generation nitroxide spin-probe for DNA dynamics studies *Bioorg. Med. Chem. Lett.* **1994,** *4* (8), 981-986.
63. Miller, T. R.; Alley, S. C.; Reese, A. W.; Solomon, M. S.; McCallister, W. V.; Mailer, C.; Robinson, B. H.; Hopkins, P. B., A probe for sequence-dependent nucleic-acid dynamics. *J. Am. Chem. Soc.* **1995,** *117* (36), 9377-9378.
64. Edwards, T. E.; Cekan, P.; Reginsson, G. W.; Shelke, S. A.; Ferre-D'Amare, A. R.; Schiemann, O.; Sigurdsson, S. T., Crystal structure of a DNA containing the planar, phenoxazine-derived bi-functional spectroscopic probe Ç. *Nucleic Acids Res.* **2011,** *39* (10), 4419-4426.
65. Shelke, S. A.; Sigurdsson, S. T., Noncovalent and Site-Directed Spin Labeling of Nucleic Acids. *Angew. Chem.-Int. Edit.* **2010,** *49* (43), 7984-7986.
66. Cekan, P.; Jonsson, E. O.; Sigurdsson, S. T., Folding of the cocaine aptamer studied by EPR and fluorescence spectroscopies using the bifunctional spectroscopic probe C. *Nucleic Acids Res.* **2009,** *37* (12), 3990-3995.
67. Cekan, P.; Sigurdsson, S. T., Single base interrogation by a fluorescent nucleotide: each of the four DNA bases identified by fluorescence spectroscopy. *Chem. Commun.* **2008,** (29), 3393-3395.
68. Hobartner, C.; Sicoli, G.; Wachowius, F.; Gophane, D. B.; Sigurdsson, S. T., Synthesis and Characterization of RNA Containing a Rigid and Nonperturbing Cytidine-Derived Spin Label. *J. Org. Chem.* **2012,** *77* (17), 7749-7754.
69. Tkach, I.; Pornsuwan, S.; Hobartner, C.; Wachowius, F.; Sigurdsson, S. T.; Baranova, T. Y.; Diederichsen, U.; Sicoli, G.; Bennati, M., Orientation selection in distance measurements between nitroxide spin labels at 94 GHz EPR with variable dual frequency irradiation. *Phys. Chem. Chem. Phys.* **2013,** *15* (10), 3433-7.
70. Marko, A.; Denysenkov, V.; Margraf, D.; Cekan, P.; Schiemann, O.; Sigurdsson, S. T.; Prisner, T. F., Conformational Flexibility of DNA. *J. Am. Chem. Soc.* **2011,** *133* (34), 13375-13379.
71. Schiemann, O.; Cekan, P.; Margraf, D.; Prisner, T. F.; Sigurdsson, S. T., Relative orientation of rigid nitroxides by PELDOR: beyond distance measurements in nucleic acids. *Angew. Chem. -Int. Ed.* **2009,** *48* (18), 3292-3295.
72. Marko, A.; Margraf, D.; Cekan, P.; Sigurdsson, S. T.; Schiemann, O.; Prisner, T. F., Analytical method to determine the orientation of rigid spin labels in DNA. *Phys. Rev. E* **2010,** *81* (2).
73. Schweiger, A.; Jeschke, G., *Principles of pulse electron paramagentic resonance*. Oxford University Press: 2001.
74. Weil, J. A.; Bolton, J. R., *Electron Paramagnetic Resonance: Elementary Theory and Practical Applications*. 2nd ed.; John Wiley & Sons, Inc.: 2007.
75. Gerlach, W.; Stern, O., The experimental evidence of direction quantistion in the magnetic field. *Z. Phys.* **1922,** *9*, 349-352.

76. Gerlach, W.; Stern, O., The magnetic moment of silver atoms. *Z. Phys.* **1922,** *9*, 353-355.
77. Gerlach, W.; Stern, O., The directional quantisation in the magnetic field. *Ann. Phys.-Berlin* **1924,** *74* (16), 673-697.
78. Abragam, A.; Pryce, M. H. L., Theory of the Nuclear Hyperfine Structure of ParamagneticResonance Spectra in Crystals. *Proceedings of the Royal Society of London Series a-Mathematical and Physical Sciences* **1951,** *205* (1080), 135-153.
79. Hu, K. N.; Bajaj, V. S.; Rosay, M.; Griffin, R. G., High-frequency dynamic nuclear polarization using mixtures of TEMPO and trityl radicals. *J. Chem. Phys.* **2007,** *126* (4), 7.
80. Schneider, D. J.; Freed, J. H., *Biological magnetic Resonance: Spin labeling: Theory and applications*. Plenum Press: 1989; Vol. 8.
81. Schiemann, O.; Prisner, T. F., Long-range distance determinations in biomacromolecules by EPR spectroscopy. *Q. Rev. Biophys.* **2007,** *40* (1), 1-53.
82. Jeschke, G., DEER distance measurements on proteins. *Annu. Rev. Phys. Chem.* **2012,** *63*, 419-446.
83. Milov, A. D.; Salikohov, K. M.; Shirov, M. D., Application of ENDOR in electron-spin echo for paramagnetic center space distribution in solids. *Fiz. Tverd. Tela* **1981,** *23* (4), 975-982.
84. Milov, A. D.; Ponomarev, A. B.; Tsvetkov, Y. D., Electron electron double-resonance in electron-spin echo - model biradical systems and the sensitized photolysis of decalin. *Chem. Phys. Lett.* **1984,** *110* (1), 67-72.
85. Martin, R. E.; Pannier, M.; Diederich, F.; Gramlich, V.; Hubrich, M.; Spiess, H. W., Determination of end-to-end distances in a series of TEMPO diradicals of up to 2.8 nm length with a new four-pulse double electron electron resonance experiment. *Angew. Chem.-Int. Edit.* **1998,** *37* (20), 2834-2837.
86. Pannier, M.; Veit, S.; Godt, A.; Jeschke, G.; Spiess, H. W., Dead-time free measurement of dipole-dipole interactions between electron spins. *J. Magn. Reson.* **2000,** *142* (2), 331-340.
87. Kattnig, D. R.; Reichenwallner, J.; Hinderberger, D., Modeling Excluded Volume Effects for the Faithful Description of the Background Signal in Double Electron-Electron Resonance. *J. Phys. Chem. B* **2013,** *117* (51), 16542-16557.
88. Jeschke, G.; Chechik, V.; Ionita, P.; Godt, A.; Zimmermann, H.; Banham, J.; Timmel, C. R.; Hilger, D.; Jung, H., DeerAnalysis2006 - a comprehensive software package for analyzing pulsed ELDOR data. *Appl. Magn. Reson.* **2006,** *30* (3-4), 473-498.
89. Larsen, R. G.; Singel, D. J., Double electron-electron resonance spin-echo modulation - spectroscopic measurement of electron-spin pair seperations in orientationally disordered solids. *J. Chem. Phys.* **1993,** *98* (7), 5134-5146.
90. Maryasov, A. G.; Tsvetkov, Y. D.; Raap, J., Weakly coupled radical pairs in solids: ELDOR in ESE structure studies. *Appl. Magn. Reson.* **1998,** *14* (1), 101-113.
91. Stoll, S.; Schweiger, A., EasySpin, a comprehensive software package for spectral simulation and analysis in EPR. *J. Magn. Reson.* **2006,** *178* (1), 42-55.
92. Tkach, I.; Sicoli, G.; Höbartner, C.; Bennati, M., A dual-mode microwave resonator for double electron-electron spin resonance spectroscopy at W-band microwave frequencies. *J. Magn. Reson.* **2011,** *209* (2), 341-346.
93. Schoeps, P.; Spindler, P. E.; Marko, A.; Prisner, T. F., Broadband spin echoes and broadband SIFTER in EPR. *J. Magn. Reson.* **2015,** *250*, 55-62.
94. Doll, A.; Jeschke, G., EPR-correlated dipolar spectroscopy by Q-band chirp SIFTER. *Phys. Chem. Chem. Phys.* **2016,** *18* (33), 23111-23120.
95. Marko, A.; Prisner, T. F., An algorithm to analyze PELDOR data of rigid spin label pairs. *Phys. Chem. Chem. Phys.* **2013,** *15* (2), 619-627.

96. Godt, A.; Schulte, M.; Zimmermann, H.; Jeschke, G., How flexible are poly(para-phenyleneethynylene)s? *Angew. Chem.-Int. Edit.* **2006,** *45* (45), 7560-7564.
97. Prisner, T. F.; Marko, A.; Sigurdsson, S. T., Conformational dynamics of nucleic acid molecules studied by PELDOR spectroscopy with rigid spin labels. *J. Magn. Reson.* **2015,** *252*, 187-198.
98. Denysenkov, V. P.; Prisner, T. F.; Stubbe, J.; Bennati, M., High-field pulsed electron-electron double resonance spectroscopy to determine the orientation of the tyrosyl radicals in ribonucleotide reductase. *Proc. Natl. Acad. Sci. U. S. A.* **2006,** *103* (36), 13386-13390.
99. Denysenkov, V. P.; Biglino, D.; Lubitz, W.; Prisner, T. F.; Bennati, M., Structure of the tyrosyl biradical in mouse R2 ribonucleotide reductase from high-field PELDOR. *Angew. Chem.-Int. Edit.* **2008,** *47* (7), 1224-1227.
100. Margraf, D.; Bode, B. E.; Marko, A.; Schiemann, O.; Prisner, T. F., Conformational flexibility of nitroxide biradicals determined by X-band PELDOR experiments. *Mol. Phys.* **2007,** *105* (15-16), 2153-2160.
101. Margraf, D.; Cekan, P.; Prisner, T. F.; Sigurdsson, S. T.; Schiemann, O., Ferro- and antiferromagnetic exchange coupling constants in PELDOR spectra. *Phys. Chem. Chem. Phys.* **2009,** *11* (31), 6708-6714.
102. Savitsky, A.; Dubinskii, A. A.; Zimmermann, H.; Lubitz, W.; Möbius, K., High-Field Dipolar Electron Paramagnetic Resonance (EPR) Spectroscopy of Nitroxide Biradicals for Determining Three-Dimensional Structures of Biomacromolecules in Disordered Solids. *The Journal of Physical Chemistry B* **2011,** *115* (41), 11950-11963.
103. Reginsson, G. W.; Schiemann, O., Pulsed electron-electron double resonance: beyond nanometre distance measurements on biomacromolecules. *Biochem. J.* **2011,** *434*, 353-363.
104. Reginsson, G. W.; Hunter, R. I.; Cruickshank, P. A.; Bolton, D. R.; Sigurdsson, S. T.; Smith, G. M.; Schiemann, O., W-band PELDOR with 1 kW microwave power: molecular geometry, flexibility and exchange coupling. *Journal of magnetic resonance (San Diego, Calif. : 1997)* **2012,** *216*, 175-82.
105. Reginsson, G. W.; Kunjir, N. C.; Sigurdsson, S. T.; Schiemann, O., Trityl Radicals: Spin Labels for Nanometer-Distance Measurements. *Chem.-Eur. J.* **2012,** *18* (43), 13580-13584.
106. Bode, B. E.; Plackmeyer, J.; Prisner, T. F.; Schiemann, O., PELDOR measurements on a nitroxide-labeled Cu(II) porphyrin: Orientation selection, spin-density distribution, and conformational flexibility. *J. Phys. Chem. A* **2008,** *112* (23), 5064-5073.
107. Lovett, J. E.; Bowen, A. M.; Timmel, C. R.; Jones, M. W.; Dilworth, J. R.; Caprotti, D.; Bell, S. G.; Wong, L. L.; Harmer, J., Structural information from orientationally selective DEER spectroscopy. *Phys. Chem. Chem. Phys.* **2009,** *11* (31), 6840-6848.
108. Polyhach, Y.; Godt, A.; Bauer, C.; Jeschke, G., Spin pair geometry revealed by high-field DEER in the presence of conformational distributions. *J. Magn. Reson.* **2007,** *185* (1), 118-129.
109. Marko, A.; Margraf, D.; Yu, H.; Mu, Y.; Stock, G.; Prisner, T., Molecular orientation studies by pulsed electron-electron double resonance experiments. *J. Chem. Phys.* **2009,** *130* (6), 064102-1-064102-9.
110. Savitsky, A.; Dubinskii, A. A.; Flores, M.; Lubitz, W.; Mobius, K., Orientation-resolving pulsed electron dipolar high-field EPR spectroscopy on disordered solids: I. Structure of spin-correlated radical pairs in bacterial photosynthetic reaction centers. *J. Phys. Chem. B* **2007,** *111* (22), 6245-6262.
111. Jeschke, G., Conformational dynamics and distribution of nitroxide spin labels.

Prog. Nucl. Magn. Reson. Spectrosc. **2013,** *72*, 42-60.
112. Hagelueken, G.; Ward, R.; Naismith, J. H.; Schiemann, O., MtsslWizard: In Silico Spin-Labeling and Generation of Distance Distributions in PyMOL. *Appl. Magn. Reson.* **2012,** *42* (3), 377-391.
113. Klose, D.; Klare, J. P.; Grohmann, D.; Kay, C. W. M.; Werner, F.; Steinhoff, H. J., Simulation vs. Reality: A Comparison of In Silico Distance Predictions with DEER and FRET Measurements. *PLoS One* **2012,** *7* (6), 17.
114. Dastvan, R.; Brouwer, E. M.; Schuetz, D.; Mirus, O.; Schleiff, E.; Prisner, T. F., Relative Orientation of POTRA Domains from Cyanobacterial Omp85 Studied by Pulsed EPR Spectroscopy. *Biophys. J.* **2016,** *110* (10), 2195-2206.
115. Abe, C.; Klose, D.; Dietrich, F.; Ziegler, W. H.; Polyhach, Y.; Jeschke, G.; Steinhoff, H. J., Orientation selective DEER measurements on vinculin tail at X-band frequencies reveal spin label orientations. *J. Magn. Reson.* **2012,** *216*, 53-61.
116. Marko, A.; Denysenkov, V. P.; Margraf, D.; Cekan, P.; Schiemann, O.; Sigurdsson, S. T.; Prisner, T. F., Conformational flexibility of DNA. *J. Am. Chem. Soc.* **2011,** *133*, 13375-13379.
117. Grytz, C. M.; Marko, A.; Cekan, P.; Sigurdsson, S. T.; Prisner, T. F., Flexibility and conformation of the cocaine aptamer studied by PELDOR. *Phys. Chem. Chem. Phys.* **2016,** *18* (4), 2993-3002.
118. Grytz, C. M.; Kazemi, S.; Marko, A.; Cekan, P.; Guntert, P.; Sigurdsson, S. T.; Prisner, T. F., Determination of helix orientations in a flexible DNA by multi-frequency EPR spectroscopy. *Phys. Chem. Chem. Phys.* **2017,** *19* (44), 29801-29811.
119. Bonomi, M.; Heller, G. T.; Camilloni, C.; Vendruscolo, M., Principles of protein structural ensemble determination. *Curr. Opin. Struct. Biol.* **2017,** *42*, 106-116.
120. Ravera, E.; Sgheri, L.; Parigi, G.; Luchinat, C., A critical assessment of methods to recover information from averaged data. *Phys. Chem. Chem. Phys.* **2016,** *18* (8), 5686-5701.
121. Dornberger, U.; Hillisch, A.; Gollmick, F. A.; Fritzsche, H.; Diekmann, S., Solution structure of a five-adenine bulge loop within a DNA duplex. *Biochemistry* **1999,** *38* (39), 12860-12868.
122. Andrałojć, W.; Ravera, E.; Salmon, L.; Parigi, G.; Al-Hashimi, H. M.; Luchinat, C., Inter-helical conformational preferences of HIV-1 TAR-RNA from maximum occurrence analysis of NMR data and molecular dynamics simulations. *Phys. Chem. Chem. Phys.* **2016,** *18* (8), 5743-5752.
123. Salmon, L.; Bascom, G.; Andricioaei, I.; Al-Hashimi, H. M., A general method for constructing atomic-resolution RNA ensembles using NMR residual dipolar couplings: The basis for interhelical motions revealed. *J. Am. Chem. Soc.* **2013,** *135* (14), 5457-5466.
124. Yang, Y. H.; Ramelot, T. A.; McCarrick, R. M.; Ni, S. S.; Feldmann, E. A.; Cort, J. R.; Wang, H.; Ciccosanti, C.; Jiang, M.; Janjua, H.; Acton, T. B.; Xiao, R.; Everett, J. K.; Montelione, G. T.; Kennedy, M. A., Combining NMR and EPR methods for homodimer protein structure determination. *J. Am. Chem. Soc.* **2010,** *132* (34), 11910-11913.
125. Rao, J. N.; Jao, C. C.; Hegde, B. G.; Langen, R.; Ulmer, T. S., A combinatorial NMR and EPR approach for evaluating the structural ensemble of partially folded proteins. *J. Am. Chem. Soc.* **2010,** *132* (25), 8657-8668.
126. Duss, O.; Yulikov, M.; Jeschke, G.; Allain, F. H.-T., EPR-aided approach for solution structure determination of large RNAs or protein-RNA complexes. *Nat. Commun.* **2014,** *5*, 1-9.
127. Stojanovic, M. N.; de Prada, P.; Landry, D. W., Fluorescent sensors based on aptamer self-assembly. *J. Am. Chem. Soc.* **2000,** *122* (46), 11547-11548.
128. Stojanovic, M. N.; de Prada, P.; Landry, D. W., Aptamer-based folding fluorescent

sensor for cocaine. *J. Am. Chem. Soc.* **2001,** *123* (21), 4928-4931.
129. Neves, M. A. D.; Reinstein, O.; Johnson, P. E., Defining a Stem Length-Dependent Binding Mechanism for the Cocaine-Binding Aptamer. A Combined NMR and Calorimetry Study. *Biochemistry* **2010,** *49* (39), 8478-8487.
130. Bode, B. E.; Margraf, D.; Plackmeyer, J.; Dürner, G.; Prisner, T. F.; Schiemann, O., Counting the monomers in nanometer-sized oligomers by pulsed electron - Electron double resonance. *J. Am. Chem. Soc.* **2007,** *129* (21), 6736-6745.
131. Jeschke, G.; Polyhach, Y., Distance measurements on spin-labelled biomacromolecules by pulsed electron paramagnetic resonance. *Phys. Chem. Chem. Phys.* **2007,** *9* (16), 1895-1910.
132. Zheng, G. H.; Lu, X. J.; Olson, W. K., Web 3DNA-a web server for the analysis, reconstruction, and visualization of three-dimensional nucleic-acid structures. *Nucleic Acids Res.* **2009,** *37*, W240-W246.
133. Güntert, P.; Mumenthaler, C.; Wüthrich, K., Torsion angle dynamics for NMR structure calculation with the new program DYANA. *J. Mol. Biol.* **1997,** *273* (1), 283-298.
134. Güntert, P.; Buchner, L., Combined automated NOE assignment and structure calculation with CYANA. *J. Biomol. NMR* **2015,** *62* (4), 453-471.
135. Endeward, B.; Marko, A.; Denysenkov, V. P.; Sigurdsson, S. T.; Prisner, T. F., Advanced EPR methods for studying conformational dynamics of nucleic acids. *Methods Enzymol.* **2015,** *564*, 403-425.
136. Bailor, M. H.; Sun, X.; Al-Hashimi, H. M., Topology links RNA secondary structure with global conformation, dynamics, and adaptation. *Science* **2010,** *327* (5962), 202-206.
137. Duchardt-Ferner, E.; Weigand, J. E.; Ohlenschläger, O.; Schmidtke, S. R.; Suess, B.; Wöhnert, J., Highly modular structure and ligand binding by conformational capture in a minimalistic riboswitch. *Angew. Chem. -Int. Ed.* **2010,** *49* (35), 6216-6219.
138. Shevelev, G. Y.; Krumkacheva, O. A.; Lomzov, A. A.; Kuzhelev, A. A.; Rogozhnikova, O. Y.; Trukhin, D. V.; Troitskaya, T. I.; Tormyshev, V. M.; Fedin, M. V.; Pyshnyi, D. V.; Bagryanskaya, E. G., Physiological-temperature distance measurement in nucleic acid using triarylmethyl-based spin labels and pulsed dipolar EPR spectroscopy. *J. Am. Chem. Soc.* **2014,** *136* (28), 9874-9877.
139. Weigand, J. E.; Sanchez, M.; Gunnesch, E. B.; Zeiher, S.; Schroeder, R.; Suess, B., Screening for engineered neomycin riboswitches that control translation initiation. *RNA-Publ. RNA Soc.* **2008,** *14* (1), 89-97.
140. Schmidtke, S. R.; Duchardt-Ferner, E.; Weigand, J. E.; Suess, B.; Wohnert, J., NMR resonance assignments of an engineered neomycin-sensing riboswitch RNA bound to ribostamycin and tobramycin. *Biomol. NMR Assign.* **2010,** *4* (1), 115-118.
141. Neves, M. A. D.; Reinstein, O.; Saad, M.; Johnson, P. E., Defining the secondary structural requirements of a cocaine-binding aptamer by a thermodynamic and mutation study. *Biophys. Chem.* **2010,** *153* (1), 9-16.
142. Epel, B.; Gromov, I.; Stoll, S.; Schweiger, A.; Goldfarb, D., Spectrometer manager: A versatile control software for pulse EPR spectrometers. *Conc. Magn. Reson. 26B* **2005**, 36-45.

12 List of Figures and Tables

13 List of publications

- Grytz, C.M., Kazemi, S., Marko, A., Cekan, P., Güntert, P.; Sigurdsson, S.Th., and Prisner, T. (2017) Determination of helix orientations in highly flexible DNAs by multi-frequency EPR spectroscopy, *Phys.Chem.Chem.Phys.,*19, 29801-29811

- Grytz, C.M., Marko, A., Cekan, P., Sigurdsson, S.Th., and Prisner, T. (2016), Flexibility and conformation of the cocaine aptamer studied by PELDOR. *Phys.Chem.Chem.Phys.,*18, 2993-3002

- Zhuang, J.L., Kind, M., Grytz, C.M., Farr, F., Diefenbach, M., Tussupbayev, S., Holthausen, M. C. and Terfort, A. (2015), Insight into the Oriented Growth of Surface-Attached Metal-Organic Frameworks: Surface Functionality, Deposition Temperature, and First Layer Order. J. Am. Chem. Soc., 137, 8237-8243

- Krstic, I., Marko, A., Grytz, C.M., Endeward, B. and Prisner, T.F. (2013), Structure and conformational dynamics of RNA determined by pulsed EPR. *RNA Structure and Folding, Biophysical Techniques and Prediction Methods ed. Hrsg. v. Klostermeier, D. and Hammann, Ch.,* De Gruyter, Chapter 11, 261-286

14 Conference contributions

- 5th European EPR Summer School on Advanced EPR Spectroscopy, Konstanz, Germany, 05.-12.09.2010 (poster)
- EUROMAR Magnetic Resonance Conference 2011, Frankfurt am Main, Germany, 21.-25.08.2011 (poster)
- EUROMAR Magnetic Resonance Conference 2012, Dublin, Ireland, 01.-05.07.2012 (poster)
- 'Kick-off' Meeting SFB 902, KTC Königstein, 28.-29.10.12 (talk)
- 6th European EPR Summer School 2013, Rehovot, Israel, 12.-18.01.2013 (poster)
- Seminar of the Institute of Physical and Theoretical Chemistry 2013, Hirschegg, Austria, 18.-22.3.2013 (talk)
- Workshop on RNA methods SFB902, Bad Homburg, Germany, 13.-14.12.2013 (talk)
- EUROMAR Magnetic Resonance Conference 2014, Zurich, Switzerland, 29.06-03.07.2014 (poster)
- 3rd Conference on Regulating with RNA in Bacteria, Würzburg, Germany, 04-08.06.2013 (poster)
- Winterschool SFB902 2014, Obergurgel, Austria, 13.-17.01.2014 (talk)
- Integrating spectroscopy and theoretical methods to analyse molecular machines, Schloss Ringberg, Kreuth, Germany, 10.-13.12.2014 (poster)
- Seminar of the Institute of Physical and Theoretical Chemistry 2016, Hirschegg, Austria, 21.-25.03.2016 (talk)
- 37th FGMR discussion meeting, Darmstadt, Germany, 07.-10.9.2015 (poster)
- ISMAR 2015 The 19th International Society of Magnetic Resonance Conference, Shanghai, China, 16.-21.8.2015 (poster)
- Chianti Workshop Magnetic resonance for cellular structural biology, Principina Terra (Grosseto), Italy, 05-10.06.2016 (talk)
- Seminar of the Institute for Physical and Theoretical Chemistry, Frankfurt am Main, Germany, 20.06.2016 (talk)

- RNA Club, Frankfurt am Main, Germany, 29.06.2016 (talk)
- RNA Structural Biology SFB902, Bad Homburg, Germany, 28.-29.11.2016 (talk)
- EUROMAR Magnetic Resonance Conference 2017, Warsaw, Poland, 02.-06.07.2017 (talk and poster)